REGULATION OF CARDIAC AUTOPHAGY

IN RESPONSE TO LIPID OVERLOAD

by

Bharat Prasad Jaishy

A dissertation submitted to the faculty of
The University of Utah
in partial fulfillment of the requirements for the degree of

Doctor of Philosophy

Department of Biochemistry

The University of Utah

August 2013

The University of Utah Graduate School

STATEMENT OF DISSERTATION APPROVAL

The dissertation of **Bharat Prasad Jaishy**

has been approved by the following supervisory committee members:

E. Dale Abel	, Chair	**6/6/2013** Date Approved
Donald A. McClain	, Member	**6/6/2013** Date Approved
Jared P. Rutter	, Member	**6/6/2013** Date Approved
Janet E. Lindsley	, Member	**6/6/2013** Date Approved
Andrew S. Weyrich	, Member	**6/6/2013** Date Approved

and by **Christopher P. Hill** , Chair of the Department of **Biochemistry**

and by Donna M. White, Interim Dean of The Graduate School.

ABSTRACT

Obesity is an independent risk factor for several cardiac pathologies. Sustained exposure to nutrient overload in obesity overwhelms cellular homeostatic apparatus, leading to metabolic disorders and organelle dysfunction. The integrity of homeostatic machinery is crucial for the heart to meet its energy need and for cardiomyocytes to survive. Recently, autophagy has emerged as a major catabolic process in maintaining energy and organelle homeostasis.

Growing evidence suggest a role for autophagy in obesity related cardiac pathologies. Yet, the regulation of cardiac autophagy in obesity is unclear. In this study, we explored mechanisms regulating cardiac autophagy in an invivo mouse model of diet-induced obesity and an invitro cell culture model of lipid overload. 12 weeks of high-fat diet (HFD) (45% kcal fat) significantly increased the autophagy marker protein LC3-II and autophagosome number in the murine heart independently of canonical upstream signaling through mTORC1 and AMPK. Interestingly, high-fat fed mice displayed a defective autophagosome turnover that may have led to autophagosome accumulation. Alteration in Beclin1 expression had no effect on HFD-induced autophagy, ruling out a major contribution of autophagy initiation pathways in this process. In vitro, cultured H9C2 cardiomyocytes displayed a biphasic autophagic response to palmitate. To explore the mechanism of early autophagic response to lipid overload, we performed

most experiments after 4 h of treatment when features of ER stress and cell death were absent. Similar to HFD, palmitate increased autophagosome accumulation primarily via an impairment in autophagosome turnover. Oleate alone had no effect on autophagy but cotreatment normalized the palmitate-induced autophagosome accumulation. Moreover, palmitate treatment led to a massive accumulation of superoxide which correlated with impaired lysosomal acidification and pH-dependent lysosomal enzyme activity. Using specific inhibitors and siRNA mediated gene silencing, we identified Nox2 as the major source of superoxide production. The activation of Nox2 was dependent on the palmitate-induced activation of classical PKCs. Together, our study has identified a novel mechanism wherein palmitate-induced activation of PKC-Nox2 pathway led to impaired lysosomal enzyme activity and diminished autophagic turnover in cardiomyocytes. The Nox2-mediated inhibition of autophagic flux might contribute to other known pathological roles of Nox2-mediated oxidative stress in obesity.

TABLE OF CONTENTS

LIST OF FIGURES

LIST OF TABLES

LIST OF ABBREVIATIONS

+dP/dt: Peak rate left-ventricular pressure increase

Akt/PKB: Protein kinse B, a nonspecific serine-threonine protein kinase

AMPK: AMP-activated protein kinase

APdia: Diastolic arterial pressure

APsys: Systolic arterial pressure

Atg: Autophagy-related gene

ATP: Adenosine-5'-triphosphate

Atp6v1h: vATPase, V1 subunit H

BCAA: Branch chain amino acid

Bcl2: B-cell lymphoma 2

Bec1+/-: Mouse heterozygous for Beclin1 in the whole body

Bec1-Tg: Mouse with cardiac specific (αMHC-driven) expression of Beclin1

BMI: Body mass index

Cat (or Cts) A or D or F or L: Cathepsin A or D or F or L

Clcn7: Chloride channel, voltage-sensitive 7

CM: Cardiomyocytes

CMA: Chaperone mediated autophagy

CoA: Coenzyme A

CPT1: Carnitine palmitoyl transferase 1

CVD: Cardio vascular disease

DAG: Diacyl glycerol

DIO: Diet-induced obesity

-dP/dt: Peak rate of left-ventricular pressure decrease

DRAM: Damage-regulated autophagy modulator

EF: Ejection fraction

eIF2α: eukaryotic translation initiation factor alpha

ER: Endoplasmic reticulum

ESR: Electron spin resonance spectroscopy

FABPpm: Plasma membrane fatty acid binding protein

$FADH_2$: Flavin adenine dinucleotide reduced

FAO: Fatty acid oxidation

FAT: Fatty acid translocase

FATP: Fatty acid transporter protein

FFA: Free fatty acid

FIP200: Family interacting protein of 200 kD

FoxO: Forkhead box O family of transcription factors

FS: Fractional shortening

Gba: Glucosidase, beta

Gla: Galactosidase, alpha

GLUT-4: Glucose transporter, type 4

Gns: Glucosamine (N-acetyl)-6-sulfatase

Hexa: Hexosaminidase A

HFD: High-fat high sucrose diet

HR: Heart rate

Hsc70: Heat shock cognate 70

I/R: Ischemia and reperfusion

IRE1α: Inositol requiring enzyme 1 alpha

IVSd: Interventricular septum thickness in diastole

IVSs: Interventricular septum thickness in systole

JNK1: c-Jun N-Terminal Protein Kinase 1

Keap1: Kelch-like ECH-associated protein 1

Lamp1/2A: Lysosome associated membrane protein 1 or 2A

LC3- I or II : Myosin light chain 3- I or II

LVDevP: Left-ventricular developed pressure

LVEDP: Left-ventricular end diastolic pressure

LVIDd: Left-ventricular internal diameter in diastole

LVIDs: Left-ventricular internal diameter in systole

LVMP: Left-ventricular mean pressure

LVPWd: Left-ventricular posterior wall thickness in diastole

LVPWs: Left-ventricular posterior wall thickness in systole

LVSP: Left-ventricular systolic pressure

MCLC3: Mouse with cardiac specific (αMHC-driven) expression of mCherry LC3

Mcoln1: Mucolipin 1

mETC: mitochondrial Electron transport chain

αMHC: Myosin heavy chain, alpha

mTORC1: Mammalian target of rapamycin complex 1

$NADH/NAD^+$: Nicotinamide adenine dinucleotide reduced/oxidised

NCD: Normal chow diet

NIX: NIP3-like protein X

Nox 2 or 4 : NADPH oxidase 2 or 4

Nrf2: Nuclear respiratory factor 2

OXPHOS: Oxidative phosphorylation

p62/SQSTM1: Sequestosome 1

PDH: Pyruvate dehydrogenase

PERK: PKR-like ER kinase

PFK-1: Phosphofructokinase 1

PI3KC3: Class III phosphatidylinositol 3-kinase

PI3P: Phospatidyl inositol-3 phosphate

PINK1: PTEN-induced kinase 1

PKC: Protein kinase C

Rab7: Ras-associated protein

RNS: Reactive nitrogen species

ROS: Reactive oxygen species

SOD2: Mitochondrial manganese superoxide dismutase

SPT1: Serine-palmitoyl transferase 1

sTAB: severe Thoracic aortic banding

STZ: Streptozotocin

SV: Stroke volume

T1DM: Type 1 diabetes mellitus

T2DM: Type 2 diabetes mellitus

TAC: Transverse aortic constriction

TCA: Tricarboxylic acid

TFEB: Transcription factor EB

TG: Triglycerides

TIGAR: TP53-induced glycolysis and apoptosis regulator

TLR: Toll-like receptor

Tom20: Translocase of outer mitochondrial membrane 20

Ulk 1 or 2: Unc-51-like kinase 1 or 2

UPR: Unfolding protein response

UPS: Ubiquitin proteosomal system

vATPase: vacuolar Adenosine 5'-triphosphatase

Vps15 or 34: Vacuolar protein sorting-associated protein 15 or 34

WAT: White adipose tissue

XBP1: X-box binding protein 1

ACKNOWLEDGEMENTS

I would like to take this moment to express my sincere gratitude to my wife, Manju, for her encouragement, support, love and patience throughout this work and beyond. She maintained our family remarkably well and made sure that I could focus on my research free of family responsibilities. Without her behind-the-curtain effort, this work would not have come to its fruition.

My sincere thanks goes to all my lab members who brought their unique personality and perspective that shaped my research. They made my lab-life a truly enjoyable journey and made me feel as if the lab was a home-away-from-home. I would also like to thank all my student volunteers who spent several hours a week to help me with my experiments despite their busy undergraduate life.

I am grateful to all my committee members for providing their valuable insights and constructive criticism throughout my Ph.D. work. Their constant guidance encouraged me to work harder and realize the importance of my work.

I am greatly indebted to my advisor and mentor, Dr. E. Dale Abel for providing me this tremendous opportunity to work under his supervision. His constant support, encouragement, valuable guidance, friendly conversation, and understanding are the corner stone of my Ph.D. work. His unique ability to identify the major scientific

questions and guide me toward solving them with thoughtful experimental design streamlined the completion of my research. I remember going to his office with a handful of what I thought were negative data to have him help me interpret them to a useful conclusion. Despite his extremely busy schedule and increasing responsibilities, he provided ample time to guide me throughout my career and personal struggles.

The success of my Ph.D. work also goes to my two little wonderful daughters– Yashaswi and Smriti. They always welcomed me home with great smiles, which evaporated all the worries I might have brought home from my day of work. Being a father has endowed me with great responsibility and patience that successfully translated to my success as a scientific researcher.

And finally, I would like to thank my parents who devoted their entire life for the wellbeing of their children. They have always put my education ahead of all their priorities. Despite my being away from home for so many years, they always remained close-knit with me and my family. They take great pride in my every little achievement and encouraged me to set and achieve even higher goals in life.

CHAPTER 1

INTRODUCTION

1.1. Obesity: a major health risk factor

Obesity is a complex metabolic condition that contributes to the development of type 2 diabetes (T2DM), high blood pressure, cardiovascular disease (CVD), and heart failure. It is an independent risk factor for hypertension, dyslipidemia, osteoarthritis, sleep apnea, hypoxia, ischemic heart injury, and certain types of cancers (Kenchaiah et al., 2002; Wellman and Friedberg, 2002; Wilson et al., 2002). Environmental factors such as excessive caloric intake and sedentary lifestyles significantly contribute to obesity epidemic. In addition, the obesity is also influenced by social, economic, behavioral, cultural, and genetic factors (1998).

The prevalence of obesity has dramatically increased in the United States and around the world over the past 30 years. Between 2009-2010, estimates indicate that in the US alone, about 35.7% of adults and 17% of children are obese, with a body mass index (BMI) $\geq$ 30 kg/m^2 (Ogden et al., 2012). The rate of obesity tightly correlates with an increased incidence of T2DM and heart diseases nationwide. Moreover, obesity related diseases are among the leading causes of deaths in the US: heart disease (ranked 1) and diabetes (ranked 7) (Murphy et al., 2012). The medical costs associated with obesity were estimated $147 billion for 2008 (Finkelstein et al., 2009) and is expected to rise to approximately $860-$960 billion by 2030 (Wang et al., 2008).

The obesity is not limited to developed countries. Underdeveloped countries with limited food supply and consumption have increasing reports of obesity. Despite rising awareness and expanding medical research, obesity remains an incompletely understood metabolic condition due to its complex etiologies.

1.2. Energy substrate metabolism in the heart

The heart is an metabolically active organ with a continuous need for energy to maintain its contractile function, basal metabolic processes, and ionic homeostasis (Lopaschuk et al., 2010). It shows remarkable metabolic flexibility and utilizes a variety of carbon substrates such as fatty acids, glucose, lactate, puruvate and amino acids based on their availability to generate adenosine-5'-triphosphate (ATP) and meet its energy demand even during periods of fasting and intense exercise (Abel et al., 2012; Gertz et al., 1988; Wisneski et al., 1990). Under basal conditions, the majority of ATP in the heart comes from mitochondrial oxidative phosphorylation (OXPHOS). The ATP production through OXPHOS is driven by high energy electrons generated from nicotinamide adenine dinucleotide reduced (NADH) and flavin adenine dinucleotide reduced (FADH2) produced in the glycolysis, the tricaboxylic acid (TCA) cycle, and β-oxidation of fatty acids (Stanley et al., 2005).

Metabolism of glucose via glycolysis and glucose oxidation accounts for about 20% of the myocardial energy content (Abel et al., 2012). Glucose uptake into the cardiac myocytes is facilitated by glucose transporters, primarily GLUT-4, which is translocated to the plasma membrane upon stimulation by insulin or AMP-activated protein kinase (AMPK) or by cardiac contractility (Abel et al., 2012; Stanley et al., 2005). Additionally, glucose is derived from glycogen stores during starvation and intense exercise. As an energy substrate, glucose is converted to pyruvate by glycolysis. Pyruvate is either reversibly converted to lactate in the cytosol or transported into the mitochondrial matrix and decarboxylated to acetyl-CoA by the pyruvate dehydrogenase (PDH) complex. Acetyl-CoA finally enters the TCA cycle and is broken down to CO_2 and H_2O to generate

ATP to complete the process of glucose oxidation (An and Rodrigues, 2006). The control of glucose metabolism in the heart is complex and occurs at various levels from the entry of glucose through glucose transporters to glycolysis and glucose oxidation. The key modes of regulation involve changes in hormonal action, nutritional status, transcriptional control, allosteric regulation, and posttranslation modification of pathway specific enzymes (Lopaschuk and Kelly, 2008). Although glucose is not the major energy substrate in the normal adult heart, the reliance on glycolysis and glucose utilization significantly increases during myocardial ischemia, hyperglycemia, and heart failure (Abel et al., 2012; Lopaschuk and Kelly, 2008; Stanley et al., 2005).

Fatty acid β-oxidation accounts for majority of ATP production (~70%) in the normal adult heart. Free fatty acids (FFAs) enter the myocardium by either passive diffusion or via membrane-bound transporters such as fatty acid translocase (FAT)/CD36, plasma membrane fatty acid binding protein ($FABP_{pm}$), and fatty acid transporter protein (FATP) (Lopaschuk et al., 2010). FFAs are esterified to fatty acyl-CoAs which are either converted to triglycerides (TGs) or transported to mitochondria to generate energy. Mitochondrial transport of fatty acyl-CoA is facilitated by carnitine palmitoyl transferase 1 (CPT1), a rate limiting enzyme in fatty acid oxidation (FAO), and CPT2. The β-oxidation generates acetyl-CoA, which enters the TCA cycle to generate NADH and FADH2 and fuel OXPHOS to produce ATP (Abel et al., 2012). The rate of FA metabolism in the heart is controlled by the availability and uptake of fatty acids into cardiomyocytes (CMs), allosteric regulation of enzymes and transporters, and transcriptional control of FAO enzymes. Insulin has also been shown to regulate fatty acid uptake by facilitating membrane translocation of CD36 translocase (Luiken et al.,

2002). Another key regulator of β-oxidation at the level of mitochondria is malonyl-CoA. It is a potent inhibitor of CPT1 and limits the uptake of fatty acyl-CoA into the mitochondria, resulting in reduced mitochondrial FAO (Kerner and Hoppel, 2000). Malonyl-CoA has a very high turnover rate and its level is tightly regulated in the heart by the action of three enzymes: AMPK, acetyl-CoA carboxylase, and malonyl-CoA decarboxylase (Stanley et al., 2005).

Glucose oxidation and FAO are interregulated in the myocardium by a process called "glucose-fatty acid cycle" or "The Randle cycle" (Randle et al., 1963). High rates of FAO increase mitochondrial acetyl-CoA/free-CoA and NADH/NAD^+ ratios which activate PDH kinase resulting in the inhibition of PDH activity and subsequent reduction in glucose oxidation (Hue and Taegtmeyer, 2009). Alternatively, an inhibtion of the FAO rates leads to an increase in glucose uptake and oxidation by (i) decreasing cytosolic citrate levels and releasing inhibition of phosphofructokinase 1 (PFK-1), a rate limiting enzyme of the glycolytic pathway, and (ii) lowering acetyl-CoA and NADH levels in mitochondria and hence relieving inhibition on PDH activity . Such interregulation of FAO and glucose oxidation allows the myocardium to control fuel selection and appropriately adapt to changes in substrate availability and demand in the CMs in coordination with hormonal control of circulating myocardial substrates (Hue and Taegtmeyer, 2009; Stanley et al., 2005).

1.3. Energy metabolism of the heart in obesity

Obesity is the major cause of insulin resistance. Lack of insulin action in adipocytes promotes lipolysis and increases circulating FFA levels. Elevated plasma FFA drive

excessive FFA uptake into the myocardium, causing an imbalance between FFA uptake and oxidation and resulting in the accumulation of toxic lipid intermediates such as long-chain acyl-CoA, diacylglycerol and ceramides. These lipid intermediates may lead to impairments in insulin-stimulated GLUT4 translocation, glucose uptake, glucose oxidation, and insulin signaling in the heart (Abel et al., 2012; Boden, 2011). Studies from our lab have shown that the metabolic switch to fatty acids as a preferred energy substrate at the expense of glucose occurs early in the course of high-fat feeding (HFF) (Wright et al., 2009). 2 weeks of HFF in mice increased FAO but reduced basal rates of glycolysis and glucose oxidation in hearts and blunted insulin-stimulated glucose uptake in CMs. GLUT4 protein levels and translocation were significantly reduced, but insulin signaling through protein kinase B (PKB or AKT) was preserved. AKT activation has been shown to facilitate the translocation of CD36 to the plasma membrane (Glatz et al., 2010), which could further increase myocardial fatty acid uptake and the subsequent accumulation of toxic lipid intermediates. The ectopic lipid deposition in the heart, termed "cardiac lipotoxicity," is the hallmark of obesity and diabetes. Cardiac lipotoxicity contributes to insulin resistance, impairment of mitochondrial function, CM hypertrophy, and apoptosis, which may ultimately lead to left-ventricular remodeling of the heart, dilated cardiomyopathy and other obesity-related cardiac pathologies (Avelar et al., 2007; Bugger and Abel, 2008; Rider et al., 2009; Unger and Orci, 2002; Wende and Abel, 2010).

1.4. Quality control mechanisms in the heart

The continuous pumping of the heart places enormous demands on its energetic need. The proper functioning of the heart requires that both contractile components and energy metabolic pathways work efficiently. CMs maintain homeostasis through adaptive mechanisms regulating contractile function, energy metabolism, cell viability and cell size. Nevertheless, being postmitotic cells with little regenerative capacity, CMs sustain various cellular and subcellular insults as a consequence of the rigorous cardiac contractility and various other mechanical, metabolic, and thermal stresses over the life span of a human being (Willis et al., 2009). To overcome such damage and maintain heart function, CMs possess three major intracellular quality control mechanisms that repair or remove dysfunctional proteins/organelles and replace them with functional ones: (1) chaperone mediated refolding of misfolded proteins; (2) the ubiquitin proteasomal system (UPS) for the degradation of short-lived proteins; and (3) autophagy for the recycling of cytoplasmic materials including long-lived proteins, complex lipids, carbohydrates, and damaged organelles via a lysosomal pathway (Figure 1.1) (Wang and Terpstra, 2012; Willis et al., 2009).

The protein synthesis and degradation in the heart are under constant surveillance, which ensures that a synthesized nascent protein is properly folded and functional. Despite an extensive protein folding machinery in the endoplasmic reticulum (ER) and other subcellular compartments, protein misfolding is inevitable. This protein misfolding is further elevated under various cellular stress. The initial attempt to deal with misfolded proteins is their refolding to native form: a function performed by a diverse family of proteins called molecular chaperones (Bukau et al., 2006). Multiple chaperones may

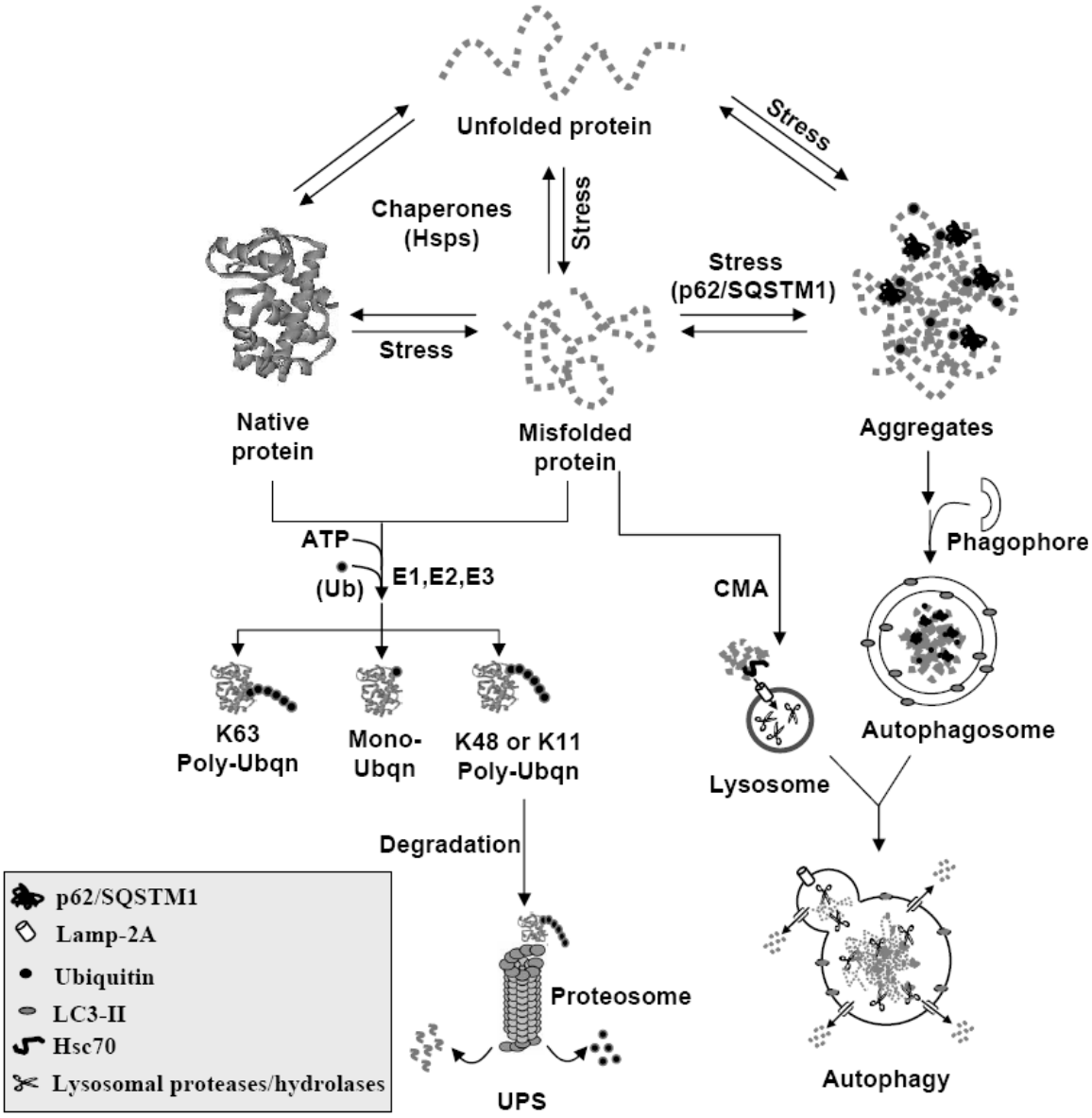

Figure 1.1. Intracellular protein quality control mechanisms in CMs. Molecular chaperones assist proteins to fold into their native form. During various cellular stresses, protein misfolding is upregulated. Misfolded proteins are either degraded by the ubiquitin proteasomal system (UPS) or chaperone mediated autophagy (CMA). Bulk protein aggregates are degraded via macroautophagy. See text for details.

coordinate a refolding event depending on subcellular localization and misfolding conditions of the protein (Patterson, 2006). The synthesis and assembly of the basic sarcomeric proteins such as actin and myosin depends heavily on chaperones to avoid misassembly and aggregation. Chaperones are abundant in CMs and are upregulated during a cardiac stress (Birnie et al., 2005; Pantos et al., 2006). Desmin-related cardiomyopathies, for example, are the consequence of loss-of-function mutations in either the molecular chaperone αB-crystallin or in desmin resulting in disorganized sarcomere and disintegrated myofibrils (Bova et al., 1999; Dalakas et al., 2000; Wang et al., 2001).

At times, the molecular chaperones are inefficient resulting in terminally misfolded proteins that can be cytotoxic. Removal of such proteins occurs via selective and non-selective pathways. The selective pathway is called the ubiquitin-proteasomal system (UPS). The degradation of intracellular proteins via UPS involved two key steps: (1) ubiquitination, where proteins targeted for degradation are covalently tagged at lysine residues with small proteins called ubiquitin (Ub) in an ATP-dependent reaction involving E1, E2, and E3 ligases, and (2) the degradation, in which polyubiquitinated proteins are delivered to and degraded by the 26S proteasome in a highly regulatory process (Zolk et al., 2006). Posttranslational modifications (PTMs), such as acetylation, phosphorylation, and sumoylation, also influence ubiquitination and degradation of target proteins (Manente et al., 2011). The ubiquitinated proteins are recognized by proteasomes either directly or via specific ubiquitin receptors (Lee and Brown, 2012; Sowa et al., 2009). Normally, proteins targeted for proteasomal degradation are tagged with at least four lysine 48 (K-48) or lysine 11 (K-11) linked ubiquitin chains (Clague and Urbe,

2010). Monoubiquitination and lysine 63 (K-63) linked polyubiquitination of proteins are involved in nonproteolytic signaling pathways (Chen and Sun, 2009). A number of muscle specific ubiquitin ligases are involved in UPS-mediated degradation of sacromeric proteins and thus play an important role in structural and functional integrity of the sarcomere (Bodine et al., 2001; Zhang et al., 2005).

Under severe cellular stress and cardiac pathologies, both chaperones and the UPS are overwhelmed by significant accumulation of misfolded proteins. Under such conditions, misfolded proteins are either selectively degraded in the lysosomal lumen via chaperone mediated autophagy or form large aggregates, which eventually leads to the formation of specialized structures called aggresomes at the microtubule organizing center (Garcia-Mata et al., 2002). Aggresome formation is thought to be a protective mechanism to sequester potentially toxic proteins into confined cytoplasmic compartments (Wang and Terpstra, 2012). However, accumulation of aggregosomes induces nonselective degradation of its content via macroautophagy (Garcia-Mata et al., 2002). Detailed mechanism of mammalian autophagy is described in section 1.5.

1.5. Autophagy: a key regulator of cardiac cellular homeostasis

Autophagy (Greek; auto=self, phagy= to eat) is an evolutionarily conserved process of cellular self-digestion. It is a catabolic process whereby long-lived proteins, damaged organelles, intracellular pathogens, and other cytoplasmic materials are degraded in the lysosomes. Depending on the mode of substrate delivery to lysosomes, autophagy is broadly classified into three different forms: microautophagy, chaperone mediated autophagy (CMA), and macroautophagy (Figure 1.2) (Yorimitsu and Klionsky, 2005).

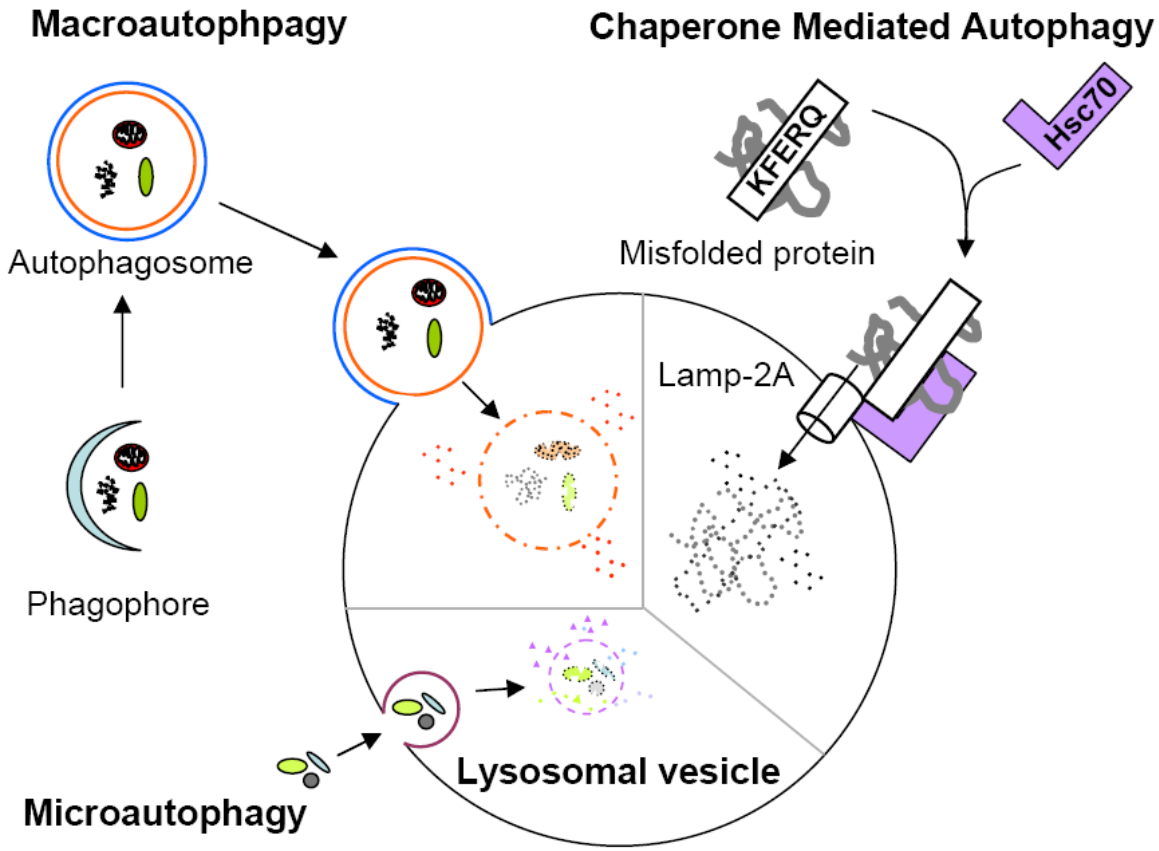

Figure 1.2. Different forms of mammalian autophagy. Three different types of autophagy are identified in mammalian cells based on the method of substrate delivery to lysosomes. In macroautophagy, cytoplasmic constituents are sequestered by a double membrane vesicle, the autophagosome, and delivered to the lysosome by heterotypic fusion. In CMA, misfolded/unfolded proteins containing KEFRQ consensus motif are selectively recognized by molecular chaperone Hsc70 and cochaperones and targeted to the lysosome via interaction with the lysosomal membrane protein Lamp-2A. In microautophagy, substrates targeted for degradation are trapped and internalized into a single membrane vesicle by direct invagination of the lysosomal membrane. The vesicle then pinches off into the lysosomal lumen to deliver the substrates. See text for details. protease Atg4 to LC3-I to expose its C-terminal glycine residue. LC3-I is then activated.

Autophagy is maintained at a low level under physiological conditions to clear proteins and organelles damaged by general wear and tear. However, it is significantly induced in response to a stress such as nutrient starvation, hypoxia, ischemia and reperfusion (I/R), mitochondrial dysfunction, ER stress, oxidative stress, and various infections (Bellot et al., 2009; Deretic, 2006; Elmore et al., 2001; Lee et al., 2012; Lum et al., 2005; Matsui et al., 2007). Autophagy is also regulated at the transcriptional and epigenetic levels (He and Klionsky, 2009). Autophagy is primarily considered as a prosurvival process providing nutrients to cells under starvation through the degradation of proteins dispensable for basic cellular function. It also protects cells by removing toxic proteins aggregates, damaged organelles, and invading pathogens via lysosomal degradation. However, uncontrolled autophagy can be detrimental and may promote cell death by excessive degradation of essential proteins and cellular organelles that are essential for survival (Bursch, 2004).

1.5.1. Mechanisms of mammalian autophagy

The activation of a particular form of autophagy depends on the nature of stimulus or stressor and types of substrates to be degraded. Of three different forms of autophagy, microautophagy is the least studied in mammals. In yeasts, both nonselective (NSM) and selective (SM) forms of microautophagy exist. In NSM, cytosolic constituents, mainly proteins, cause tubular invaginations of the lysosomal membrane from which small vesicles engulfing the target proteins are pinched off into the lysosomal lumen and degraded by lysosomal proteases and hydrolases (Mijaljica et al., 2011). In SM, specific organelles such mitochondria, peroxisomes, and part of the nucleus are targeted for

lysosomal degradation (Farre and Subramani, 2004; Kissova et al., 2007; Roberts et al., 2003). Interestingly, no direct evidence of microautophagy under physiological conditions is reported to date (Mijaljica et al., 2011).

CMA is the major form of selective autophagy for long-lived proteins in mammalian cells. In CMA, proteins containing a KFERQ or KFERQ-like pentapeptide motif are recognized by the cytosolic chaperone heat shock cognate 70 (Hsc70) and cochaperones. The substrate-chaperone complex interacts with lysosome-associated membrane protein 2A (Lamp-2A), which results in unfolding and translocation of the substrate into the lysosome for degradation (Majeski and Dice, 2004). About 30% of cytosolic proteins contain a KFERQ-like sequence that remains buried in the native protein fold. Upon misfolding of proteins, the pentapeptide sequence becomes exposed and is recognized by Hsc70, which ultimately targets misfolded proteins to CMA (Kiffin et al., 2004). Impairment of CMA leads to accumulation of oxidized proteins and protein aggregates making cells easily vulnerable to a variety of stress. Interestingly, CMA is upregulated in cells with impaired macroautophagy, probably as a prosurvival pathway to get rid of toxic cytoplasmic proteins (Kaushik et al., 2008; Massey et al., 2006).

Macroautophagy (hereafter referred to as autophagy) is the most extensively studied form of autophagy in mammalian systems. The entire process of autophagy involves five distinct steps: initiation, expansion, vesicle maturation, fusion, and cargo degradation. The initiation step starts with the formation of a small membranous structure called the isolation membrane or phagophore. The precise origin of phagophore formation in mammalian cells is still unclear and may originate from the ER, mitochondria, the Golgi or the plasma membrane depending on the nature and degree of autophagic induction

(Mari et al., 2011). The phagophore expands with the acquisition of extra lipids to enclose the intracellular material targeted for degradation. Subsequent maturation of the phagophore resulted into a double-membrane vesicle called autophagosome. Mature autophagosomes were suggested to fuse first with late endosomes to form amphisomes and then with lysosomes to form autophagolysosomes or autolysosomes. Finally, the inner autophgosomal membrane and enclosed cargo are degraded by the lysosomal proteases and hydrolases into simple metabolites that are transported back into the cytosol to fuel essential cellular function (He and Klionsky, 2009; Mari et al., 2011).

Autophagy is tightly regulated at every step of the process to ensure that cellular homeostasis is maintained during its evolution. Autophagosome formation alone requires 18 different core autophagy (Atg) proteins in addition to an increasing number of upstream signaling molecules that fine tune autophagy in response to various stimuli (Weidberg et al., 2011) . In a prototypic case, mammalian target of rapamycin complex 1 (mTORC1) acts as a master regulator of autophagy (Figure 1.3). Under normal conditions, growth factor signaling activates mTORC1. Activated mTORC1 directly interacts with the Ulk1/2-Atg13-FIP200 complex and inhibits Ulk1/2 kinase activity and autophagy by phosphorylating Ulk1/2 and Atg13. Inactivation of mTORC1 such as during nutrient deprivation dissociates it from the Ulk1/2-Atg13 complex, resulting in the dephosphorylation and activation of Ulk1/2. This leads to phosphorylation of Atg13, FIP-200, and Ulk1/2, and induction of autophagy. An active Ulk1/2-Atg13-FIP200 complex provides the initial signal for autophagy induction (Chan, 2009). Initiation of autophagy is regulated by various factors through direct or indirect regulation of mTORC1.

Figure 1.3. Molecular mechanism of mammalian autophagy. Multiple signaling molecules coordinate different steps in autophagy: initiation, expansion, vesicle maturation, fusion, and cargo degradation. An inducer such as starvation relieves inhibitory phosphorylation of mTORC1 on the Ulk1/2 complex to initiate autophagy (step 1). The activated Ulk1/2 complex in turn activates Beclin1-Vps34 (PI3KC3) complex either through Ambra1 or other factors. The kinase activity of Vps34 is regulated by Beclin1, which in turn is controlled by an inhibitory interaction with Bcl-2. The catalytic activity of Vps34 results in the formation of PI3P: a key lipid molecule involved in interaction with various factors that supply membrane and protein components to the growing isolation membrane (phagophore) of unknown origin (step 2). In addition to these initiating regulatory complexes, autophagosome expansion and maturation requires two ubiquitin-like conjugation systems: Atg5-Atg12 and LC3 (mammalian Atg8) (step 3). The LC3 (Atg8) conjugation is also required for the selection of autophagic cargo (substrate), determining autophagosome size and membrane curvature, and, in association with microtubule proteins, for the bidirectional movement of autophagosomes towards lysosomes for fusion. Mature autophagosomes either fuse with late endosomes to form amphisomes or with lysosomes to form autolysosomes (step 4). The autophagic cargo is degraded in autolysosomes by lysosomal proteases and hydrolases into simple substrates which are effluxed back into the cytosol to be utilized for energy production and biomolecule synthesis that are vital for cellular homeostasis (step 5).

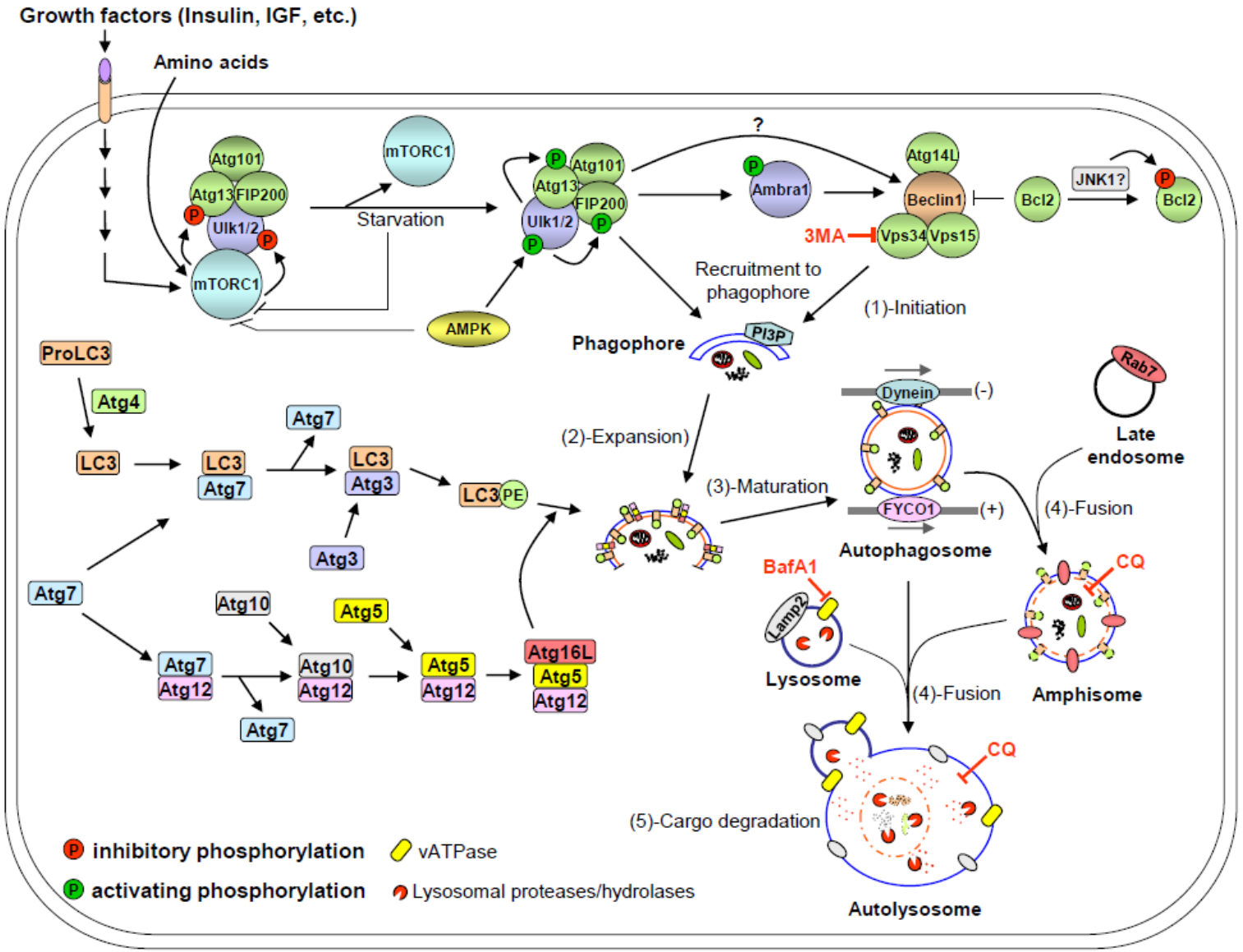
Growth factors (Insulin, IGF, etc.)
Amino acids
Atg101
Atg13
FIP200
Ulk1/2
mTORC1
Starvation
mTORC1
Atg101
Atg13
FIP200
Ulk1/2
?
Ambra1
Atg14L
Beclin1
Vps34
Vps15
3MA
Bcl2
JNK1?
Bcl2
Recruitment to phagophore
(1)-Initiation
AMPK
Phagophore
PI3P
ProLC3
Atg4
LC3
LC3
Atg7
Atg7
LC3
Atg3
Atg3
LC3 PE
(2)-Expansion)
(3)-Maturation
Dynein
(-)
FYCO1
(+)
Autophagosome
Rab7
Late endosome
(4)-Fusion
Atg7
Atg7
Atg12
Atg10
Atg10
Atg12
Atg5
Atg5
Atg12
Atg16L
Atg5
Atg12
BafA1
Lamp2
Lysosome
(4)-Fusion
CQ
Amphisome
CQ
(5)-Cargo degradation
Autolysosome
inhibitory phosphorylation
activating phosphorylation
vATPase
Lysosomal proteases/hydrolases

Recently, mTOR independent pathways of autophagy induction have also been documented in mammalian system (Sarkar et al., 2009; Williams et al., 2008). Uponautophagic stimulation, a Beclin1-class III phosphatidylinositol 3-kinase (PI3KC3 or Vps34) complex consisting of Beclin1, Vps34, Vps15, Atg14L (Barkor), and Ambra1, is formed at the phagophore by an unclear mechanism. Beclin1 plays a crucial role in Vps34 activation and the Beclin1-Vps34 interaction is required for autopahgic induction. Beclin1 constitutively binds to its antiapoptotic partner Bcl2, which prevents Beclin1-Vps34 interaction. However, in amino acid depleted condition, Beclin1 dissociates from Bcl2: a process mediated by multiple factors including Bcl2 degradation, competitive binding of Bcl2 with other proteins, and JNK1 phosphorylation of Bcl2 (Lavallard et al., 2012). The dissociated Beclin1 binds to Vps34 and enhances its lipid kinase activity resulting in the formation of phospatidyl inositol-3 phosphate (PI3P). In autophagy, PIP3 mediates the localization of several regulatory Atg proteins to the phagophore which is essential for the expansion of the autophagosome (Weidberg et al., 2011).The expansion of autophagosome also requires two ubiquitin-like (UBL) systems: Atg12-Atg5 and myosin light chain3 or LC3 (mammalian Atg 8) conjugation systems. In the Atg12-Atg5 system, Atg12 is initially activated by Atg7, an E1-like ubiqutin enzyme, and then transferred to Atg10, an E2-like ligase, which covalently attaches Atg12 to Atg5. Finally, the Atg12-Atg5 complex noncovalently attaches to Atg16L (mammalian Atg16-like protein) to form a larger Atg12-Atg5-Atg16L complex (Mizushima et al., 2003; Weidberg et al., 2011). The recruitment of this complex to the autophagosomal membrane may depend on PI3P formation (Weidberg et al., 2011). Interestingly, the complex dissociates from the membrane upon autophagosome formation and thus serves

as a specific marker of the phagophore (Mizushima et al., 2003). In the LC3 (Atg 8) conjugation system, a larger precursor form of LC3 is first cleaved by the cysteine by an E1-like enzyme, Atg7, and transferred to an E2-like ligase, Atg3, which lapidates LC3-I by covalent attachment of phosphatidyl ethanol amine (PE) to the glycine residue resulting into the formation of LC3-II (or LC3-PE) (Kim et al., 2001; Kirisako et al., 2000). LC3-II is recruited to the growing autophagosome by Atg5-At12-Atg16L complex (Mizushima et al., 2001). Translocation of LC3-II to the membrane helps membrane expansion and closure of the double membrane structure to form the mature autophagosome (Lavallard et al., 2012). Among Atg proteins, only LC3-II remains attached to autophagosomes during their fusion with lysosomes and gets degraded in autolysosomes. Hence, LC3-II is used as a reliable biomarker for monitoring autophagy (Klionsky et al., 2007). Fusion of autophagosomes with lysosomes and degradation of the autophagosomal content is the final step of autophagy. Several motor proteins of the cytoskeleton such as Dynein and FYCO1 promote bidirectional movements of mature autophagosomes to microtubule organizing centers where they fuse with lysosomes (Pankiv et al., 2010; Ravikumar et al., 2005). The fusion is mediated by classical endocytotic pathway proteins such as Rab7, which interacts with autophagosomes and facilitates their fusion with lysosomes in a Lamp1/Lamp2 dependent manner (Jager et al., 2004).

Autophagy is also regulated at the transcriptional level. The forkhead box O family of transcription factors (FoxO) and transcription factor EB (TFEB) are implicated in the transcriptional control of autophagy genes. Constitutively active FoxO1 has been shown to prevent insulin dependent reduction in autophagy gene expression in hepatocytes

(Lavallard et al., 2012). Recently, TFEB has been identified as a master transcriptional regulator of a network of genes involved in autophagy and lysosomal biogenesis (Palmieri et al., 2011; Sardiello et al., 2009).

Although bulk autophagy is largely considered a nonselective process, several studies showed autophagy to be highly selective for the targeting of cytoplasmic proteins and specific organelles for lysosomal degradation (Figure 1.4). Most cytosolic proteins targeted for selective autophagy are ubiquitinated and bound to ubiquitin-binding adapter protein p62/SQSTM1 (hereafter called p62) through its ubiquitin binding domain (UBD) (Figure 1.1). The self-oligomerization of p62 facilitates incorporation of more ubiquitinated proteins. The p62-target protein complexes are delivered to autophagosome through a direct interaction of LC3-interacting region (LIR motif) of p62 with specific residues within LC3 (Ichimura et al., 2008; Pankiv et al., 2007). Consistent with these observations, several in vivo studies showed the accumulation of p62-positive aggregates of ubiquitinated proteins when autophagic turnover was impaired (Bjorkoy et al., 2005; Gal et al., 2007; Settembre et al., 2008).

Like proteins, various intracellular organelles and macromolecules also undergo selective autophagy. In mitophagy, mitochondria are selectively targeted for autophagic degradation. In vitro studies demonstrate that uncoupled mitochondria with diminished mitochondrial membrane potential are specifically recognized by the PTEN-induced kinase 1 (PINK1) which recruits the E3-ubiquitin ligase Parkin to the damaged mitochondria. Parkin ubiquitinates mitochondrial substrates which are recognized by p62 to facilitate the engulfment of damaged mitochondria by autophagosomes

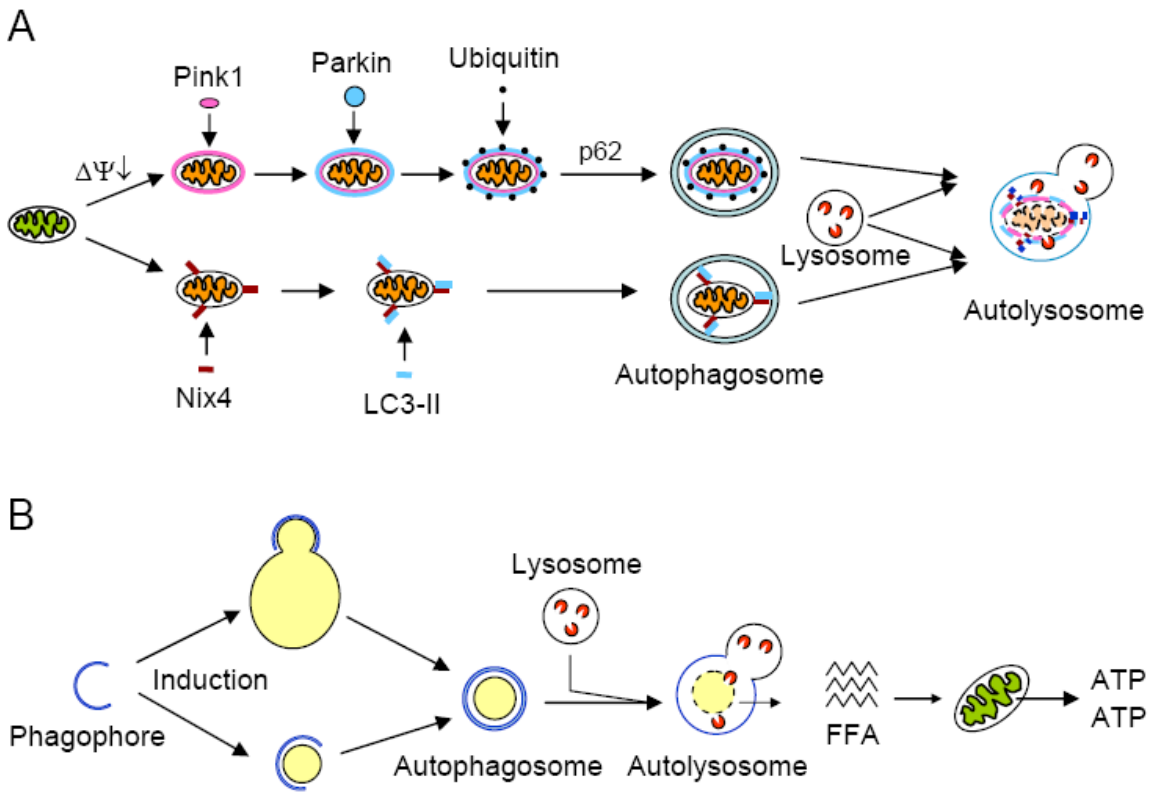

Figure 1.4. Two major types of organelle specific autophagy. (**A**) In mitophagy, damaged mitochondria with diminished membrane potential (ΔΨ↓) are selectively recognized by PINK1 which recruits the E3-ubiquitin ligase Parkin to mitochondria. Parkin ubiquitinates mitochondrial proteins, which are recognized by p62 to facilitate autophagic degradation of damaged mitochondria. Selective removal of normal mitochondria in maturing reticulocytes occurs via binding of Nix4 to mitochondria. Nix4 directly interacts with LC3-II to direct mitochondria for autophagic degradation. (**B**) In lipophagy, small LDs or a portion of a large LD are sequestered by a growing autophagosomal membrane. The lipid droplets in mature autophagosomes are then degraded by lysosomal hydrolases to generate FFAs, which are utilized for ATP production in mitochondria to maintain cellular energy homeostasis. See text for details.

(Youle and Narendra, 2011). Mitophagy is also involved in the clearance of normal mitochondria in reticulocytes, which mature into mitochondria-deficient red blood cells. This form of mitophagy involves a different mechanism in which the outer mitochondrial membrane protein NIP3-like protein X (NIX) directly interacts with LC3 through its WXXL-like motif facing the cytosol to target mitochondria for autophagic degradation (Novak et al., 2010). Like mitochondria, defective ER, peroxisomes, and ribosomes are also selectively degraded by reticulophagy, pexophagy and ribophagy, respectively (Weidberg et al., 2011).

Lipid droplets (LDs) are the other important organelles that are degraded by lipophagy (autophagy of LDs) to provide FFAs as substrates for ATP production. Recent reports suggest that lipophagy is an important process in the mobilization of esterified lipids in LDs in addition to previously known intracellular lipolysis (Singh and Cuervo, 2012; Singh et al., 2009a). The mechanism of lipophagy is not well established. LC3 is found to be associated with LDs, however, if it directly interacts with LDs or remains associated with classical autophagosomes wrapping LDs is unclear (Shibata et al., 2009). The evidence for the involvement of autophagy in LDs catabolism came from knockdown of Atg5 in cultured hepatocytes. Normal hepatocytes responded to acute oleic acid challenge by increasing lipolysis which would prevent enlargement of LDs, whereas hepatocytes with Atg5 knockdown displayed increasing number and size of LDs upon acute oleic acid challenge. Likewise, in vivo, liver specific deletion of another Atg gene (Atg7) in mice resulted in the development of liver steatosis (Singh et al., 2009a). These studies also showed that lipophagy is involved in LDs metabolism both under basal and starvation conditions. Given the epidemic of fat-related diseases such as obesity and

T2DM, the role of autophagy in lipid metabolism and homeostasis in normal and disease states and in other organ systems requires further study.

1.5.2. Regulation of lysosomal function

Lysosomes are the final destination for macromolecules and cytoplasmic organelles bound for degradation through autophagy. Lysosomes contain about 50 different hydrolytic enzymes that perform their maximal activity at low pH. The acidic pH of lysosomes (pH≤5) is largely maintained by a vacuolar ATPase that pumps protons into the lysosomal lumen (Saftig and Klumperman, 2009). The acidic pH of the lysosome is critical for the degradation of the autophagic substrates. However, the mechanism of lysosomal acidification is complex and not entirely clear (Mindell, 2012). The proton pumping of the vATPase separates electric charge (greater positive charge in the lysosomal lumen than in the cytoplasm), which generates a transmembrane voltage. Therefore, a counter ion must move to dissipate this voltage for net proton pumping to occur. Although the molecular identity of such counterion channel remains elusive, it is generally agreed that both ClC-7, a Cl^-/H^+ antiporter, and a putative cation transporter (primarily a K^+-channel) may contribute to the acidification of lysosomes (Graves et al., 2008; Kornak et al., 2001; Mindell, 2012). The relative contribution of different channels may be context dependent and could vary in different cell types. More importantly, the assembly of the vATPase subunits, namely membrane-bound V_0 and cytosolic V_1, are also affected by various conditions which could, in turn, impair lysosomal acidification and lysosomal enzymatic activity (Sautin et al., 2005; Sumner et al., 1995).

1.5.3. Autophagy in the heart

Autophagy in the heart plays a critical role in cellular homeostasis and a defect in autophagy can be deleterious to the heart as evidenced by the deregulation of autophagy in many cardiomyopathies such as ischemic heart disease, Danon disease, myocardial infarction (MI), and heart failure (Gustafsson and Gottlieb, 2008; Martinet et al., 2007). Under baseline conditions, autophagy seems to maintain normal cardiac function and structure. For example, upregulation of autophagy in the murine heart in response to fasting suggests an important prosurvival role of autophagy in starvation (Mizushima et al., 2004). In contrast, disruption of basal autophagy by conditional deletion of cardiac-specific Atg5 leads to accumulation of abnormal mitochondria, disruption of sarcomeric structure, and development of cardiac dysfunction (Nakai et al., 2007). Likewise, in Danon's cardiomyopathy, defective autophagic clearance due to a deficiency in the lysosomal protein Lamp-2 results in a massive accumulation of autophagosomes (Nishino et al., 2000; Tanaka et al., 2000). Conversely, studies indicate that excessive autophagy may impair cardiac function. CMs from patients with cardiovascular diseases such as aortic stenosis, hypertensive heart disease, chronic ischemia, and dilated cardiomyopathy have increased numbers of autophagosomes in dying cells (Hein et al., 2003; Kostin et al., 2003; Yan et al., 2005). Whether autophagy plays a causal role in cell death or is upregulated in an attempt to rescue dying cells is not clear.

1.5.3.1. Autophagy in cardiac hypertrophy and heart failure

In response to hemodynamic stress, such as pressure overload, CMs increase in size resulting in cardiac hypertrophy. Autophagy was suppressed during cardiac hypertrophy

in the heart induced by 1 week of transverse aortic constriction (TAC) with no cardiac dysfunction (Nakai et al., 2007; Yamaguchi et al., 2003). Studies suggest that autophagy might play a protective role in compensatory cardiac hypertrophy. For example, cardiac hypertrophy induced by β-adrenergic stimulation by isoproterenol infusion leads to left ventricular dilation and cardiac dysfunction in conditional Atg5-deficient mice but not in wildtype controls (Nakai et al., 2007). In contrast, activation of autophagy by rapamycin treatment not only prevents cardiac hypertrophy induced by thyroid hormone treatment or aortic banding but also regresses existing hypertrophy in parallel with improved cardiac function (Ha et al., 2005; Kuzman et al., 2007; McMullen et al., 2004). Together, these data suggest that autophagy facilitates hypertrophic response in the heart. Interestingly, conditional Atg5-deficient mice undergo same degree of hypertrophy as wildtype mice in response to TAC, disputing the role of autophagy in TAC-induced cardiac hypertrophy or suggesting that an alternative hypertrophic response exists to compensate for autophagy (Nakai et al., 2007).

Contrary to compensatory cardiac hypertrophy, autophagy was upregulated in heart failure in both patients and animal models (Nishida et al., 2009). In failing hearts, increased autophagy has been observed in dead or dying CMs together with apoptosis and necrosis (Kostin et al., 2003). However, it is unclear if CM death is caused by autophagy or is the consequence of impaired autophagic turnover in failing myocardium. Zhu et al. study suggested that in mice subjected to severe thoracic aortic banding (sTAB), autophagy plays a role in transition from cardiac hypertrophy to heart failure (2007). Compared to conventional TAC, sTAB mice showed rapid onset of clinical heart failure accompanied by a significant increase in autophagosome number. Suppression of

autophagy in Beclin1$^{+/-}$ mice decreased pathological remodeling of the heart following sTAB. In contrast, enhancement of autophagy by Beclin1 overexpression exacerbates cardiac remodeling. The conclusion from these data conflicts with an earlier study by Nakai et al. on Atg5-deficient mice which suggests that autophagy is an adaptive response to hemodynamic stress (2007). This discrepancy may be due to different genetic models used to suppress autophagy: while Atg5-deletion completely blocks basal autophagy, Beclin1$^{+/-}$ brings about only 50% reduction. Data from a recent study suggest that the improved cardiac function observed in sTAB-operated Beclin1+/- mice could be due to disinhibition of autophagic flux and consequential decrease in autophagosome number, implying that autophagy could be adaptive in the setting of sTAB-induced cardiac remodeling (Ma et al., 2012). Overall, an emerging consensus is that autophagic activation must be in an optimal, adaptive range to have beneficial effects in load-induced cardiac hypertrophy.

1.5.3.2. Autophagy in oxidative stress

Oxidative stress is a common feature of several systemic and cardiac abnormalities such as obesity, dyslipidemia, insulin resistance, diabetes, I/R, heart failure, cancer, neurodegeneration, and aging. Oxidative stress occurs excessive reactive oxygen species (ROS) production overwhelms cellular antioxidant defense system. The mitochondrial electron transport chain (mETC) and the membrane-bound NADPH oxidase (Nox) are the major producers of ROS. The accumulated ROS indiscriminately oxidizes and damages various cellular constituents such as proteins, DNA, and lipids. Superoxide anion ($O_2^{\bullet}$-) and hydrogen peroxide (H_2O_2) are two major forms of ROS in the heart.

As a prosurvival pathway, autophagy has long been envisioned as playing a key role in oxidative stress and associated pathologies. Studies have shown that both $O_2^{\bullet-}$ and H_2O_2 induce autophagy which, in turn, serves as an adaptive response to minimize further oxidative damage (Scherz-Shouval and Elazar, 2011). Since ROS are short lived and interconvertible, it is likely that multiple ROS coordinately mediate oxidative stress-induced autophagy. For example, mitophagy is triggered by the generation of ROS, both $O_2^{\bullet-}$ and H_2O_2, which impairs mETC leading to the loss of mitochondrial membrane potential ($\Delta\Psi_m$) and enhanced mitochondrial fragmentation. Consequently, the damaged mitochondria are eliminated by autophagy to prevent further ROS-induced damage (Lee et al., 2012; Scherz-Shouval and Elazar, 2011).

Depending upon the site of ROS generation and the nature of stress, a specific ROS could regulate autophagic induction. For instance, superoxide is the major mitochondrial ROS regulating autophagy. In HeLa cells, $O_2^{\bullet-}$ has been shown to mediate glucose-deprivation induced autophagy which is inhibited by overexpression of mitochondrial manganese superoxide dismutase (SOD2) and induced by siRNA mediated depletion of SOD2 (Chen et al., 2009). However, the mechanism inducing mitochondrial $O_2^{\bullet-}$ production in starvation is unclear (Chen et al., 2009). A separate study showed that H_2O_2 also mediates starvation induced autophagy partially through PI3KC3 (Scherz-Shouval et al., 2007). H_2O_2 acts as a direct modifier of the cysteine-protease Atg4 by oxidizing the protein and enhancing its ability to convert LC3-I into LC3-II. Similarly, a number of autophagy genes have been identified as the direct target of redox modifications which lead to deregulation of autophagy under oxidative stress (Lee et al., 2012). It is important to emphasize that ROS usually react or cross-talk with reactive nitrogen species (RNS)

and other reactive molecules that may modulate their effect on autophagy. Therefore, in several pathologies oxidative and nitrosative stresses often coexist with altered autophagy.

The role of NOX-borne ROS in autophagy is less known. The ROS produced by the NOX isoform 2 (Nox2) was recently shown to induce antibacterial autophagy in phagoycytes (Huang et al., 2009). Upon induction, NOX2 translocates to the phagosomal membrane and generates superoxide by transferring electrons from cytosolic NOX to oxygen in the phagosomal lumen. The generation of ROS was necessary to target LC3 to phagosomes and subsequent degradation of phagosomes within lysosomes. A recent study linked NOX2 activation to toll-like receptor (TLR)-mediated induction of autophagy in inflammatory bowel diseases (Huang et al., 2009).

The ROS/RNS also regulates autophagy at the transcriptional level by modifying key transcription factors and altering their activity. One such target is the Nrf2 /Keap1 pathway (Itoh et al., 1997). Nrf2 not only induces the transcription of antioxidant and cellular detoxification genes but also induces autophagy by increasing p62 expression (Jain et al., 2010). A second major transcription factor activated by ROS is p53. The activation of p53 leads to the induction of both pro- and antiautophagic gene expression. The TIGAR (TP53-induced glycolysis and apoptosis regulator) is the direct target of p53 and its overexpression has been shown to attenuate starvation or glucose/hypoxia induced autophagy (Bensaad et al., 2009). Another p53 target DRAM (damage-regulated autophagy modulator), on the other hand, promotes autophagy (Crighton et al., 2006).

Oxidative stress also affects lysosomal integrity and function (Kurz et al., 2008). The lysosomal compartment is rich in iron released from macromolecules and damaged

mitochondria during autophagic degradation. The labile pool of iron reacts with H_2O_2 generated during oxidative stress to form extremely reactive hydroxyl radical ($OH^{\bullet}$). The $OH^{\bullet}$ causes oxidative damage to lysosomal membrane proteins and lipids, which subsequently leads to lysosomal membrane destabilization and enzyme leakage. Additionally, diffusion of H_2O_2 into lysosomes results in oxidative accumulation of undegradable intralysosomal material, called lipofuscin, which over time occupies most of the lysosomal volume especially in long-lived postmitotic cells including CMs. Lipofuscin accumulation redirects lysosomal enzymes away from lysosomes. Collectively, the dysfunctional lysosomes in oxidative stress result in the inhibition of autophagic turnover and accumulation of large autophagosomes as often observed in oxidative-stress associated pathologies such as aging and neurodegeneration.

1.5.3.3. Cardiac autophagy in obesity and diabetes

Obesity contributes to various metabolic disorders including dyslipidemia, hypertension, reduced high-density lipoprotein (HDL) cholesterol, and glucose intolerance which greatly increase the risk for several diseases including CVD and T2DM (Malnick and Knobler, 2006). Insulin resistance, characterized by reduced insulin action, is central to the pathogenesis of CVD and T2DM. In obesity, excessive expansion of visceral adipose tissue causes adipose tissue dysfunction resulting in the increased production of FFA due to uncontrolled lipolysis and release of inflammatory cytokines release from adipose tissue. High levels of circulating FFAs and inflammatory cytokines suppress insulin signaling in many tissues including liver, skeletal muscles and the heart (Abel et al., 2012; Chess and Stanley, 2008). In the heart, increased delivery of FFA leads

to the accumulation of toxic lipid intermediates which inhibit local insulin action via protein kinase C-Φ dependent inhibitory phosphorylation of insulin receptor substrate proteins. Accumulation of toxic lipid metabolites also invokes diverse pathological responses including oxidative stress, ER stress, mitochondrial dysfunction, and apoptosis (Abel et al., 2012). The effect of lipotoxicity is multifactorial and could result from alterations in various homeostatic cellular pathways.

Autophagy is an important cellular homeostatic pathway and has been shown to play critical roles in the regulation of metabolism in many organ systems (Rabinowitz and White, 2010). Derangement of metabolic pathways in obesity is well documented. Recent studies suggest a link between autophagy and obesity; however, the precise role of autophagy in the development of obesity is unclear (Lavallard et al., 2012; Xu and Ren, 2012). Most studies on autophagy in relation to obesity are focused on insulin sensitive tissues and reveal opposing and tissue specific effects of autophagy.

The role of basal autophagy in pancreatic islet homeostasis is demonstrated by the studies on β-cell specific Atg7 knockout (Atg7-KO) mice (Ebato et al., 2008). Morphologically, loss of autophagy in Atg7-KO β-cells displayed increased accumulation of ubiquitinated proteins, deformed and branched mitochondria, distended ER, decreased β-cell mass, and reduced numbers of insulin vesicles accompanied by an increase in apoptosis and the loss of β-cell proliferation. Functionally, Atg7-KO β-cells exhibited impaired glucose-stimulated insulin secretion. Consequently, the KO mice became hypoinsulinemic and hyperglycemic suggesting a protective role of autophagy in β-cell function. More importantly, when mice were challenged with a high-fat diet, autophagy was significantly upregulated in wildtype β-cells, whereas lack of autophagy

Atg7-KO β-cells resulted in accumulation of ubiqutinated proteins, lower β-cell mass, increased apoptosis, degeneration of islets and more severe glucose intolerance. Furthermore, autophagy was also upregulated in type 2 diabetic (db/db) mouse model compared to nondiabetic controls (Ebato et al., 2008; Fujitani et al., 2009). These data suggest that induction of autophagy in diet-induced obesity and T2DM is an adaptive response and protects pancreatic islets from deleterious effects underlying these metabolic diseases (Hur et al., 2010).

Obesity is the direct consequence of the expansion of white adipose tissue (WAT) mass due to increased number and size of adipocytes. Adipocytes are the primary storage site of body fat and are generated from fibroblast-like preadiopocytes through a differentiation process called adipogenesis. Several studies have shown that the lysosomal-degradation pathway is an important regulator of cellular differentiation (Taniguchi et al., 2010; Zhang et al., 1995). Since autophagy is involved in the lysosomal degradation pathway, its role in adipogenesis in obesity has been studied extensively in recent years (Singh et al., 2009b; Zhang et al., 2009). Inhibition of autophagy by knocking down Atg7 or Atg5 gene blocked the differentiation of 3T3-L1 preadiopcytes and impaired adipogenesis or lipid accumulation. In congruence, adipose-tissue specific deletion of Atg7 resulted in leaner mice with reduced WAT mass and differentiation. (Singh et al., 2009b). In obese people, the degree of induction of autophagy is correlated with the degree of obesity and the size of white adipocytes (Kovsan et al., 2011). This induction of autophagy in adipose tissue has been found to be deleterious leading to the development of obesity. For instance, adipose tissue specific Atg7-KO mice were resistant to diet-induced obesity (DIO) with improved insulin sensitivity. Inhibition of

autophagy by ablation of the Atg5 gene impaired adipogenesis suggesting that induction of autophagy contributes to adipogenesis and development of obesity (Baerga et al., 2009).

Under baseline conditions, hepatic autophagy is involved in the maintenance of blood glucose and amino acid levels, and the regulation of Insulin response (Ezaki et al., 2011; Yang et al., 2010). Upon starvation, hepatic autophagy increases the production of gluconeogenic amino acids, some of which are fed into hepatic gluconeogensis to produce glucose and maintain blood-glucose level (Yang et al., 2010). In contrast to autophagy in pancreas and adipose tissue, hepatic autophagy was significantly suppressed in obesity (Codogno and Meijer, 2010; Czaja, 2010). In parallel, obesity markedly induced the calcium-dependent protease calpain 2 which presumably resulted in the degradation of autophagy proteins and subsequent inhibition of the autophagic pathway (Yang et al., 2010). Obesity-induced defective hepatic autophagy contributes to elevated ER stress and possibly to insulin resistance in the liver. In fact, restoration of autophagy by Atg7 overexpression reduced ER stress and improved hepatic insulin sensitivity (Yang et al., 2010). Hepatic autophagy has also been shown to regulate intracellular lipid metabolism by lipophagy (Singh et al., 2009a). While a moderate increase in lipid supply induces lipophagy to provide FFAs for ATP production, sustained availability of lipids such as in ob/ob or high-fat fed mice, inhibits hepatic autophagic turnover (Codogno and Meijer, 2010; Yang et al., 2010).

In the heart, the regulation of autophagy in obesity is one of the least understood processes in insulin sensitive tissues. While some studies suggest that autophagy in the heart is upregulated in obesity, there are conflicting data indicating that cardiac

autophagy is suppressed in obesity resulting in obesity-related cardiac dysfunction. For instance, in two different mouse models of T2DM, namely db/db and recombinant congenic strain (RCS)-10, markers of autophagy such as LC3-II, Beclin1, and Atg5-12 conjugate were significantly upregulated. Notably, the RSC10 mice exhibited increased left ventricular (LV) mass while fractional shortening and LV end systolic (ESD) and end diastolic (EDD) diameters largely remained unchanged. Conversely, db/db mice exhibited both diastolic and systolic dysfunction in the absence of cardiac hypertrophy (Wellnitz, 2009). These results suggest that autophagy is activated in the diabetic heart irrespective of the functional status of the myocardium. Similarly, a recent study on a mouse model of DIO showed that 20 weeks of HFF significantly increased cardiac autophagy as measured by an increase in LC3-II and p62 levels (Xu et al., 2012). Surprisingly, the AKT-mTORC1 signaling which is known to suppress autophagy is also activated upon HFF. Although the increase in autophagy was suggested to be due to AKT2-mediated suppression of lysosomal biogenesis, how AKT2 impairs lysosomal biogenesis is not entirely clear. Importantly, the role of activated AKT-mTORC1 signaling was not investigated. Functionally, HFF resulted in cardiac dysfunction manifested by increased LV mass, increased LV-ESD and LV-EDD, and decreased fractional shortening. The study concluded the inhibition of autophagy upon HFF as maladaptive since the restoration of autophagic turnover by AKT2 ablation partially preserved the cardiac function in HFF mice. However, the study did not address if the improvement in cardiac function is solely due to autophagy or due to other AKT2 isoform specific functions.

The studies which contradict the idea of induced cardiac autophagy in obesity are based on the notion that under nutrient rich conditions such as obesity, the AKT-mTOR signaling is activated which in turn suppresses autophagy. Recently, the mTOR signaling and autophagy was examined in Ossabaw pigs with metabolic syndrome (MetS), characterized by obesity, dyslipidemia and insulin resistance. In MetS pig hearts, the mTOR signaling was markedly activated while autophagy was significantly regressed as assessed by lower Beclin1, Ulk1 and LC3-II levels (Li et al., 2012). Similarly, cardiac autophagy was inhibited in type I diabetic (T1DM) mouse model. The hearts from T1DM mice, induced by streptozotocin (STZ) injection or β-cell calmodulin overexpression (OVE26), showed significant reduction in autophagy evidenced by reduced LC3II level (Xie et al., 2011a; Xie et al., 2011b). Restoration of autophagy by chronic activation of AMPK with metformin prevented diabetic cardiomyopathy in T1DM mice. These data suggest a beneficial effect of metformin in preventing the onset and development of diabetic cardiomyopathy via activation of AMPK and subsequently of autophagy. However, the involvement of mechanisms independent of autophagy in the beneficial effect of metformin cannot be ruled out in these studies.

The available data on the regulation of cardiac autophagy in obesity provide an unclear picture of how the rate of autophagic turnover is affected in the obese heart and if the altered autophagy is beneficial or detrimental to heart function. Moreover, most of the studies based their conclusion on the static observation of molecular markers of a very dynamic process of autophagy, which could explain the inconsistency in the available data. A dynamic observation of the regulation of autophagy is crucial to understand the precise role of cardiac autophagy in obesity. In fact, studies have shown that the

autophagic process is highly dynamic based on the duration and severity of the stimulus with different functional consequences (Menon et al., 2011; Papackova et al., 2012; Patschan et al., 2008). Therefore, further studies are needed to reconcile the conflicting findings on the regulation and functional significance of cardiac autophagy in obesity and associated pathologies.

1.6. Summary and rationale

Basal autophagy functions primarily as a quality control process by constantly removing damaged proteins and organelles. Under low nutrient conditions, the process acts as a life support by providing substrates essential for energy production and maintenance of vital cellular functions. Studies showed that autophagic activity must be maintained within a narrow range to have a beneficial effect. Both diminished and excessive autophagy can cause cell death. Likewise, defective autophagic turnover at the level of lysosomes is detrimental to cell survival. The heart is a metabolically demanding organ that requires a constant supply of energy to maintain its contractility. With no apparent regenerative capacity, CMs rely heavily on quality control mechanisms such as autophagy to maintain their healthy status. Autophagy plays a role in most of the cardiac pathologies namely I/R injury, hypertension and heart failure, presumably as an attempt to rescue CMs from injury. However, the role of autophagy in cardiac metabolism is largely underappreciated. The detrimental effect of nutrient excess in the heart is well documented in obesity-related pathologies. Yet, there is no comprehensive study on what role autophagy plays in the cardiac adaptations to obesity. Furthermore, it is unclear whether altered cardiac autophagy in obesity is an adaptive or maladaptive response of the heart. Clearly, more

studies are required to understand the precise mechanism and role of cardiac autophagy in obesity. Such studies may identify molecular mediators that could be potential therapeutic targets to attenuate the pathological outcomes of obesity related cardiac diseases.

The objective of this study is to understand the mechanisms that regulate autophagy in response to lipid overload both in vivo in a mouse model of DIO and in vitro in cultured embryonic CMs. The autophagic flux–defined as the rate of progression of autophagy–can vary temporally based on the severity and duration of a stress. Current data on the regulation of autophagy in obesity have been based on static observations of autophagy at single time points. Higher autophagosome abundance may result from either increased formation of autophagosomes or their decreased turnover or both, and static observations fail to account for such changes (Figure 1.5). In this study, we will monitor autophagy flux both in vivo and in vitro by using pharmacological inhibitors of the degradation steps of autophagy. Furthermore, this study examines the regulation of autophagy in the murine heart in response to short-term HFF and in cultured CMs following acute lipid overload. Such acute treatments allow us understand the mechanism of initial autophagic response in the absence of such cytotoxic response as apoptosis and necrosis, which normally occurs following more protracted lipotoxic stimuli. Finally, lysosomal activity is an essential component of autophagic flux. However, lysosomal functions have been relatively understudied in obesity and associated diseases. Therefore, this study also evaluates lysosomal function in vitro in response to fatty acid treatment to better understand the role of lysosomal activity in the regulation of autophagy.

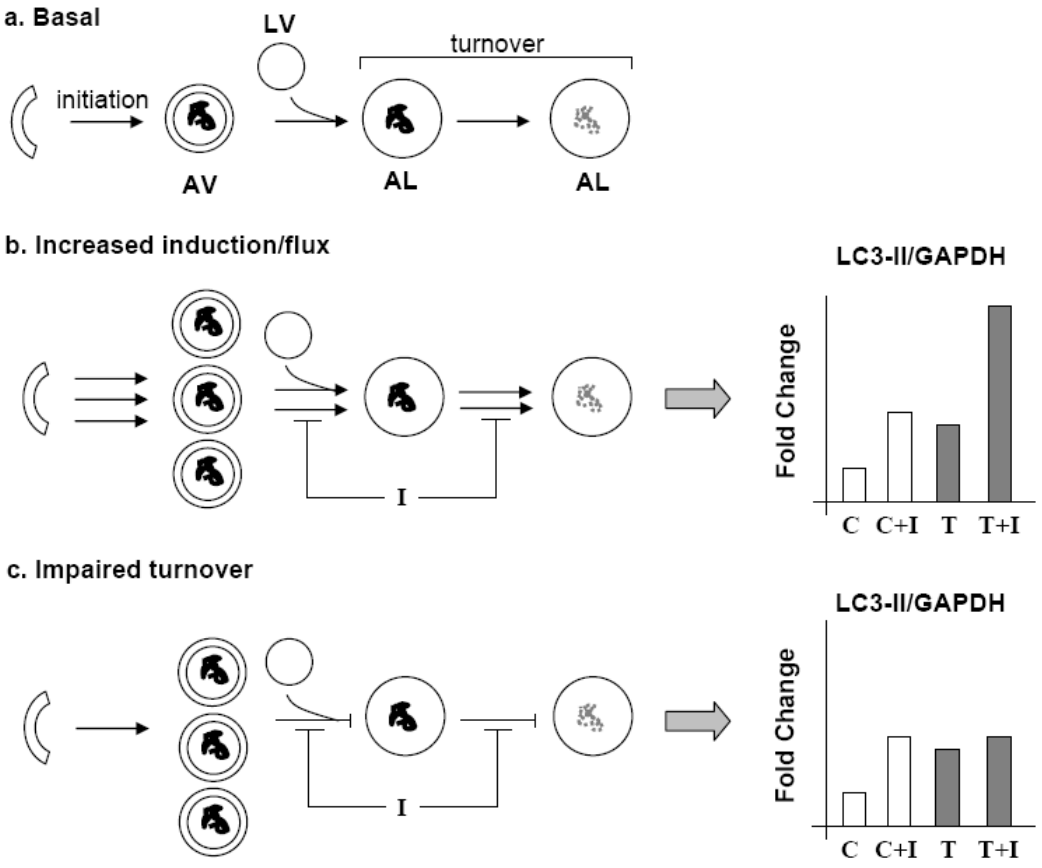

Figure 1.5. Measurement of autophagic flux. (a) At a basal steady-state level [C], autophagosomes (AVs) are constantly formed and turned over in autolysosomes (ALs) upon fusion with lysosomes (LVs). AV abundance increases due to either increased flux or reduced turnover. (b) If a treatment [T] stimulates autophagic initiation, the rate of AV formation is increased. The inhibition [I] of turnover leads to a proportionally higher accumulation of AVs in treated samples [T+I] than in control [C+I], i.e., [T+I]/[T] > [C+I]/[C]. (c) If a treatment inhibits AV turnover, the additional inhibition of AV turnover [T+I] results in either no additional or less than a proportional increase in AV accumulation compared to control, i.e., [T+I]/[T] < [C+I]/[C].

Together, this is the first study which specifically investigates the mechanism(s) by which the initial autophagic response is altered in the presence of lipid overload both in vivo and in vitro. The outcome of this study will provide novel understanding of the regulation of autophagy flux including an evaluation of the role of lysosomal activity and expands our knowledge of potential mechanisms for autophagic alterations in obesity, diabetes and cardiovascular diseases.

CHAPTER 2

HIGH-FAT FEEDING INCREASES AUTOPHAGOSOMAL ABUNDANCE IN THE MOUSE HEART BY IMPAIRING AUTOPHAGOSOME TURNOVER

2.1. Introduction

Elevated levels of FFA in obesity are believed to be one of the major contributing factors in the pathogenesis of T2DM and CVD. Studies from our lab have shown that mice fed with a high-fat, high-sucrose diet (HFD) for 10 weeks became hyperinsulinemic and glucose intolerant (Wright et al., 2009). The insulin signaling through AKT remained intact in high-fat fed mouse hearts. However, glucose utilization was significantly altered in the heart as early as 2 weeks of HFF leading to reduced glycolysis and glucose oxidation with a concomitant increase in FAO. Notably, these changes in cardiac substrate utilization occurred in the absence of any obesity phenotype or cardiac dysfunction. Chronic HFF leads to obesity phenotype in mice with the development of cardiac insulin resistance, cardiac hypertrophy, contractile dysfunction, and impaired intracellular Ca^{2+} handling and mitochondrial function (Dong et al., 2007; Turdi et al., 2011). However, the pathogenesis of cardiac hypertrophy and cardiac dysfunction and the factors involved in transition to impaired myocardial function following HFF still remain elusive.

Autophagy is highly regulated in various tissues such as liver, adipocytes, skeletal muscles, and pancreatic β-cells, and plays an important role in preserving their normal function and architecture in the face of nutrient excess (Ebato et al., 2008; Sandri, 2010; Singh et al., 2009b; Yang et al., 2010). Although autophagy is regulated in various cardiac pathologies, its role in cardiac metabolism and function in the setting of obesity is unclear (Xu and Ren, 2012). While some data suggest an increase in cardiac autophagy following HFF, others suggest a decrease or no change (He et al., 2012; Xu et al., 2012). These studies did not assess autophagic flux or lysosomal function. Therefore, it is

difficult to interpret which step in autophagy was affected by HFF. Preliminary studies from our lab have shown that in the left ventricles of insulin resistant pigs and in the left atrial appendages of diabetic and nondiabetic human subjects, autophagy was markedly increased (Zhang, Q.J.; unpublished data). The characteristics of the pig model and human subjects used in these studies have been published (Anderson et al., 2009; Edwards et al., 2010). Surprisingly, AKT phosphorylation was significantly increased despite an increase in autophagy. Moreover, the increase in autophagosomes was independent of changes in mTOR and AMPK signaling.

Based on available data, we hypothesize that lipid overload by HFF in mice increases autophagosome abundance in the heart primarily by suppressing autophagosome degradation and not by increasing autophagic flux. To test this hypothesis, we placed wild type mice on a HFD regimen and examine upstream signals of autophagy, core autophagic proteins, and lysosomal proteins. We also pharmacologically inhibited autophagosomal-lysosomal fusion to identify the step(s) in the autophagic pathway are altered in response to HFF.

2.2. Methods

2.2.1. Animals

The study was approved by the Institute of Animal Care and Use Committee of the University of Utah. Control (WT) and transgenic mice expressing mCherry-LC3 in CMs (αMHC-mCherryLC3 or MCLC3) on C57BL/6 background were housed in our animal facility at 22 ^{o}C and on a 12-h light/dark cycle (6AM, light on) with free access to water

and a normal-chow (NCD, 13% kcal fat, 53% kcal carbohydrate, and 34% kcal protein, Teklad 8656, Madison, WI).

2.2.2. High-fat diet regimen

Eight-week old male WT or MCLC3 mice were fed with either a HFD (45% kcal fat, 35% kcal carbohydrate, and 20% kcal protein, Research Diets Inc. D12451, New Brunswick, NJ) or the NCD (Teklad 8656) for 12 weeks. The gain in body weight was calculated as the difference in body weight measured before placing the animals on a diet regimen and at the time of harvest. For all studies, mice were fasted for 6 h (from 6 AM to 12 PM) and blood glucose levels were measured by a standard glucometer (Bayer, IN) before sacrifice.

2.2.3. Measurement of hormones and metabolites in the heart and serum

The heart was excised from anaesthetized mice and kept frozen in -80 ^{o}C until use. To measure TG content in the heart, 50 mg of tissue was homogenized in 1 ml of chloroform/methanol in TissueLyser II (Qiagen, Valencia, CA). The TGs were extracted by rocking the samples at room temperature for 3 h. Eight hundred µl of H_2SO_4 was added to each sample and centrifuged at 218xg for 10 min. Fifty µl of organic (bottom) layer was dried in a speedvac for 15 min. Three hundred µl of triglyceride assay buffer (Sigma-Aldrich, St. Louis, MO) was added to each sample and incubated at 37 ^{o}C for 15 min with occasional mixing. Samples were loaded in 250 µl onto a 96-well plate and absorbance was measured at 562 nm. Glycerol standard was used to generate the standard curve (Sigma-Aldrich, St. Louis, MO).

Blood was collected from the submendibular vein of the mouse in a microfuge tube containing a small piece of Teflon. The serum was removed from the clotted blood by centrifugation and preserved in -80 ºC until use. Circulating levels of insulin, glucagon and leptin were measured using the MEGPIX™ (Luminex, Austin, TX), a multiplex enzyme-linked immunosorbent assay (ELISA), using a specific antibody-coated magnetic microsphere kit (Milliplex Map Kit; Millipore, Billerica, MA). Circulating levels of FFAs and TGs were measured in serum samples using kits from Wako Diagnostics (Richmond, VA).

2.2.4. Metabolomics analysis of the heart and serum

Hearts from NCD- or HFD- fed mice (heretofore NCD or HFD mice) were flash-frozen in liquid nitrogen. Metabolomics analysis was performed by using gas chromatography-mass spectrometry (GC-MS) at the University of Utah Metabolomics Core Facility. The identity of the metabolites was verified by comparing with GC-MS profiles of known metabolites in the library. The amount of a metabolite in a sample was reported as the area under the peak for the corresponding metabolite in the chromatogram and was normalized to the starting tissue weight.

Serum samples were prepared as described in section 2.2.3. GC-MS analysis was performed as above for heart samples, and the metabolite content in each sample was normalized to the serum volume (40 µl).

2.2.5. Histology and stereology

The apical half of the heart was fixed in 10% zinc formalin (Thermo Fisher Scientific, Waltham, MA) for 1 h, embedded in paraplast, and sliced into 5 µM transverse sections (T.S). The T.S. was stained with hematoxylin-eosin and Masson's trichrome stains. Images were acquired with an Olympus LX81 inverted light microscope equipped with an Olympus Microfire Digital Camera (New York, NY), and volume density was measured for CMs and interstitial fibrotic tissue as described (Mandarim-de-Lacerda, 2003).

2.2.6. Cryosectioning and fluorescence microscopy

The apical half of the heart from MCLC3 mice fed with NCD or HFD were embedded in Optimal Cutting Temperature (OCT) compound (Sakura Finetek, Torrence, CA) on dry ice for 25 min and sliced in 5 µM T.S. on a cryostat (Leica, Buffalo Grove, IL) at -20 ^{o}C. Tissue fixation/staining and confocal imaging were performed essentially as described previously (Perry et al., 2009). Briefly, the T.S. was fixed in 4% paraformaldehyde for 15 min, stained with Hoechst 33342 for 30 min, and mounted with ProLong Gold antifade reagent (Invitrogen, Grand Island, NY) for 2 h in the dark. Fluorescent images were taken using an Olympus IX81 FV1000 confocal microscope equipped with x40 dry objective (NA 0.80) and 488 nM (for Hoechst 33342) and 633 nM (for mCherry) lasers. The images representing different Z-sections were merged using ImageJ software (NIH, Bethesda, MD) to obtain a representative image.

2.2.7. Insulin stimulation of the heart

Mice were anaesthetized by intraperitoneal (ip) injections of chloral hydrate (0.7 mg/g body weight) before harvesting the tissues or prior to insulin injections. Anaesthetized mice were injected with 0.01 unit of human regular insulin (Novolin R) or an equal volume of saline via the inferior vena cava (ivc) as described previously (Kim et al., 2008). Five minutes following insulin injection, the heart was removed and kept frozen until further analysis.

2.2.8. Activation of mTOR and inhibition of autophagic turnover

For mTOR activation, mice were injected ip with a branch-chain amino acid (BCAA) solution (46 mM isoleucine, 91 mM, leucine, 61 mM, and 35 mM arginine, pH 7.4) at a daily of dose of 100 µl/g body weight for 2 weeks prior to harvest.

For the inhibition of autophagic turnover, mice were injected ip with three doses of the autophagosome-lysosome fusion inhibitor chloroquine (CQ) at 48 h (30 mg/kg body weight), 24 h (30 mg/kg), and 2 h (50 mg/kg) prior to harvest. Control animals were injected with an equal volume of saline.

2.2.9. RNA isolation and quantitative RT-PCR

Total RNA was extracted from hearts with TRIzol reagent (Invitrogen, Carlsbad, CA) and purified using RNAeasy kit (Qiagen, Valencia, CA). Total mRNA was reverse transcribed and individual gene expression was determined indirectly by quantitative real-time polymerase chain reaction (qRT-PCR) using an ABI Prism 7900 HT instrument (Applied Biosystems, Foster City, CA) as described previously (Riehle et al., 2011).

Each reaction was performed in triplicate in a 384-well plate using SYBR Green I chemistry and ROX internal reference dye (Invitrogen, Carlsbad, CA). Data were normalized to Cyclophilin mRNA level. The sequence of primers used was described previously (Liu et al., 2009).

2.2.10. Immunoblotting

Total proteins were extracted by homogenizing frozen tissues in a lysis buffer containing 50 mM HEPES (pH 7.5), 150 mM NaCl, 10% Glycerol, 1% Triton X-100, 1.5 mM $MgCl_2$, 1 mM EGTA, 10 mM $Na_4P_2O_7$, 100 mM NaF, and 1X Halt protease and phosphatase inhibitor cocktail (Thermo Scientific), and analyzed by western blotting as previously described (Riehle et al., 2011). Antibodies against LC3 (Sigma, St. Louis, MO); Beclin1, GAPDH, phospho and total mTOR, AKT, AMPK and S6 (Cell Signaling, Danvers, MA); phospho FOXO1/3 and Ulk1 (Cell Signaling); total FOXO, total Ulk1, and Cathepsin D (Santa Cruz, Santa Cruz, CA) were used for immunodetection. IRDye 800CW anti-Mouse (LICOR, Lincoln, NE) and Alexa Fluor anti-Rabbit (Invitrogen, Carlsbad, CA) were used as secondary antibodies. Fluorescence intensity of a protein band was detected and quantified by using the LICOR Odyssey Imager.

2.2.11. Statistical analysis

All data are presented as mean ± SEM. Unpaired Student's t-test was performed to determine p-values when comparing between two groups. 1-way Analysis of variance (ANOVA) was used to compare data across multiple groups with one independent variable. Multiple groups with two or more independent variables were analyzed by 2-

way ANOVA. Statistical significance was determined by Bonferroni's post-hoc analysis using the GraphPad Prism 5 software (La Jolla, CA). For all analyses, $p<0.05$ was considered statistically significant.

2.3. Results

2.3.1. Body weight and systemic metabolic variables

Mice on HFD for 12 weeks gained about 15 g of body weight compared to 5 g in NCD-fed littermate controls (Table 2.1). The fasting blood glucose levels were significantly increased in HFD mice compared to NCD mice. However, the fasting blood glucose levels in HFD mice (188.6 mg/dL) were below the diabetic level (>300 mg/dL) (von Herrath et al., 1995). The HFD mice had a significant rise in serum insulin and leptin levels compared NCD controls. In addition, circulating levels of FFAs and TGs were significantly elevated in HFD mice compared to NCD controls. Although, body composition (fat mass and lean mass) was not measured in this study, mice on HFD showed marked accumulation of both visceral and subcutaneous adipose tissue. Supporting this observation, a previous study from our group have shown a significant increase in both gonadal fat pad mass and total fat mass in mice following 14 weeks of HFF compared NCD controls (Tanner et al., 2010). Taken together, 12 weeks of HFF manifested the basic hallmarks of diet induced obesity and the metabolic syndrome.

2.3.2. Cardiac phenotype in HFD and NCD fed mice

Consistent with a gain in body weight, 12 weeks of HFF led to an increase in heart weight (~8.8%) and biventricular weight (~10%) compared to NCD controls (Table 2.2).

Table 2.1. Phenotypic and metabolic characteristics of mice fed HFD or NCD for 12 weeks. *p<0.05 vs. NCD (n=10-12).

Parameters	NCD	HFD
Age	21 ± 0.5	21 ± 0.5
Body weight (g)	28 ± 0.5	39.9 ± 1.1*
Body weight/tibia length (g/mm)	1.6 ± 0.03	2.3 ± 0.57*
Blood glucose (mg/dL)	142.5 ± 8.1	188.6 ± 11.5*
Insulin (pg/ml)	92.82 ± 27.2	641.6 ± 176.4*
Leptin (pg/ml)	363.8 ± 147.3	19441 ± 3782.7*
Serum free fatty acids (mM)	0.33 ± 0.01	0.85 ± 0.04*
Serum triglycerides (mg/dL)	24.47 ± 2.08	34.81 ± 4..67*

Table 2.2. Cardiac parameters of mice fed with HFD or NCD for 12 weeks. *p<0.05 vs. NCD (n=10-12).

Parameters	NCD	HFD
Heart weight (mg)	130.0 ± 2.2	142.5 ± 3.3*
Heart weight/tibia length (mg/mm)	7.5 ± 0.2	8.1 ± 2.0*
Biventricular weight/tibia length (mg/mm)	7.1 ± 0.12	7.8 ± 1.9*
Heart triglycerides (μg/mg Tissue)	0.20 ± 8.1	0.31 ± 0.04*

The increase in heart weight is usually accompanied by CM hypertrophy or increased fibrosis in the heart. CM size, examined by H&E staining, was similar in high-fat fed and normal-chow fed animals (Figure 2.1). Moreover, Masson's trichrome staining of the T.S. of the heart showed no fibrosis in HFD mice. The histology data suggest that mice on HFD had normal cardiac growth. However, the HFF significantly increased TG content (~1.6 fold) in the heart (Table 2.2). The ectopic deposition of fat in TG might contribute to an increase in the heart and biventricular weight.

2.3.3. Profiles of circulating metabolites from NCD and HFD fed mice

To identify the obesity-related changes in the levels of circulating small metabolites, serum samples from 13-week NCD or HFD mice were analyzed by GS-MS analysis (Table 2.3). The initial goal of this analysis was to determine the changes in the circulating levels of amino acids. However, a generic extraction and analysis protocol allowed us to analyze several other metabolites including FFAs, carbohydrates, TCA cycle and glycolytic intermediates. Most surprisingly, the level of serum glucose was significantly low in HFD animals. Although most of the TCA cycle and glycolytic intermediates tended to be reduced the in HFD groups, no significant difference was observed compared to NCD controls. Notably, the circulating levels of most of the common nonesterified free fatty acids including palmitic acid and linoleic acid were significantly reduced in the HFD group which is in contrast with well-known observation of high circulating levels of glucose and free fatty acids in obesity and T2DM. Since the GC-MS experimental protocol was optimized for amino acid analysis, such optimization

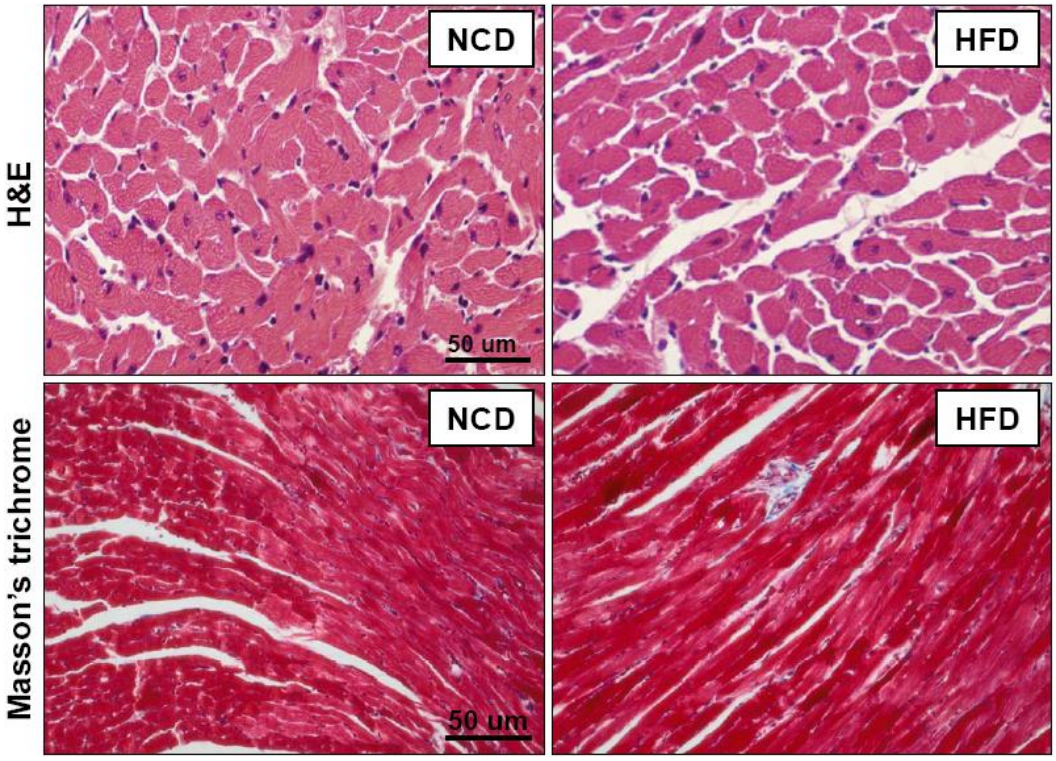

Figure 2.1. No cardiac hypertrophy and fibrosis in mice following 12 weeks of high-fat feeding. Mice fed with HFD or NCD for 12 weeks were examined for CM size by H&E staining (upper panel). The presence of fibrotic tissue in the heart was assessed by Masson's trichrome staining (lower panel). The fibrotic tissues stain blue on Masson's trichrome staining. Scale= 50 µm.

Table 2.3. Levels of circulating metabolites in the serum from NCD or HFD mice.

Glycolysis and TCA Cycle				
Metabolite	**NCD**	**HFD**	**HFD-fold change**	**p-value**
lactic acid	777.2	769.3	1.0	0.881
pyruvic acid	585.9	519.4	0.9	0.682
glycerol	8.8	4.3	0.5	0.039
glyceric acid	59.8	42.1	0.7	0.252
citric acid	574.3	584.3	1.0	0.869
aconitic acid	17.9	16.0	0.9	0.423
isocitric acid	67.7	34.6	0.5	0.135
2-ketoglutaric acid	52.1	63.2	1.2	0.244
succinic acid	118.6	64.1	0.5	0.311
fumaric acid	131.4	93.6	0.7	0.164
malic acid	221.7	164.1	0.7	0.191
2-hydroxyglutarate	14.4	16.5	1.1	0.365
DHAP	8.89	1.70	0.2	0.117
galactose or isomer	2785.82	2379.16	0.9	0.217
glucose	23092.73	16993.45	0.7	0.021
glucose-1-phosphate	5.81	3.58	0.6	0.120
glucose-6-phosphate	59.25	35.52	0.6	0.080
Amino Acids				
2-aminoadipic acid	23.9	27.8	1.2	0.286
lysine	93.7	182.9	2.0	0.045
valine	658.7	490.3	0.7	0.028
leucine	2013.1	1383.5	0.7	0.008
isoleucine	1379.4	922.0	0.7	0.001
threonine	250.9	265.0	1.1	0.642
glycine	125.4	91.4	0.7	0.014
serine	76.4	76.7	1.0	0.978
alanine	227.7	233.7	1.0	0.821
glutamic acid	25.2	15.6	0.6	0.075
glutamine	1128.4	1111.5	1.0	0.910
proline	649.8	669.5	1.0	0.808
aspartic acid	120.0	74.1	0.6	0.011
asparagine	16.0	13.6	0.8	0.140
methionine	251.0	224.0	0.9	0.393
cysteine	18.7	27.6	1.5	0.142
homocysteine	0.9	0.7	0.8	0.337
phenylalanine	271.5	238.8	0.9	0.197
tyrosine	55.3	44.1	0.8	0.186

Table 2.3. (continued)

Amino Acids				
Metabolite	**NCD**	**HFD**	**HFD-fold change**	**p-value**
tryptophan	706.6	964.7	1.4	0.094
histidineND	4.6	7.7	1.7	0.049
ornithine	15.2	19.9	1.3	0.066
Triglyceride and Cholesterol				
phosphate	7829.8	5758.2	0.7	0.088
diphosphate	631.9	885.2	1.4	0.031
phosphoglycerol	260.6	255.5	1.0	0.935
3-phosphoglycerate	9.6	2.7	0.3	0.058
1-monooleoylglycerol	43.6	40.3	0.9	0.582
1-monostearylglycerol	154.9	187.0	1.2	0.199
1-monopalmitoylglycerol	260.9	207.9	0.8	0.090
1-monopalmitolylglycerol	2.7	1.3	0.5	0.001
cholesterol	1107.1	1054.6	1.0	0.710
Carbohydrate				
fructose	660.7	690.9	1.0	0.869
ribose	45.6	23.0	0.5	0.003
sorbitol	27.8	21.7	0.8	0.662
galacitol	70.7	73.4	1.0	0.829
inositol	3117.2	1378.9	0.4	0.0001
myo-inositol phosphate	136.3	159.5	1.2	0.414
disaccharide	192.6	98.1	0.5	0.176
Fatty Acids (nonesterified)				
lauric acid	54.0	48.9	0.9	0.359
myristic acid	149.1	137.1	0.9	0.542
palmitiladic acid	151.9	108.3	0.7	0.246
palmitic acid	3127.2	3211.5	1.0	0.842
linoleic acid	500.4	508.5	1.0	0.917
oleic acid	649.1	1114.5	1.7	0.014
elaidic acid	45.5	60.8	1.3	0.074
stearic acid	1738.9	2131.8	1.2	0.039
arachidonic acid	27.8	28.4	1.0	0.911

Table 2.3. (continued)

Purine, Pyrimidine Metabolism and Other Metabolites				
Metabolite	**NCD**	**HFD**	**HFD-fold change**	**p-value**
xanthine	112.7	28.6	0.3	0.018
adenosine	2.2	2.8	1.3	0.506
adenine	2.4	2.0	0.8	0.423
uracil	55.1	40.0	0.7	0.374
phosphoenolpyruvate	9.9	1.0	0.1	0.136
3-indoleacetic acid	5.0	5.1	1.0	0.891
inosine	23.1	14.0	0.6	0.117
rhamnose	0.5	0.3	0.6	0.048
tyramine	1.4	1.1	0.8	0.316
tartaric acid	0.3	18.4	55.0	0.153

could affect other analyses. Therefore, the levels of other metabolites in this study may not reflect their true levels in the serum. The GC-MS results contradict our own finding of increased fatty acid and triglycerides levels in the serum HFD animals (Table 2.1). Nevertheless, the GC-MS data clearly showed that circulating levels BCAAs such as valine (0.7 fold, p=0.043), isoleucine (0.6 fold, p=0.011), and leucine (0.3 fold, p=0.099) were significantly or near significantly low in HFD mice compared to NCD controls.

2.3.4. Metabolomics profile of the heart from NCD and HFD mice

Obesity has been known to increase fatty acid flux into the heart, which could alter various metabolic pathways. A previous study from our lab has shown that 5 weeks of HFF suppressed glycolysis, glucose oxidation rate, expression and membrane translocation of Glut4, and impaired insulin stimulated glucose uptake (Wright et al., 2009). Accordingly, in the present study, the analysis of small metabolites and pathway intermediates by GC-MS showed that 12 weeks of HFD markedly reduced the abundance of key glycolytic intermediates in the heart (Table 2.4). For example, glucose-6-phosphate was reduced by 80% and glucose-1-phosphate by 70% in HFD hearts compared to NCD controls. Interestingly, lactate and pyruvate levels were not changed between the two groups. Furthermore, free glucose levels in the heart was similar in both groups. In contrast to glycolytic intermediates, the levels of most TCA cycle intermediates remained fairly unchanged. The most notable changes observed between the two groups were in the level of amino acids. Most importantly and consistent with serum metabolomics data, the levels of BCAAs were significantly reduced in HFD hearts

Table 2.4. Levels of small molecule metabolites in the heart from NCD or HFD mice.

TCA Cycle				
Metabolite	**NCD**	**HFD**	**HFD-fold change**	**p-value**
citrate	22394.2	25006.4	1.1	0.576
aconitate	47.9	51.0	1.1	0.791
isocitrate	316.1	295.3	0.9	0.793
2-ketoglutarate	145.6	166.4	1.1	0.865
succinate	1774.6	881.8	0.5	0.213
fumarate	1217.6	821.2	0.7	0.293
malate	1736.0	1602.7	0.9	0.798
2-hydroxyglutarate	78.7	66.8	0.8	0.244
Glycolysis				
glucose-6-phosphate	627.2	95.8	0.2	0.142
glucose-1-phosphate	148.8	40.3	0.3	0.155
DHAP (Di-OH-acetone-P)	8.0	5.7	0.7	0.344
3-phosphoglycerate	179.0	81.6	0.5	0.145
2-phosphoglycerate	19.1	10.2	0.5	0.102
lactate	1324.5	1146.1	0.9	0.334
pyruvate	372.6	320.0	0.9	0.775
Amino Acids				
alanine	1480.9	1883.4	1.3	0.212
glycine	1736.9	1067.5	0.6	0.081
serine	7575.8	9526.0	1.3	0.250
lysine	97.3	65.9	0.7	0.352
valine	4385.8	2927.1	0.7	0.043
leucine	1615.2	561.2	0.3	0.099
isoleucine	1722.6	976.2	0.6	0.011
threonine	2800.2	2803.6	1.0	0.993
glutamate	11672.1	8418.7	0.7	0.011
glutamine	4544.9	2449.5	0.5	0.128
proline	227.8	179.6	0.8	0.289
2-hydroxyyproline	4.6	2.6	0.6	0.138
aspartate	5407.4	6138.3	1.1	0.596
methionine	763.8	707.2	0.9	0.742
phenylalanine	2026.6	954.7	0.5	0.025
tryptophan	9.2	0.6	0.1	0.195
tyrosine	31.9	31.5	1.0	0.956
ornithine	19.0	8.2	0.4	0.036

Table 2.4. (continued)

Fatty Acids (nonesterified)				
Metabolite	**NCD**	**HFD**	**HFD-fold change**	**p-value**
phosphoethanolamine	1096.7	681.0	0.6	0.016
decanoic acid	44.8	26.0	0.6	0.048
lauric acid	92.5	60.8	0.7	0.063
myristic acid	53.4	39.5	0.7	0.028
palmitiladic acid	195.0	64.2	0.3	0.009
palmitate	10610.1	6250.1	0.6	0.045
linoleic acid	988.1	657.6	0.7	0.036
oleic acid	636.1	565.3	0.9	0.493
elaidic acid	106.7	99.1	0.9	0.789
stearate	6492.4	4800.5	0.7	0.165
arachidonic acid	24.1	9.1	0.4	0.313
arachidic acid	53.0	34.3	0.6	0.021
pantothenoic acid	496.0	321.5	0.6	0.031
Cabohydrates				
glucose	26897.0	23031.1	0.9	0.337
fructose	59.9	50.9	0.8	0.339
galactose or isomer	5.3	3.5	0.7	0.047
gluconic acid	27.9	12.1	0.4	0.0005
inositol	12634.3	5948.0	0.5	0.001
Cholesterol, Purine-Pyrimidine,and Small Metabolites				
Cholesterol	1802.4	1799.8	1.0	0.996
monostearin	2525.3	1928.9	0.8	0.219
creatinine	1637.0	1428.9	0.9	0.447
adenosine	1134.3	494.3	0.4	0.122
uracil	59.6	38.0	0.6	0.102
cytosine	172.9	135.8	0.8	0.076
urea	14.3	15.6	1.1	0.672

compared to NCD controls: valine (0.7 fold, p=0.043), isoleucine (0.6 fold, p=0.011), and leucine (0.3 fold, p=0.099). The GC-MS analysis of the metabolites did not show any anticipated increase in the level of free fatty acids in the hearts of HFD animals.

2.3.5. Insulin-stimulated AKT signaling was preserved in the hearts of HFD mice

To examine if 12 weeks of HFF alters insulin signaling in the mouse heart, insulin-stimulated AKT phosphorylation was assessed by western blot in the heart of HFD animals injected via IVC with insulin or saline and compared to NCD controls (Figure 2.2). Insulin significantly increased AKT phosphorylation both in NCD and HFD groups relative to respective saline controls as assessed by pAKT-S473/AKT fold change (NCD-saline: 1.0 ± 0.061, NCD-insulin: 27.27 ± 2.157, HFD-saline: 0.82 ± 0.079, and HFD-insulin: 22.59 ± 1.438). However, no significant difference was observed in insulin-stimulated AKT phosphorylation between NCD and HFD groups, meaning that HFF did not alter insulin signaling through AKT in the mouse heart. Furthermore, basal AKT phosphorylaton was also similar between the two groups.

2.3.6. High-fat feeding regulates cardiac autophagy in mice

In the heart, the role of autophagy and its mechanistic regulation following HFF are unclear from previous studies (Xu and Ren, 2012). To understand the mechanism of regulation of cardiac autophagy upon HFF, changes in autophagy markers and pathway specific upstream signaling molecules were examined in the heart of mice fed with NCD or HFD.

(A)

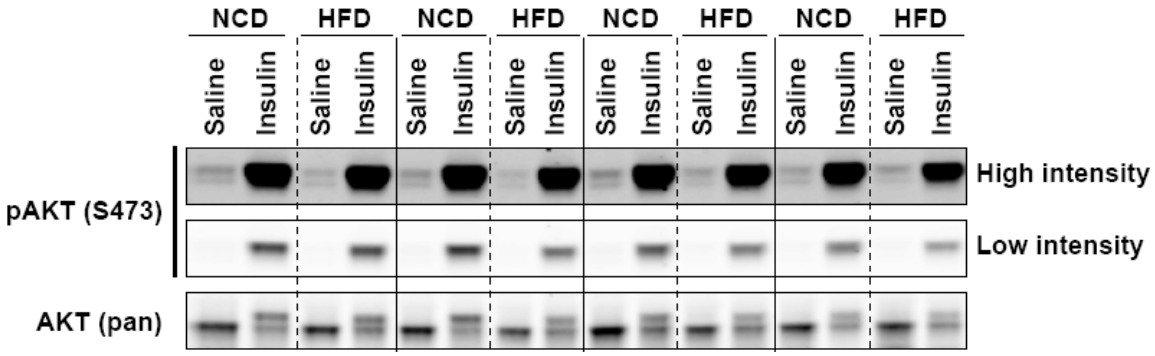

(B)

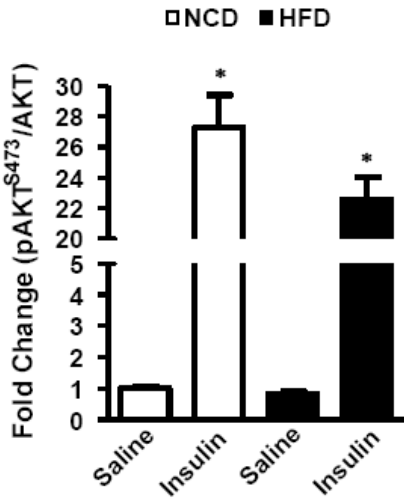

Figure 2.2. Basal and insulin stimulated AKT signaling in the heart are not altered by high-fat feeding. Mice fed with either NCD or HFD for 12 weeks were administered saline or 0.01 U insulin via IVC injection. (A) Insulin signaling through AKT was assessed in the heart by immunoblotting. (B) Graph represents the data quantified from the immunoblot shown in panel (A). *p<0.0001 vs. NCD-saline, n=4-5.

2.3.6.1. High-fat feeding alters autophagy markers in the heart

12 weeks of HFD in mice significantly increased autophagy in the heart compared NCD controls. The western blot showed that LC3-II level, measured by LC3-II/GAPDH fold change, was increased by 40% in HFD hearts compared to NCD hearts (Figure 2.3.A) (NCD: 1.0 ± 0.082, HFD: 1.4 ± 0.025). Consistent with western blot data, HFF increased cardiac autophagosome abundance as evidenced by a 2.5-fold increase in the number of mCherry-LC3-positive puncta in the heart sections of HFD- MCLC3 mice compared to NCD-MCLC3 mice (Figure 2.3.B).

2.3.6.2. High-fat feeding-induced changes in autophagy is independent of canonical autophagy-induction pathways

Insulin signaling through AKT is known to suppress autophagy through mTORC1 activation (Kanazawa et al., 2004). To determine if an increase in autophagy upon HFF is due to an impairment in insulin signaling through AKT, and its downstream targets in autophagy FoxO1 and FoxO3 were assessed by western blotting. The data show that phosphorylation of AKT (at T-308 and S-473) was normal in the heart of HFD mice, suggesting normal AKT kinase activity (Figure 2.4.A). Downstream of AKT, FoxO1 (T24) and FoxO3 (T32) phosphorylation was also intact in HFD hearts. These data suggest that canonical Insulin-AKT-FoxO1 signaling regulating autophagy remains normal in HFD hearts and is unlikely to regulate HFD-induced autophagy. Autophagy is also induced by AMPK in the heart under various conditions including glucose deprivation. Since glucose uptake in the heart was impaired by 10 weeks of HFF in our previous study, we examined if AMPK is activated upon 12 weeks of HFF. However, the

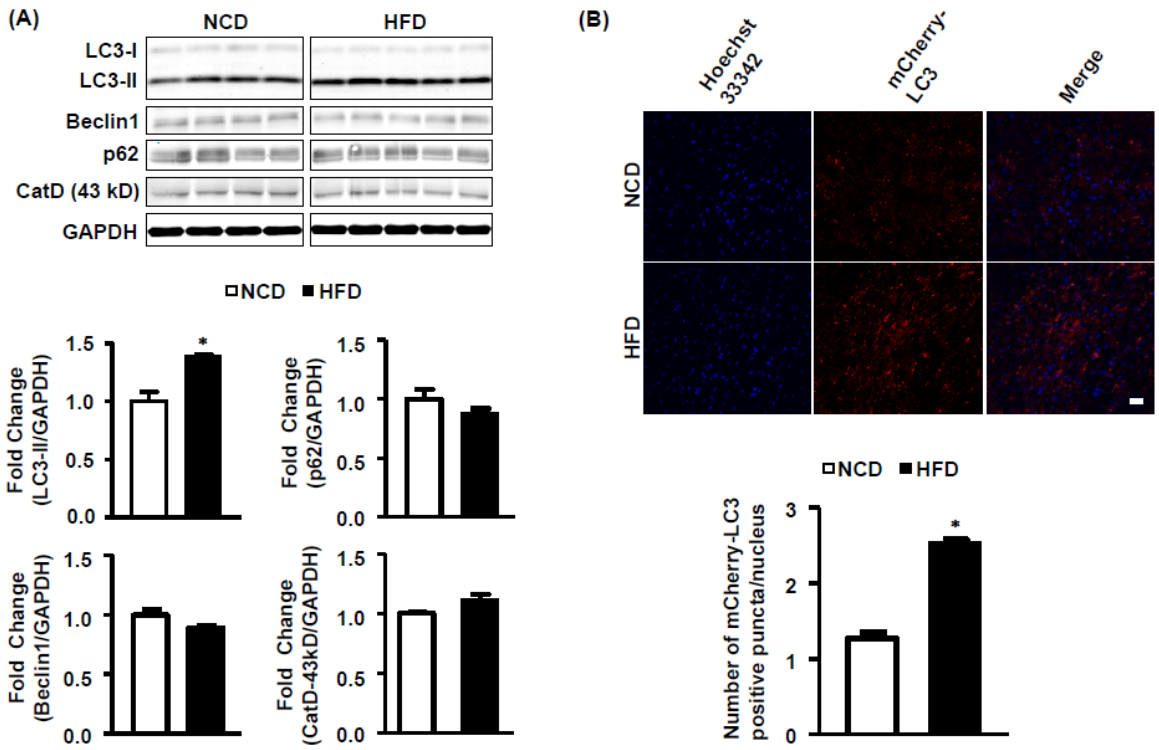

Figure 2.3. Increased autophagic abundance in the heart of HFD mice. (A) Representative western blots of the autophagy proteins LC3-I, LC3-II, Beclin1, and p62, and lysosomal hydrolase Cathepsin D (CatD) from the total heart homogenates of NCD or HFD mice. GAPDH was used as a normalizer. Graphs represent mean ± SEM. *p=0.0042 vs. NCD, n=9-11. (B) Representative confocal microscopic images of transverse sections of the heart from NCD or HFD mice expressing cardiac specific mCherry-LC3. The red puncta represent mCherry-LC3 positive autophagosomes and autolysosomes. The nuclei were counterstained blue with Hoechst 33342. Scale bar is 50 µm. *p<0.0001 vs. NCD, n=5.

Figure 2.4. High-fat diet-induced autophagy is not regulated by canonical autophagy signaling pathways. (A) Representative western blots of key signaling molecules regulating initiation of autophagy. Posttranslational modifications by phosphorylation of proteins regulating autophagic initiation were analyzed in the whole heart homogenate of mice fed with NCD or HFD for 12 weeks (n=7-9). GAPDH was used as a normalizer. (B) The mRNA level of autophagic genes in the heart from NCD and HFD mice (n=4-5). The mRNA level of target genes was normalized with Cyclophilin A mRNA level. See text for details.

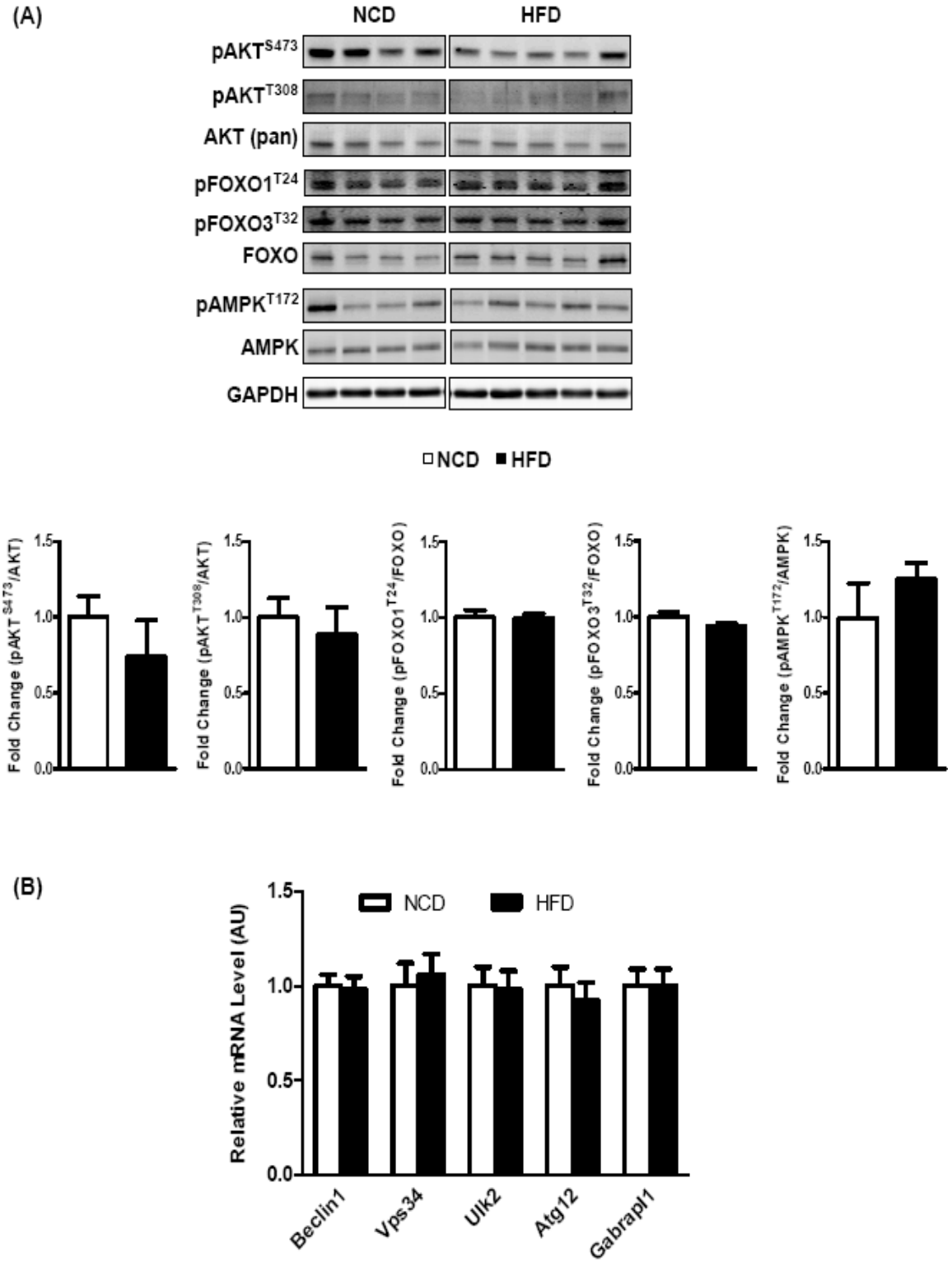
(A)
NCD
HFD
pAKT S473
pAKT T308
AKT (pan)
pFOXO1 T24
pFOXO3 T32
FOXO
pAMPK T172
AMPK
GAPDH
NCD
HFD
Fold Change (pAKT S473/AKT)
Fold Change (pAKT T308/AKT)
Fold Change (pFOXO1 T24/FOXO)
Fold Change (pFOXO3 T32/FOXO)
Fold Change (pAMPK T172/AMPK)
1.5
1.0
0.5
0.0
(B)
NCD
HFD
Relative mRNA Level (AU)
Beclin1
Vps34
Ulk2
Atg12
Gabrapl1

phosphorylation of AMPK in HFD hearts was similar to that in NCD hearts, suggesting an AMPK-independent autophagic regulation by HFF (Figure 2.4.A).

Transcriptional regulation of autophagic genes by FoxO is also known to induce autophagy in the heart (Sengupta et al., 2009). To examine if HFD induced autophagy is regulated at the transcriptional level, mRNA levels of autophagic genes under direct control of FoxO transcriptional activity were examined by qRT-PCR (Figure 2.4.B). The data indicate that the expression level of all the autophagic genes examined remained unchanged in HFD hearts compared NCD hearts. These data suggest that FoxO does not regulate autophagic gene expression in the heart of HFD mice. This is consistent with a lack of change in FoxO1 and FoxO3 phosphorylation as assessed by western blot.

2.3.6.3. High-fat diet-induced autophagy is independent of changes in mTOR signaling

As described earlier, mTORC1 forms a critical node converging multiple upstream signaling to regulate autophagy in response to various stimuli. The mTORC1 activation inhibits autophagy, whereas its suppression enhances the process. The regulation of mTOR signaling was examined in the heart of NCD or HFD animals. Consistent with increased autophagy, phosphorylation of mTOR was repressed in HFD hearts by ~ 34% compared to controls (NCD: 1.0 ± 0.116, HFD: 0.66 ± 0.036) (Figure 2.5.A). The decrease in mTOR phosphorylation was accompanied by the reduced phosphorylation of mTOR targets. The phsophorylation of Ulk1 at S757 was decreased by ~ 40% (NCD: 1.0 ± 0.123, HFD: 0.6 ± 0.059) and of ribosomal protein S6 was reduced by ~ 69% (NCD: 1.0 ± 0.261, HFD: 0.21 ± 0.055) in HFD mice compared to NCD controls.

.

Figure 2.5. Regulation of cardiac autophagy by high-fat feeding is independent of changes in mTOR signaling. (A) Mice fed with either NCD or HFD for 12 weeks were analyzed for mTOR signaling in the heart by western blotting. Representative blots of total and phosphorylated proteins are shown. *$p<0.05$ vs. NCD, n=4-5. (B) Mice fed with NCD or HFD for 12 weeks were injected daily with BCAA solution for the last 2 weeks and analyzed for indicated proteins by western blotting. *$p<0.05$ vs. NCD-PBS, n=4-5. See text for details.

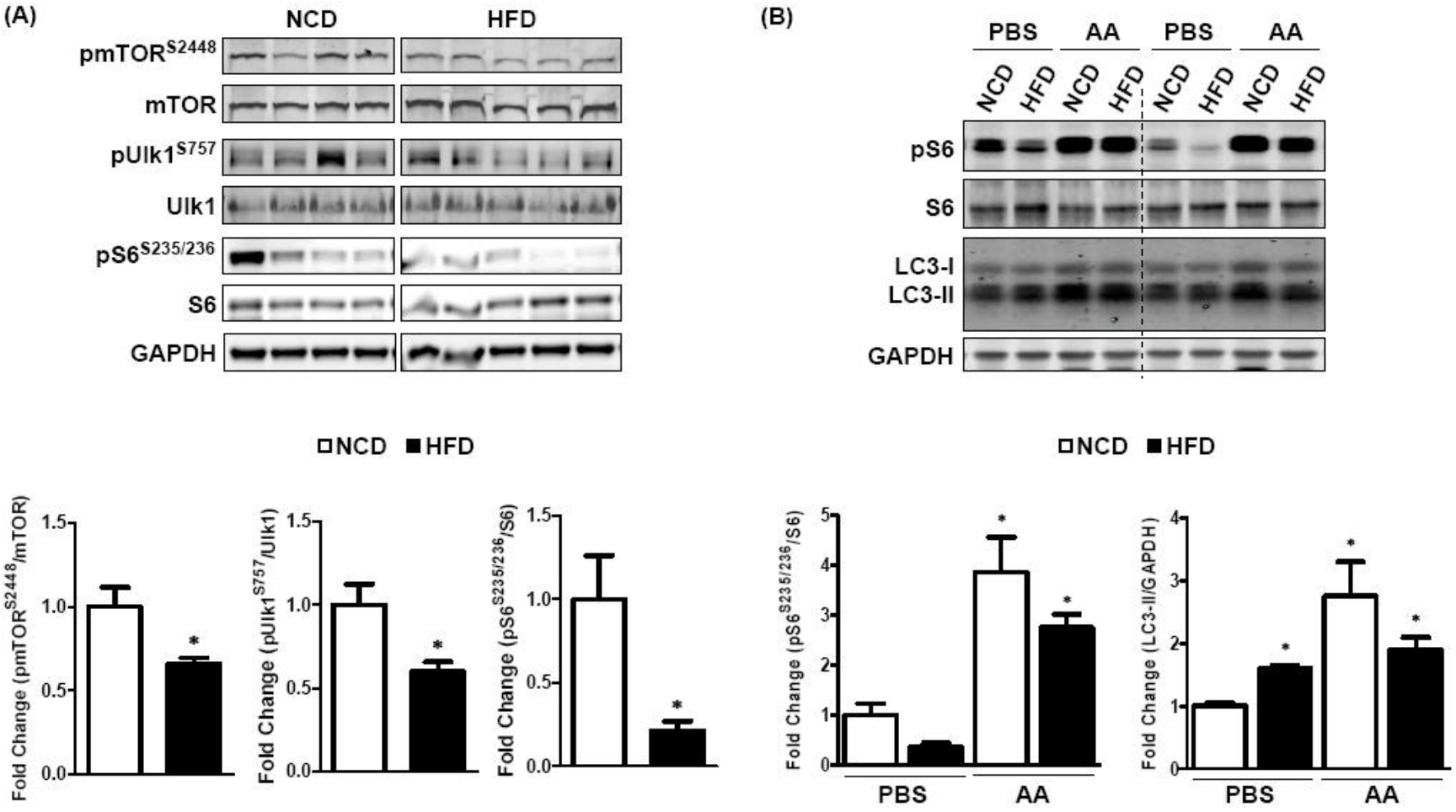
(A)
NCD
HFD
pmTOR^{S2448}
mTOR
pUlk1^{S757}
Ulk1
pS6$^{S235/236}$
S6
GAPDH
NCD HFD
Fold Change (pmTOR^{S2448}/mTOR)
Fold Change (pUlk1^{S757}/Ulk1)
Fold Change (pS6$^{S235/236}$/S6)
(B)
PBS
AA
PBS
AA
NCD
HFD
NCD
HFD
NCD
HFD
NCD
HFD
pS6
S6
LC3-I
LC3-II
GAPDH
NCD HFD
Fold Change (pS6$^{S235/236}$/S6)
Fold Change (LC3-II/GAPDH)
PBS
AA
PBS
AA

The downregulation of mTOR signaling was consistent with decreased levels of BCAA in the heart (Table 2.3 and section 2.3.4) and in the serum (Table 2.4 and section 2.3.5) of HFD mice. The lower level of BCAA could contribute to the suppression of mTOR activity, which in turn induces autophagy. To determine if HFD-induced autophagy is regulated by mTOR, mTOR signaling was stimulated by injecting mice with a BCAA solution. Western blot analysis showed that mTOR signaling was induced in hearts of both NCD and HFD fed mice upon BCAA injection compared to phosphate buffered saline (PBS)-injected controls (Figure 2.5.B). The phosphorylation of mTOR target S6 was significantly increased in BCCA injected NCD or HFD mouse hearts compared to controls (NCD-PBS: 1.0 ± 0.231, HFD-PBS: 0.4 ± 0.067, NCD-AA: 3.9 ± 0.698, HFD-AA: 2.8 ± 0.260). However, despite activation of mTOR signaling, autophagy assessed by LC3-II levels in HFD mice remained significantly induced even after mTOR signaling was induced by BCAA (NCD-PBS: 1.0 ± 0.058, HFD-PBS: 1.6 ± 0.058, NCD-AA: 2.8 ± 0.548, HFD-AA: 2.8 ± 0.200). Unexpectedly, BCAA treatment was associated with higher LC3-II despite induced mTOR phosphorylation in NCD mice.

2.3.6.4. High-fat diet-induced autophagosomal abundance is secondary to impaired autophagosome turnover

The major signaling pathways known to induce autophagic initiation either remained intact or were altered independently of any changes in HFD-induced autophagy. Since autophagic abundance is also increased by the reduced rate of autophagosome degradation independently of changes in autophagic initiation, we examined if autophagosome turnover is impaired in the heart by HFF. Autophagosome degradation in

the lysosome was blocked by increasing lysosomal pH (lysosomal basification) with CQ. Lysosomal basification blocks the activity of lysosomal hydrolases/proteases which work optimally at an acidic pH. CQ injection led to a significant increase in the level of the autophagy marker LC3-II in NCD hearts compared to control NCD hearts (NCD-cont: 1.0 ± 0.309, NCD-CQ: 2.04 ± 0.091) (Figure 2.6). However, CQ treatment did not cause any additional increase in LC3-II levels in HFD mice compared to control HFD mice (HFD: 1.95 ± 0.391, HFD-CQ: 2.15 ± 0.027). These results suggest that the increased autophagic abundance in the heart upon HFF was primarily due to impaired degradation of autophagosomes and that CQ treatment could not further impair the turnover process so that no further accumulation of autophagosomes occured.

2.4. Discussion

Obesity is a common risk factor in various cardiac pathologies such as ischemic heart disease, hypertension, CVD, heart failure, and diabetic cardiomyopathy. Autophagy is highly-regulated under these pathological conditions (Mellor et al., 2013a; Nemchenko et al., 2011). Yet, the mechanism by which obesity regulates autophagy is not clearly defined. Our preliminary studies in insulin resistant porcine model and on diabetic human subjects showed increased autophagosomes independent of changes in insulin and mTOR signaling. Other studies also observed a dissociation between autophagy and mTOR signaling in the heart (Li et al., 2012; Xu et al., 2013). In this study we tested the hypothesis that autophagic abundance in the hearts of HFD mice is primarily due to the impaired degradation of autophagic vesicles.

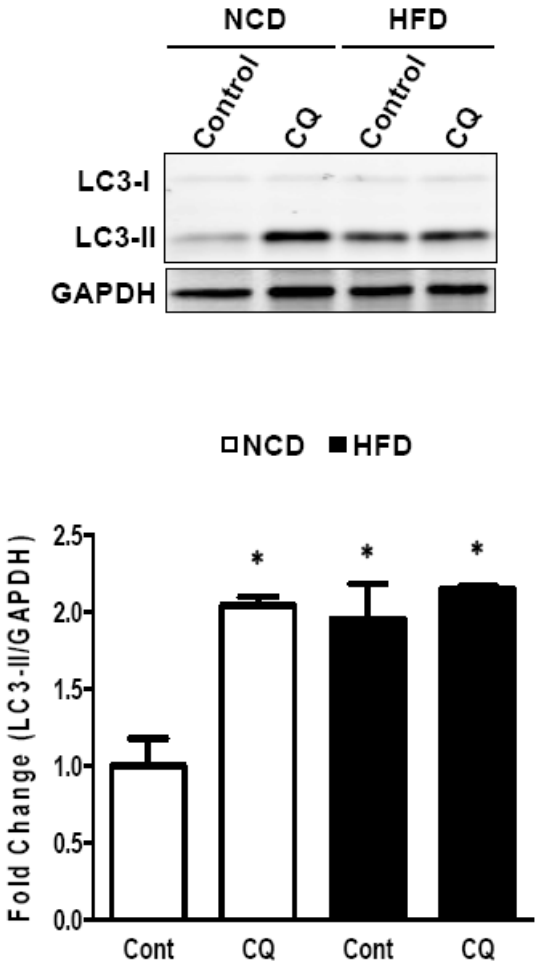

Figure 2.6. Impairment of autophagic turnover in the HFD murine heart. Mice fed either HFD or NCD were injected with or without chloroquine (CQ) for 3 days prior to harvest. Representative western blots for LC3-I, LC3-II and GAPDH in total heart homogenates of NCD or HFD mice. ∗$p<0.05$ vs. NCD-control (n=4-5). See text for details.

Twelve weeks of HFD significantly increased body weight in mice in parallel with elevated circulating levels of TGs, FFAs, fasting blood glucose, insulin, and leptin. Metabolomics analyses of serum showed a trend towards an increase in both saturated and unsaturated fatty acid levels in HFD mice. Additionally, HFD mice exhibited marked ectopic deposition of fat in various tissues including liver, kidney, and intestinal linings together with increased deposition of both visceral and subcutaneous fat (data not shown). In the heart, the HFF significantly increased heart weight and TG levels without increasing CM size and fibrosis. Furthermore, we observed a marked decrease in several key glycolytic pathway intermediates in the metabolomics analyses of HFD hearts, which is consistent with our previous finding of reduced glucose uptake and utilization in the heart of HFD mice (Wright et al., 2009). However, insulin signaling through AKT remained intact in HFD hearts. This implies that myocardial insulin signaling may remain preserved despite a systemic impairment in insulin action. In summary, our HFD mice displayed all the major hallmarks of the metabolic syndrome.

HFD also led to a significant increase in levels of the autophagy protein LC3-II and accumulation of mCherry-LC3 positive autophagosomes in the heart. The abundance of autophagy markers is influenced by the rate of autophagosome formation and their turnover in lysosomes. Analysis of major metabolic signaling pathways regulating autophagosome formation revealed that signaling through upstream molecules such as AKT, FoxO1and FoxO3, and AMPK remained normal in the HFD heart. Recent studies suggest transcriptional activation of autophagic genes as a mechanism of inducing autophagy. The analysis of autophagic gene expression by qRT-PCR showed no

difference in the transcript level of core autophagic genes. These data imply that autophagosome formation might not be perturbed in HFD hearts.

Since mTOR can be directly regulated by nutrients such as amino acids independent of AKT, we examined mTOR signaling in the heart in response to HFF. Western blot analyses showed blunted mTOR signaling upon HFF as evidenced by reduced phosphorylation of mTOR and its downstream targets. Likewise, the levels of BCAAs activating mTOR were also reduced in serum and the heart of HFD-mice. However, administration of BCAAs, despite inducing mTOR signaling, failed to suppress autophagy, indicating an mTOR independent autophagic induction by HFF. Complete blockade of autophagic turnover by CQ did not increase autophagic abundance above that caused by HFF. Together, this study showed that accumulation of autophagosomes in HFD mouse hearts was primarily due to impairment in the degradation of autophagosomes via lysosomal pathways and not due to increased autophagy induction.

CHAPTER 3

PALMITATE INCREASES AUTOPHAGOSOME ABUNDANCE BY IMPAIRING LYSOSOMAL FUNCTION

3.1. Introduction

Obesity has long been known as an independent risk factor for the development of CVD (Hubert et al., 1983; Lavie et al., 2009). Excessive caloric intake and a sedentary lifestyle contributes to obesity and insulin resistance, and elevate circulating levels of TGs and FFAs. Chronic exposure to high levels of energy substrates can have a deleterious effect (“ lipotoxicity”) on the myocardium due to the formation toxic lipid intermediates such as ceramide, DAG, and ROS (Wende and Abel, 2010). Studies in transgenic mice overexpressing the cardiac-specific fatty-acid transporter showed that ectopic lipid accumulation itself could induce lipotoxic cardiomyopathy and premature cell death independently of any systemic metabolic effects of obesity (Chiu et al., 2001). The heart initially attempts to minimize lipotoxicity by inducing FAO and channeling excess lipids towards relatively inert TG droplets (Goldberg et al., 2012). Recent studies in mouse models uncovered that autophagy represents a novel mechanism important in regulating lipid metabolism in multiple tissues such as liver, adipocytes, neurons, and pancreatic beta cells (Ebato et al., 2008; Kaushik et al., 2011; Shibata et al., 2009; Singh et al., 2009a; Singh et al., 2009b). However, the role of autophagy in cardiac lipid metabolism and its regulation in a lipid-overloaded heart is poorly understood.

High circulating levels of fatty acids have been shown to regulate autophagy in animal models of diabetes and DIO in a tissue dependent manner. In pancreatic beta cells, autophagy is induced in both diabetic (db/db) and nondiabetic high-fat fed mice and is essential for maintaining islet homeostasis (Ebato et al., 2008). In contrast, hepatic autophagy is suppressed in high-fat fed, insulin-resistant mice (Liu et al., 2009). In the heart, autophagy is differentially regulated under numerous pathological conditions

including ischemic injury, hypertensive heart disease, and heart failure, with both beneficial and detrimental outcomes (Gustafsson and Gottlieb, 2009; Wang et al., 2010b). However, the regulation of cardiac autophagy and its role in obesity and diabetes is controversial. A previous study revealed an inhibition of cardiac autophagy by the activated mTOR complex1 (mTORC1) in HFD mice (Sciarretta et al., 2012b). In contrast, studies on two mouse models of type-2 diabetes (db/db and RCS10) reported an increase in markers and mediators of autophagy (Wellnitz, 2009). Induction of autophagy markers was also observed in HFD murine hearts despite mTORC1 activation (Xu et al., 2013). While the basis for these discrepant results is not clear, accumulating evidence suggest that the magnitude and direction of autophagic regulation are highly dependent on the duration of HFF, composition of fatty acids in the diet and to differences in genetic background strain (Mei et al., 2011; Papackova et al., 2012). Moreover, many of these studies based their conclusion on a static observation of the dynamic process of autophagy. In fact, in vitro studies in pancreatic beta cells suggest that saturated fatty acids invoke a highly fluctuating biphasic autophagy response (Komiya et al., 2010; Las et al., 2011). In the present study, we examined the dynamic regulation of autophagy by lipid overload in CMs. Our study identified a novel mechanism whereby lipid overload impairs the lysosomes' ability to degrade autophagosomes, leading to autophagosome accumulation in CMs.

3.2. Methods

3.2.1. Cell culture and reagents

H9C2 (rat embryonic cardiomyoblasts, ATCC) and Ad-293 (Agilent) cells were maintained in Dulbecco's Modified Eagle Medium (DMEM) (Invitrogen) with 25 mM glucose and 10% fetal bovine serum (FBS) (Thermo Scientific). H9C2 cardiomyoblasts were differentiated in DMEM with 5 mM glucose and 1% FBS for 5 days. Lysosomal acidification was inhibited with 80 μM chloroquine (Sigma), de-novo ceramide synthesis with 50 μM myriocin (Sigma), and CPT1 with 50 μm etomoxir (Sigma). NADPH oxidase isoform 2 (Nox2) activity was inhibited with 10 mM apocynin (4′-hydroxy-3′methoxyacetophenone), total PKC activity with 2 μM GF109203x, and classical and novel PKC-isoform specific activities with 2 μM Gö6976 and 10 μM rottlerin, respectively. Cellular superoxide was scavenged by treating cells with 10 mM tiron.

3.2.2. Free fatty acid (FFA)-bovine serum albumin (BSA) complex solution

Solutions of FFA complexed with BSA were prepared essentially as previously described (Cousin et al., 2001). Briefly, a 100 mM stock solution of FFA was prepared in 0.1 M NaOH at 70^{o}C. The stock solution was mixed with a 20% (w/v) solution of FFA-free BSA (Sigma) at 50^{o}C to prepare a 10 mM FFA-20% BSA complex solution. The solution was added to a desired concentration in DMEM with 5 mM glucose and 10% FBS and used immediately after filtration. For vehicle control, cells were incubated with 1% FFA-free BSA solution prepared identically as described above but without FFA.

3.2.3. Viral transductions

Adenovirus expressing GFP-LC3 and a retroviral expression vector for mCherry-GFP-LC3 were kindly provided by Dr. Roberta Gottlieb and Dr. Eric Adler, (University of California, San Diego), respectively. Viruses were generated and amplified in Ad-293 cells. Adenoviruses were partially purified by repeated freeze-thaw in a 10% glycerol solution in PBS followed by centrifugation at 5000 rpm for 5 min. Viral supernatant was titered and used to transduce cells as described (Huang et al., 2010). All subsequent treatments were performed 18 h posttransduction. For retroviral transduction, viral supernatant of Ad-293 cells was filtered through 0.45-μM-pore filter and added to H9C2 cell culture medium supplemented with 4 μg/ml polybrene (Millipore). Stably transduced cells were obtained by selection against puromycin (5 μg/ml; Invitrogen).

3.2.4. Western blot analyses

Total proteins were extracted from cells in a lysis buffer containing 50 mM HEPES (pH 7.5), 150 mM NaCl, 10% Glycerol, 1% Triton X-100, 1.5 mM $MgCl_2$, 1 mM EGTA, 10 mM Sodium Pyrophosphate, 100 mM Sodium Fluroride, and 1X Halt protease and phosphatase inhibitor cocktail (Thermo Scientific), and analyzed by western blotting as described previously (Riehle et al., 2011). Antibodies against LC3 and alpha-Tubulin (Sigma); phospho and total mTOR, AKT, and S6 (Cell Signaling); phospho-Ulk1 and GAPDH (Cell Signaling); Ulk1, p62 (SQSTM1), and Cathepsin D (Santa Cruz); Lamp1 (Abcam); and Nox2 (Novus Biologicals) were used for immunodetection.

3.2.5. Measurement of apoptosis

Apoptosis was assessed in H9C2 cardiomyocytes (CMs) using FITC Annexin V Apoptosis Detection Kit with PI (BioLegend) following supplier's protocol. Briefly, following each treatment, cells were washed and resuspended in a staining buffer, stained with FITC-Annexin V and propidium iodide (PI) for 15 min at room temperature, and subsequently analyzed by flow cytometry using appropriate filters.

3.2.6. Fluorescence microscopy

For live cell imaging, cells were plated on an 8-chamber coverglass (Lab-Tek, Nunc). Lysosomes were stained with 75 nM LysoTracker Red for 30 min or with 1 μM LysoSensor Yellow/Blue (Invitrogen) for 10 min and placed in an on-stage humidified incubator at 37^{o}C for image acquisition. For GFP-LC3 and mCherry-GFP-LC3 fluorescence, cells were fixed in 4% PFA. For other immunofluorescence, cells were blocked/permeabilized in 5% goat serum/5% horse serum/0.2% TritonX-100 following fixation. Fixed cells were stained with anti-Lamp1, anti-Tom20 (Santa Cruz), or anti-Ceramide (Enzo Life Sciences) primary antibody (1:250 dilution) for 1 h at 37^{o}C and with Alexa Fluor-conjugated secondary antibodies (1:500 dilution; Invitrogen) for 1 h at room temperature. Cell nuclei were counterstained with DAPI (Invitrogen). Images were obtained using an Olympus IX80 FV 1000 confocal microscope equipped with appropriate lasers. Quantification of GFP-positive puncta and other fluorescent intensity was performed from a minimum of three randomly selected sections per sample with 50 cells per section and 4 samples per treatment.

3.2.7. ATP measurement

Total ATP content in cells was measured by a bioluminescence assay based on the luciferase/luciferin reaction using the ATP assay system kit (Thermolabsystems) following supplier's protocol.

3.2.8. Lysosomal enzyme activity

Cathepsin L activity was examined by staining live CMs with Magic Red Cathepsin L substrate (Immunochemistry Technologies) for 1 h at 37ºC following supplier's protocol. Fluorescent images were acquired as described earlier. Crude lysosomal fractions, prepared as described (Parent et al., 2009), were used to measure beta-galactosidase activity using mammalian beta-galactosidase assay kit (Thermoscietific) and beta-hexosaminidase activity as described previously (Vaidyanathan et al., 2001).

3.2.9. Superoxide measurement by ESR spectroscopy

Following each treatment, cells were washed and incubated for 30 min at 37ºC with 1M HEPES buffer (pH 7.4) containing 25 μM deferoxamine mesylate and 0.2 mM 1-Hydroxy-3-methoxycarbonyl-2,2,5,5-tetramethylpyrrolidine, HCl (CMH; Alexis Corp, USA) to trap superoxide as CMH-free radical adduct. The cell sample was homogenized and aspirated into a capillary tube for the detection of the adduct by electron spin resonance (ESR) spectroscopy. ESR spectra were recorded using a Brüker EMX micro EPR spectrometer with the following settings: center field, 3511G; field sweep, 70 G; microwave frequency, 9.85 GHz; microwave power, 20 milliwatts; modulation

amplitude, 0.5G; conversion time, 5.0 ms; time constant, 1.28 ms; resolution, 1400 points; and receiver gain, 50dB.

3.2.10. Statistical analyses

All data are presented as mean ± SEM. Unpaired Student's t-test was performed to determine p-values when comparing between two groups. 1-way Analysis of variance (ANOVA) was used to compare data across multiple groups with one independent variable. Multiple groups with two or more independent variables were analyzed by 2-way ANOVA. Statistical significance was determined by Bonferroni's post-hoc analysis using the GraphPad Prism 5 software (La Jolla, CA). For all analyses, $p<0.05$ was considered statistically significant.

3.3. Results

3.3.1. Acute palmitate treatment regulates autophagy with no cytotoxic effect

To study the regulation of autophagy in lipid overload, H9C2 CMs were first incubated with 250 to 1000 μM of palmitate, the most abundant saturated circulating FFA, for 2-8 h. Treatment with 500 μM palmitate for 4 h resulted in the maximal increase in the autophagy marker protein LC3-II in the absence of ER stress and cell death (data not shown). Next, we examined if palmitate treatment exhibits time-dependent autophagic response as recently reported in pancreatic beta cells (Komiya et al., 2010; Las et al., 2011). As shown in Figure 3.1.A, palmitate induced a biphasic autophagic response in H9C2 CMs with LC3-II levels increased in the first 4 h and then

Figure 3.1. Short-term palmitate treatment regulates autophagy in H9C2 CMs without cytotoxicity. (A) H9C2 CMs were incubated with vehicle or 500 µM palmitate at indicated time points and autophagy was monitored by analyzing the levels of LC3-II normalized to GAPDH in total cell lysates. Graph represents mean ± SEM. *$p<0.05$ vs. vehicle (n=3). (B-C) H9C2 CMs were incubated with either vehicle or 500 µM palmitate for 4 h. Following vehicle or palmitate treatment, CMs were either stained with Annexin-V/FITC and propidium iodide (PI) and analyzed by flow cytometry (B), or examined for DNA fragmentation (C). CMs treated with 10 mM H_2O_2 for 1 h were used as positive controls. (D) Total ATP content in CMs treated with vehicle or palmitate (n=6). (E) Representative LC3-I and II immunoblots from CMs incubated with vehicle or palmitate for 4 h (a and b, respectively) and subsequently replaced with normal growth medium for 8 h (c and d, respectively).

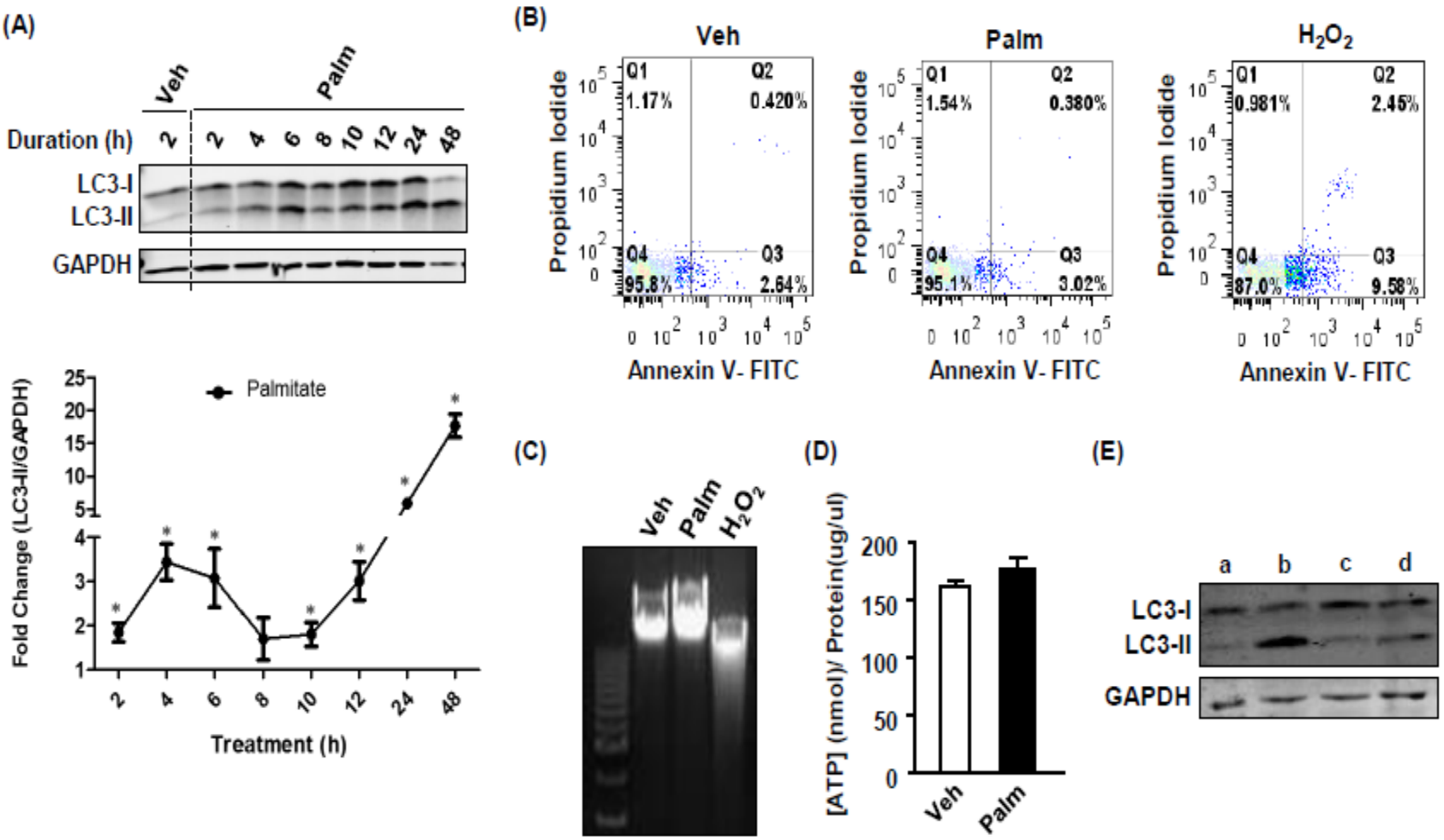
(A)
Veh
Palm
Duration (h)
2
2
4
6
8
10
12
24
48
LC3-I
LC3-II
GAPDH
Palmitate
Fold Change (LC3-II/GAPDH)
Treatment (h)
(B)
Veh
Palm
H2O2
Propidium Iodide
Annexin V- FITC
Q1
Q2
Q3
Q4
1.17%
0.420%
95.8%
2.64%
1.54%
0.380%
95.1%
3.02%
0.981%
2.45%
87.0%
9.58%
(C)
Veh
Palm
H2O2
(D)
[ATP] (nmol)/ Protein(ug/ul)
Veh
Palm
(E)
a
b
c
d
LC3-I
LC3-II
GAPDH

dropping to baseline before being increased rapidly after 8 h. As such, we chose to perform all subsequent experiments with 500 µM palmitate and 4-h incubation to study the mechanism of initial, preclinical regulation of autophagy in response to lipid overload without the confounding effect of cytotoxicity.

To verify that our treatment caused no cytotoxicity, we examined markers of apoptosis and necrosis in H9C2 CMs following palmitate treatment. Flow cytometric analysis of CMs stained with FITC-Annexin V and propidium iodide (PI) showed no difference in staining between vehicle and palmitate treated CMs. In contrast, CMs incubated with exogenous H_2O_2 as positive control showed a clear increase in Annexin V binding and PI positivity (Figure 3.1.B). Accordingly, examination of genomic DNA in vehicle and palmitate treated CMs exhibited no DNA laddering, a characteristic of apoptotic cell death, whereas H_2O_2 treatment significantly increased genomic DNA laddering in CMs (Figure 3.1.C). Moreover, we measured ATP level in H9C2 CMs since changes in cellular ATP level have been shown to induce apoptotic and necrotic cell death (Eguchi et al., 1997; Tsujimoto, 1997). As shown in Figure 3.1.D, we did not observe any change in total ATP content by palmitate treatment. Together, these data indicate that 4 h of palmitate treatment alters autophagy in H9C2 CMs without inducing a cytotoxic effect. Finally, when CMs pretreated with palmitate were returned to normal growth medium, autophagy was restored to basal levels by 8 h (Figure 3.1.E), and total cellular protein content was comparable with CMs pretreated with vehicle (data not shown), suggesting that palmitate-dependent autophagy is a transient, reversible process unlike apoptosis and necrosis which are mostly irreversible.

3.3.2. Palmitate impairs autophagosome turnover

The metabolic status of a cell is a critical factor in the regulation of autophagy. In the normal fed state, insulin signaling pathway suppresses autophagy in the heart (Mellor et al., 2013b); however, insulin action in the heart progressively declines under conditions of lipid overload as in genetic and dietary mouse models of obesity (Abel et al., 2012). To explore the potential mechanisms whereby lipid overload by palmitate alters cardiac autophagy, we examined upstream metabolic signals known to regulate the autophagic initiation process. As shown in Figure 3.2, insulin signaling through Akt-phosphorylation (at S473) remained intact in palmitate-treated CMs compared with vehicle controls. Since mTOR can be regulated by both Akt dependent and independent pathways, we assessed mTOR signaling in palmitate-treated CMs. Interestingly, phosphorylation of mTOR (at S2448) and its downstream target in autophagy, Ulk1 (at S757), were unaffected by palmitate. The classical mTOR target ribosomal protein S6 phosphorylation also remained preserved in palmitate-treated CMs. Additionally, AMPK, an important kinase sensing cellular energy status, is also known to upregulate autophagy by activating Ulk1 and inhibiting mTOR. Like AKT and mTOR signaling, we did not observe any change in AMPK signaling in palmitate-treated CMs as assessed by phosphorylation of AMPKα (at T172) and its target Ulk1 (at S555). These data indicate that canonical upstream signaling pathways regulating autophagy in insulin sensitive tissues remained normal following short-term palmitate treatment. Therefore, the observed increase in autophagic markers in response to palmitate might not be primarily due to an induction of the autophagic initiation pathway.

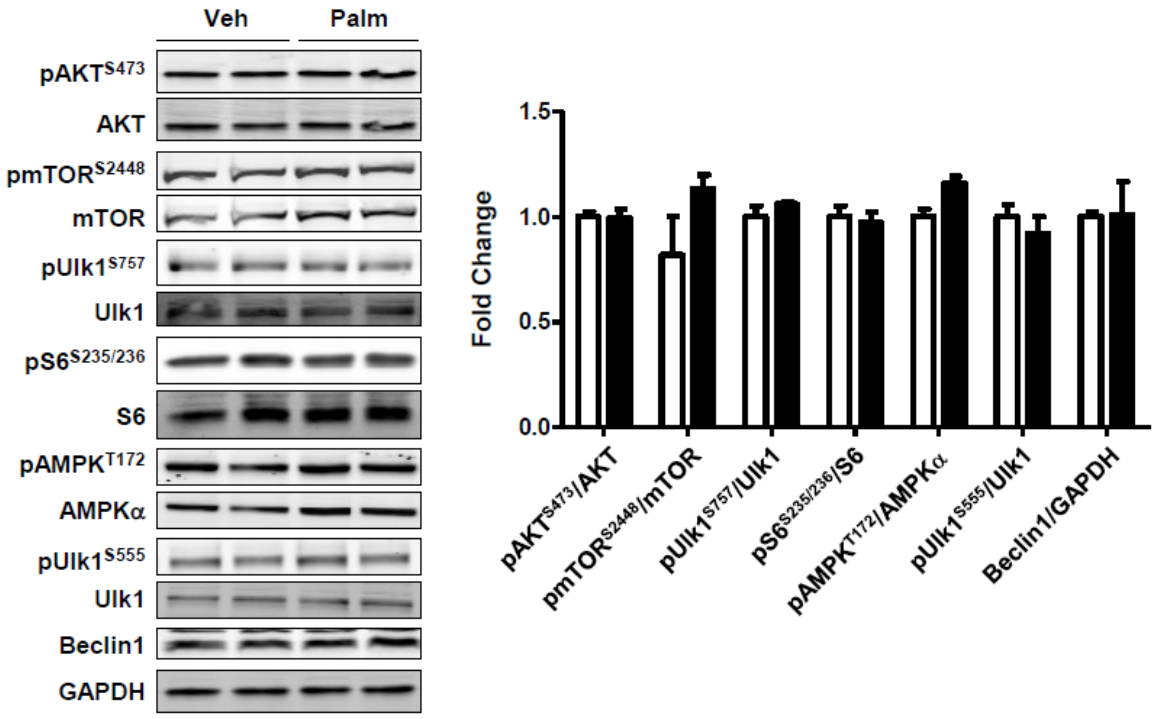

Figure 3.2. Palmitate-induced autophagy is independent of the canonical signaling pathways initiating autophagy. H9C2 CMs were incubated with either vehicle or 500 µM palmitate for 4 h. Proteins involved in autophagy initiation signaling were analyzed by immunoblotting. Graphs represent mean ± SEM (n=3-6).

The accumulation of autophagic markers is consistent with either increased autophagosome formation or reduced turnover. In the absence of changes in major signaling pathways initiating autophagy, we explored autophogosome turnover as a potential step impacted by palmitate that leads to autophagosome accumulation. Autophagosome turnover in vehicle or palmitate treated CMs was completely blocked by chloroquine (CQ) treatment for the last 1 h of incubation. While palmitate alone significantly increased LC3-II level, CQ treatment further increased accumulation of LC3-II under both conditions (vehicle: 1.0 ± 0.146, palmitate: 2.5 ± 0.113, vehicle+CQ: 3.4 ± 0.037, palmitate+CQ: 4.5 ± 0.176) (Figure 3.3.A). Interestingly, upon CQ addition, the fold increase in vehicle-treated CMs was much higher (~3.5 fold) than in palmitate-treated CMs (~1.8 fold) compared with respective non-CQ treatments. These data suggest that the palmitate-induced increase in LC3-II may primarily be due to partial impairment in autophagosome turnover. Supporting this notion, the adapter protein p62 (SQSTM1), which is degraded by autophagy, remained higher in palmitate-treated CMs, and, expectedly, in CQ-treated CMs under both conditions. To validate our observation, we repeated palmitate and CQ treatment in H9C2 CMs expressing adenoviral GFP-LC3, and scored GFP-positive autophagosomes using fluorescence microscopy (Figure 3.3.B). Consistent with immunoblot data, palmitate treatment led to significantly higher numbers of GFP-positive puncta than vehicle treatment (vehicle: 4 ± 1.364, palmitate: 16 ± 2.273). However, CQ addition increased the number of puncta more robustly in vehicle-treated CMs than in palmitate-treated ones (vehicle+CQ: 47 ± 5.455, palmitate+CQ: 37 ± 3.636). Finally, we examined autophagosome abundance in H9C2 CMs stably expressing dual fluorescence (mCherry- GFP)-tagged LC3. Both GFP (green) and mCherry (red)

Figure 3.3. Palmitate impairs autophagosome turnover in H9C2 CMs. (A-B) H9C2 CMs incubated with either vehicle (1% BSA) or 500 µM palmitate for 4 h in presence or absence of 80 µM Chloroquine (CQ) for the last 1 h were analyzed for LC3-I, LC3-II and p62 levels by immunoblotting. Data represent mean ± SEM. (n=6). (B and C) H9C2 cells transiently expressing adenoviral GFP-LC3 (Ad GFP-LC3) (B), or stably expressing mCherry-GFP-LC3 (C) were incubated with vehicle or palmitate in presence or absence of CQ as described in panel A. (B) Confocal images showing distribution of Ad-GFP-LC3 (green). Graph represents average number of GFP-positive puncta/cell ± SEM (n=6). (C) Confocal images showing GFP (green) and mCherry (red) fluorescence of mCherry-GFP-LC3. DAPI (blue) stains the nuclei. Scale bars represent 10 µm. $*p<0.05$ vs. vehicle-saline and $^{\#}p<0.05$ vs. palmitate-saline.

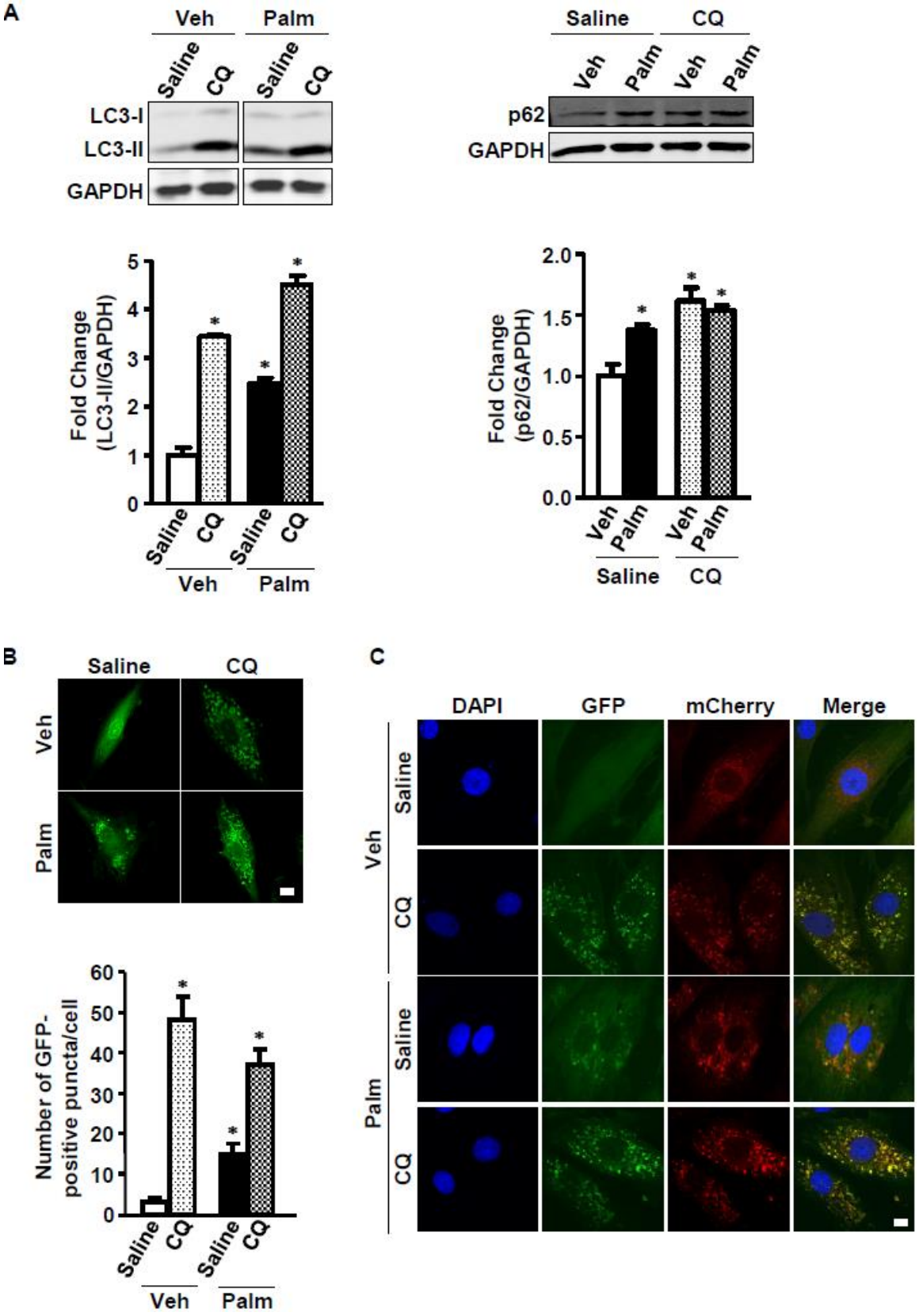
A
Veh
Palm
Saline
CQ
LC3-I
LC3-II
GAPDH
Fold Change (LC3-II/GAPDH)
Saline
CQ
p62
Fold Change (p62/GAPDH)
B
Number of GFP-positive puncta/cell
C
DAPI
GFP
mCherry
Merge

fluoresce in autophagosomes, but GFP fluorescence is quenched when autophagosomes fuse with lysosomes because of the acidic pH of the lysosomal lumen. As shown in Figure 3.3.C, vehicle treated CMs mostly exhibited mCherry punctae with no apparent GFP puncta, suggesting a rapid autophagosome turnover. In contrast, palmitate-treated CMs predominantly exhibited dual-fluorescent positive puncta, suggesting either increased formation of autophagosomes or defective nonacidic autolysomes. Inhibition of lysosomal acidification with CQ resulted in even greater accumulation dual-fluorescent puncta in both vehicle and palmitate treated CMs similar to one observed with palmitate alone. Together, our data support an impairment in autophagosome turnover as a potential mechanism for autophagosomal abundance in palmitate-treated H9C2 CMs.

3.3.3. Palmitate induces autophagy in the absence of ER stress

ER stress is a classical hallmark of obesity and diabetes in both humans and animal models (Boden et al., 2008; Cnop et al., 2012). Several experimental models of ER stress have been shown to induce autophagy in multiple cell types (Madaro et al., 2013; Nijholt et al., 2011; Ogata et al., 2006). Therefore, we tested if ER stress mediates or precedes palmitate-induced autophagy. Immunoblot analyses showed that proteins in two different unfolding protein response (UPR) pathways (IRE1α-XBP1 and PERK-eIF2α) involved in ER stress and autophagy were not altered following 4 h of palmitate treatment (Figure 3.4). Changes in the UPR pathway were observed only after 8 h of palmitate treatment when phosphorylation of IRE1α and the active form of XBP1 (generated from alternative mRNA splicing of XBP1 by IRE1α) were significantly elevated. These data illustrate that

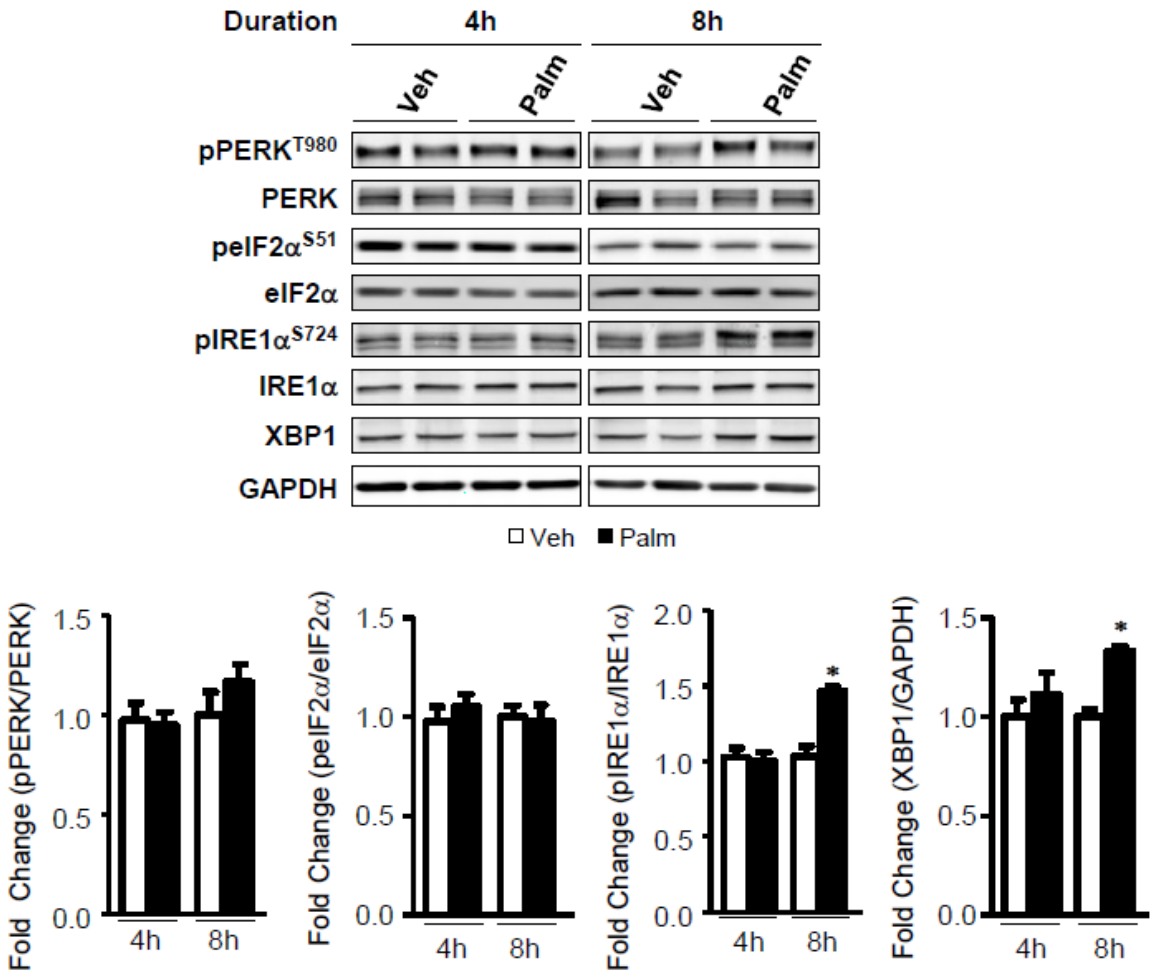

Figure 3.4. Autophagic response to palmitate is independent of ER stress. H9C2 CMs incubated with either vehicle or 500 µM palmitate for 4 h and 8 h were analyzed for proteins involved in UPR-mediated ER stress. Data represent mean ± SEM. *$p<0.05$ vs. vehicle, same duration of incubation.

autophagy precedes ER stress in palmitate-treated H9C2 CMs.

3.3.4. Palmitate-induced autophagy is independent of ceramide

Ceramide is an important byproduct of palmitate metabolism and is known to mediate cytotoxic effects of palmitate in multiple cell types (Summers, 2006). Several studies have shown that ceramide promotes autophagy (Daido et al., 2004; Pattingre et al., 2009a; Scarlatti et al., 2004). To determine if ceramide plays a role in palmitate-dependent autophagy, we first examined the level of ceramide in palmitate-treated H9C2 CMs by indirect immunofluorescence using an anticeramide antibody. Consistent with previous findings, ceramide levels were significantly elevated (~2 fold) following palmitate treatment (Figure 3.5.A). We then blocked de novo ceramide synthesis by inhibiting serine-palmitoyl transferase 1 (SPT1), an enzyme involved in ceramide biosynthesis with myriocin. While myriocin completely prevented palmitate-induced ceramide accumulation, it did not prevent palmitate-induced accumulation of the autophagy marker protein LC3-II (Figure 3.5.B). These data suggest that palmitate-induced ceramide synthesis and autophagosome accumulation are independent processes, and ceramide does not mediate palmitate's effect on autophagosomal abundance.

3.3.5. Palmitate-induced autophagosome accumulation is dependent on superoxide

Oxidative stress caused by high levels of reactive oxygen species (ROS) plays an important role in the development of cardiovascular disease associated with obesity and

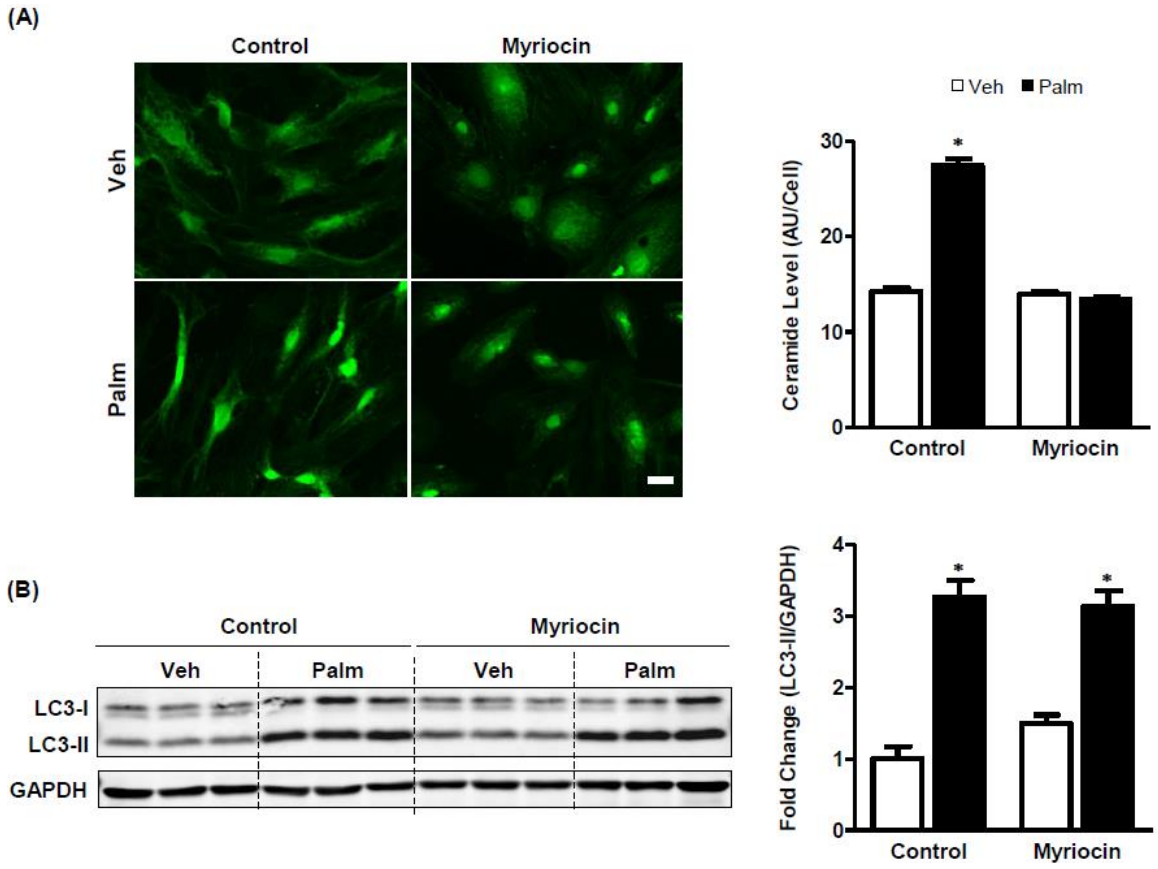

Figure 3.5. Palmitate induced autophagosome accumulation is not mediated by ceramide. (A) CMs incubated with either vehicle or palmitate for 4 h in the presence or absence of 50 µM myriocin were immunostained with anticeramide antibody and visualized by indirect immunofluorescence. *****p<0.0001 vs. vehicle, n=6. Number of CMs/n=50. Scale bar is 50 µm. (B) CMs treated identically as described in panel A were analyzed for LC3-I and II levels by immunoblotting. Data represent mean ± SEM. *****p<0.001 vs. vehicle-control.

and diabetes (Marchi et al., 2013). In vitro studies have linked palmitate-induced accumulation of ROS to various lipotoxic effects of palmitate including apoptosis and insulin resistance (Kim et al., 2010; Yuzefovych et al., 2010). Recently, both palmitateand ROS have been shown to regulate autophagy in various cell types (Azad et al., 2009; Choi et al., 2009; Scherz-Shouval and Elazar, 2011; Tan et al., 2012; Wen et al., 2011). However, it is not entirely clear from these studies if ROS mediates palmitate-dependent autophagy. To investigate the role of ROS in palmitate-dependent autophagy, we first determined the level and the identity of ROS generated by palmitate treatment in H9C2 CMs. Measurement of cellular ROS by flow-cytometry following DCFDA (2',7'–dichlorofluorescein diacetate) staining showed no difference between vehicle and palmitate treated CMs. Subsequent measurement by ESR spectroscopy using a specific spin probe revealed a massive increase in superoxide level (~3.8 fold) in palmitate-treated CMs compared to vehicle controls (Figure 3.6.A). Treatment with the generic superoxide scavenger tiron significantly lowered LC3-II level in palmitate-treated CMs (~ 35%) compared with palmitate-treated controls (palm-control: 3.2 ± 0.176, palm-tiron: 2.1 ± 0.058) (Figure 3.6.B). However, basal autophagy was not affected by tiron treatment (veh-control: 1.0 ± 0.116, veh-tiron: 1.1 ± 0.088). Moreover, tiron treatment completely blunted palmitate-induced accumulation of GFP-positive autophagosomes (punctae) in H9C2 CMs (Figure 3.6.C). These data provide clear evidence that palmitate-induced autophagosomal abundance is driven by a superoxide-dependent mechanism.

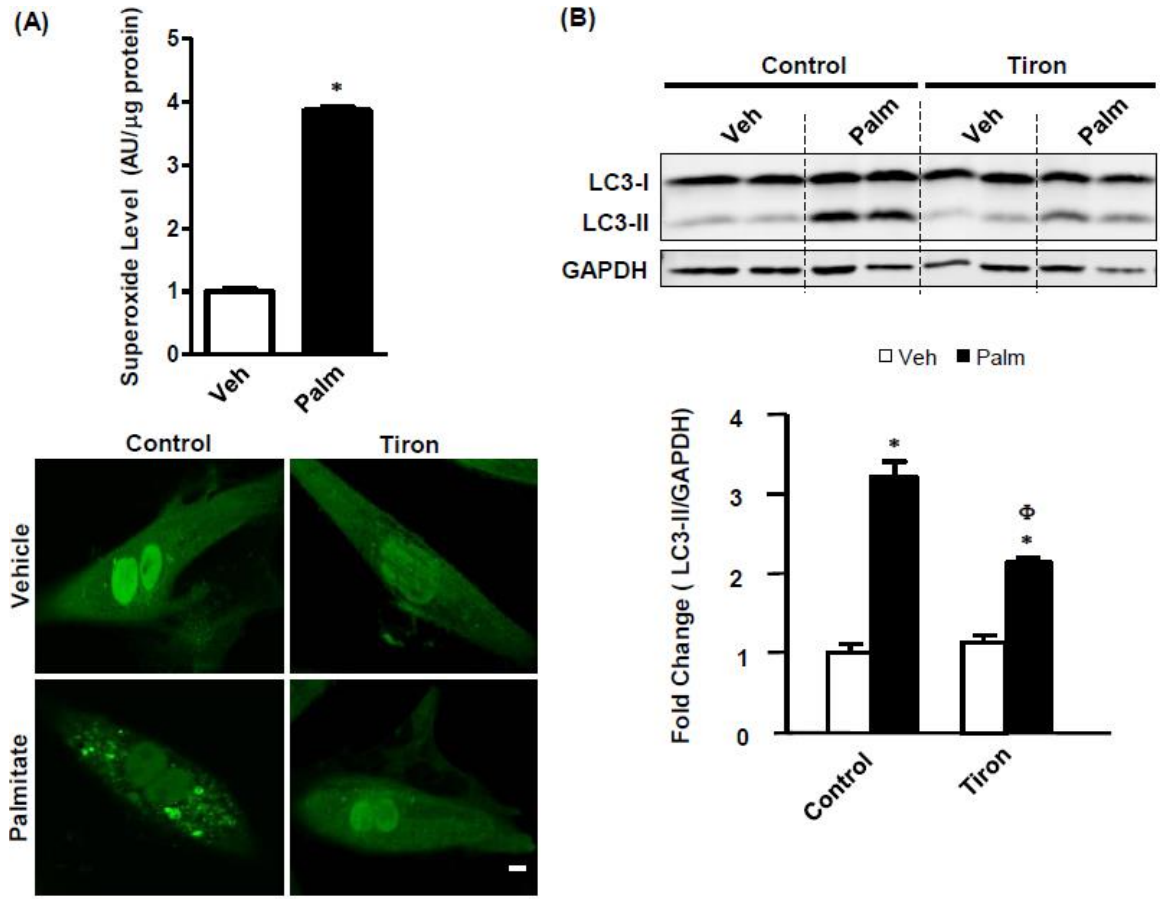

Figure 3.6. Palmitate regulates autophagy in a superoxide dependent manner. (A) Superoxide production in H9C2 CMs incubated with either vehicle or 500 µM palmitate for 4 h and was measured by ESR using CMH as a superoxide spin trap probe. ∗p<0.0001 vs. vehicle (n=5). (B) CMs were incubated with vehicle or palmitate in the presence or absence of 10 mM tiron for 4 h and analyzed for LC3-I and LC3-II by western blot. Data represent normalized LC3-II levels (n=6). *****p<0.001 vs. vehicle-control and $^{\Phi}p$<0.05 vs. palmitate-control. (C) Confocal images of GFP-LC3 in Ad GFP-LC3 expressing H9C2 CMs incubated with vehicle or palmitate in the presence or absence of 10 mM tiron. Scale bar is 10 µm.

3.3.6. Oleate reverses palmitate-induced autophagy

The elevated circulating fatty acids as in obesity and diabetes are a mixture of various FFAs and their complex derivatives. To understand if palmitate-induced autophagy is specific to palmitate or a general effect of fatty acid overload, we incubated H9C2 CMs for 4 h with 500 μM oleate– the most abundant circulating fatty acid in the body. Interestingly, autophagy remained normal in oleate-treated CMs as assessed by LC3-II immunoblot (Figure 3.7.A). Furthermore, superoxide level in oleate-treated CMs remained similar to vehicle controls (Figure 3.7.B). These data further support a superoxide-mediated regulation of autophagy in palmitate-treated CMs. Next, we examined if oleate can normalize palmitate-induced autophagy in H9C2 CMs. Coincubation with oleate not only reversed autophagic abundance in palmitate-treated CMs in a dose dependent manner but also restored autophagy to the basal level at an equimolar concentration of palmitate and oleate (Figure 3.7.C). These data suggest that palmitate exerts specific effect on autophagy. These data, therefore, uncovered a novel effect of oleate in reversing palmitate induced autophagy which may play a beneficial role in protecting cells from toxic effects of palmitate as described in previous studies.

3.3.7. Lysosomal content and autolysosome formation are not affected by palmitate

Transcriptional activation of autophagy and lysosomal genes by transcriptional factor EB (TFEB) plays a central role in starvation induced autophagy (Settembre et al., 2011). We examined if palmitate-dependent autophagic abundance involves altered transcription of lysosomal genes, since transcriptional repression of such genes may impair clearance

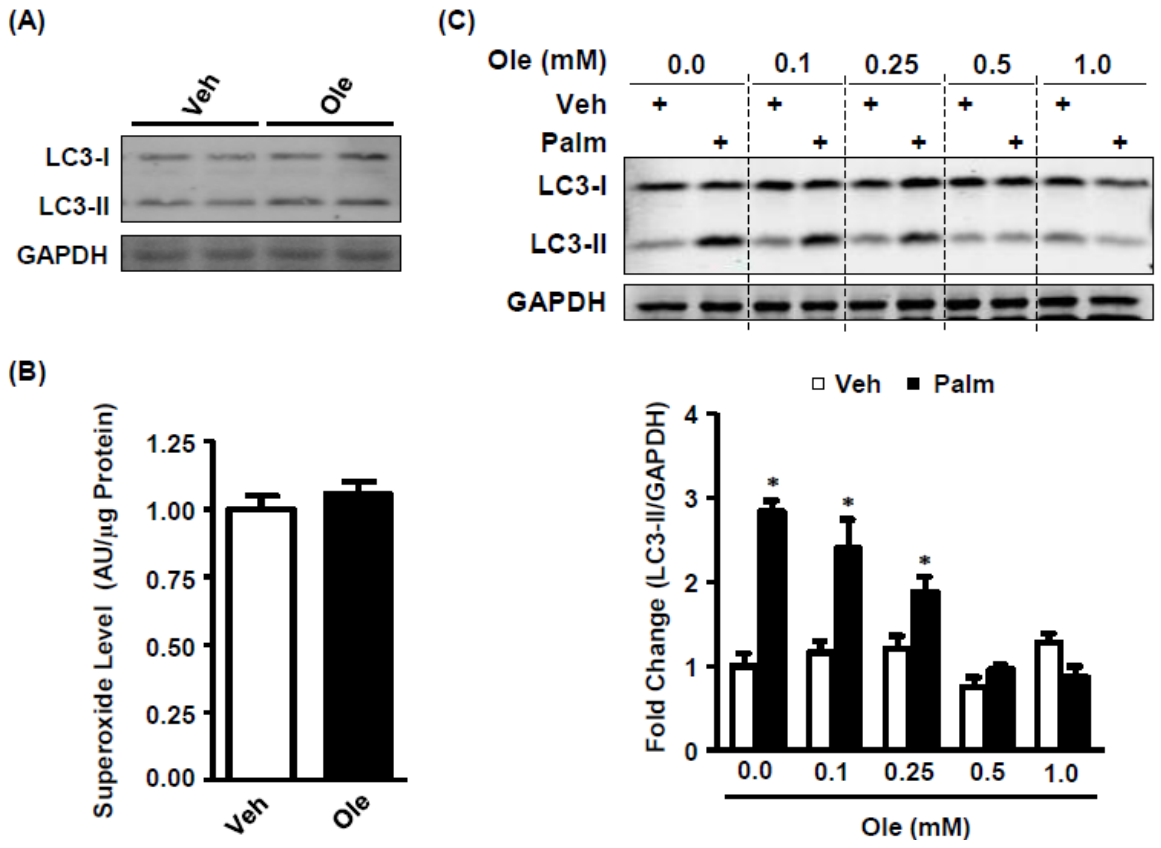

Figure 3.7. Oleate normalizes autophagy in palmitate-treated H9C2 CMs. (A and C) Western blots of LC3-I and LC3-II in H9C2 CMs treated with either vehicle or 500 μM oleate (A), or cotreated with 500 μM palmitate and varying concentration of oleate (ole) (C) for 4 h. Data represent fold change in LC3-II levels normalized to GAPDH (n=6, panel A n=3, panel C). *p<0.001 vs. vehicle alone. (B) Production of superoxide in H9C2 CMs treated with either vehicle or 500 μM oleate was measured by ESR using CMH as a superoxide spin trap probe (n=5).

of mature autophagosomes. mRNA levels of genes involved in lysosomal biogenesis, acidification and function were determined by quantitative real-time PCR (qRT-PCR). As shown in Figure 3.8.A, lysosomal gene expression largely remained intact in palmitate-treated H9C2 CMs. Accordingly, lysosome content, assessed by lysosome-associated membrane protein 1 (Lamp1) levels, was similar between vehicle and palmitate treated CMs (Figure 3.8.B). Recent studies have attributed defective autophagosome-lysosome fusion to increased autophagosome accumulation in pancreatitis and diabetic cardiomyopathy (Fortunato and Kroemer, 2009; Zhao et al., 2012). We examined if palmitate-induced autophagosome accumulation is secondary to impaired autophagosome-lysosome fusion. H9C2 CMs expressing Ad-GFP-LC3 were stained with LysotrackerRed in live cells or immunostained with Lamp1 antibody in fixed cells following palmitate treatment. Fluorescent micrographs revealed that most autophagosomes (GFP-punctae) colocalized positively with lysosomes (red punctae) both in live and fixed CMs (Figure 3.8-C and D, respectively), suggesting autophagosome-lysosome fusion to form autolysomes remained intact in palmitate-treated CMs.

3.3.8. Palmitate impairs lysosomal acidification and enzyme activity in a superoxide dependent manner

Lysosomal pH (~4.5-5.0) is a key determinant of lysosomal enzyme activity. In vitro studies have observed impairment in lysosomal acidification and enzyme activities in response to fatty acid, lipoprotein, and cholesterol overload (Cox et al., 2007; Las et al., 2011). We examined if lysosomal acidification and function were impaired in palmitate-treated CMs. Following vehicle or palmitate treatment, lysosomes were stained

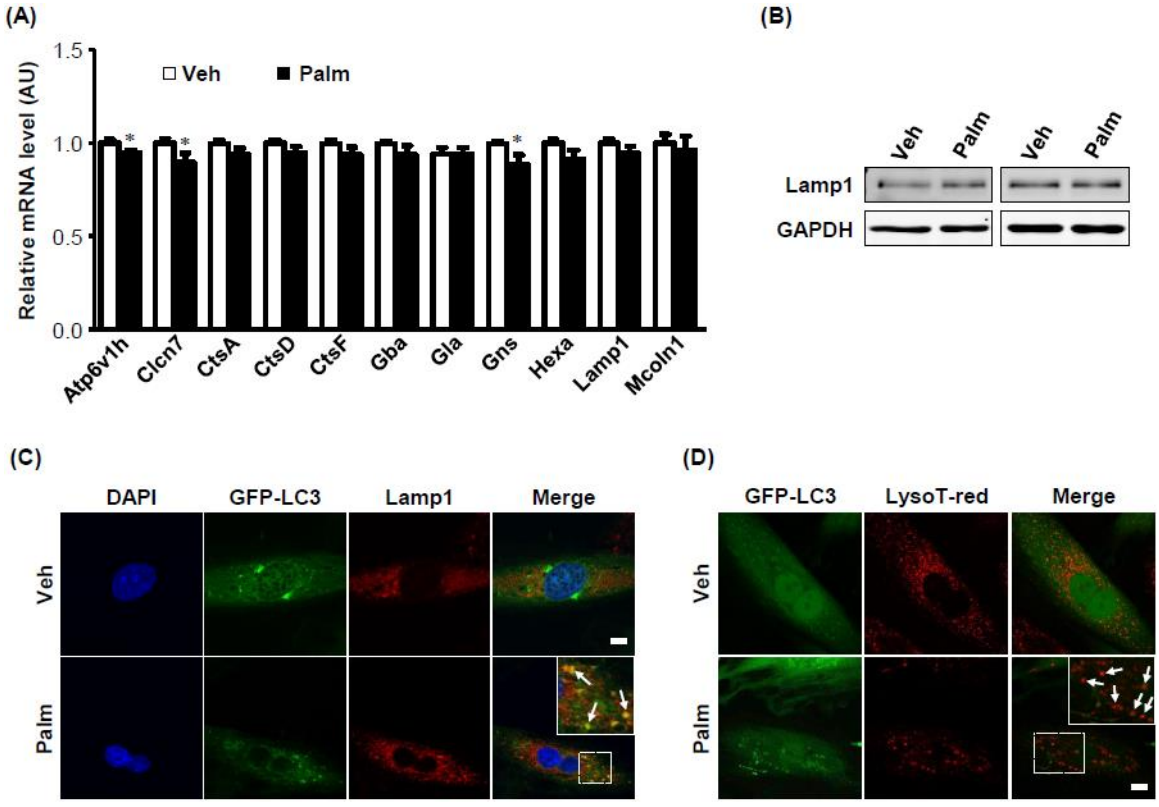

Figure 3.8. Lysosomal content and autolysome formation are not affected by palmitate treatment. (A-B) H9C2 CMs incubated with vehicle or 500 µM palmitate for 4 h were analyzed by qRT-PCR for mRNA levels of lysosomal genes normalized to cyclophilin A (A, n=5), and by western blot for Lamp1 (B, n=5). (C) Confocal images of GFP-LC3 in CMs expressing Ad GFP-LC3 following vehicle or palmitate treatment. Lamp1 was detected by indirect immunofluorescence. DAPI (blue) stains the nuclei. White arrows indicate puncta colocalized with GFP-LC3 and Lamp1. (D) Ad GFP-LC3 expressing CMs were incubated with vehicle or palmitate for 4 h and stained for lysosomes with 50 nM Lysotracker Red for 30 min. White arrows represent puncta colocalized with GFP-LC3 (green) and Lysotracker Red (red). Scale bar is 10 µm.

with the vital dye LysoSensor yellow/blue. The yellow fluorescence is pH independent, whereas blue fluorescence intensifies as lysosomal pH rises. Fluorescent micrographs showed that palmitate significantly increased lysosomal pH as evidenced by increased blue staining (Figure 3.9.A). Interestingly, lowering of superoxide levels with tiron completely abolished palmitate-induced alkalization of lysosomes, suggesting a superoxide-dependent impairment in lysosomal acidification in palmitate-treated CMs. We next examined the activity of cathepsin L (CatL), a lysosomal endopeptidase, in live CMs using MagicRed (MR), a CatL substrate which is cleaved by the enzyme into a red-fluorescent product. Consistent with impaired lysosomal acidification, CatL activity was blunted in palmitate-treated CMs but not in vehicle controls (Figure 3.9.B). Importantly, palmitate-induced inhibition of CatL activity was reversed by tiron treatment. We further examined if lysosomal enzyme function per se is diminished by palmitate treatment possibly through a superoxide- mediated oxidative damage. However, the activity of two crudely-purified lysosomal hydrolases, β-galactosidase and β-hexosaminidase, remained preserved in palmitate-treated CMs (Figure 3.9.C). Collectively, our data demonstrated that palmitate impairs lysosomal acidification possibly by a mechanism that is secondary to enhanced superoxide production which in turn impairs pH-dependent activity of lysosomal enzymes.

3.3.9. Palmitate does not alter mitochondrial superoxide production and mitophagy

Mitochondria are major producers of ROS. ROS production by mitochondria rises to pathological levels in metabolic disorders such as obesity and diabetes which could

Figure 3.9. Palmitate-induced impairment in lysosomal acidification and enzyme activity is superoxide dependent. (A) CMs incubated with vehicle or 500μM palmitate in the presence or absence of 10 mM tiron for 4 h were subsequently incubated with either LysoSensor Yellow/Blue dye during the last 10 min and visualized by confocal fluorescence microscopy. The graph represents the ratio of LysoSensor blue to yellow fluorescence. (B) CMs preincubated with vehicle or palmitate and with or without tiron were treated with MR CatL substrate during the last 1 h of incubation and visualized by confocal microscopy. The graph represents MR intensity (AU) per cell. (A-B) Data are presented as mean ± SEM, n=6. Number of cells/n=25. Scale bar is 20 μm. (C) Activities of lysosomal hydrolases β-galactosidase and β-hexosaminidase in crudely-purified enzymatic preparations from vehicle or palmitate treated H9C2 CMs (n=3).

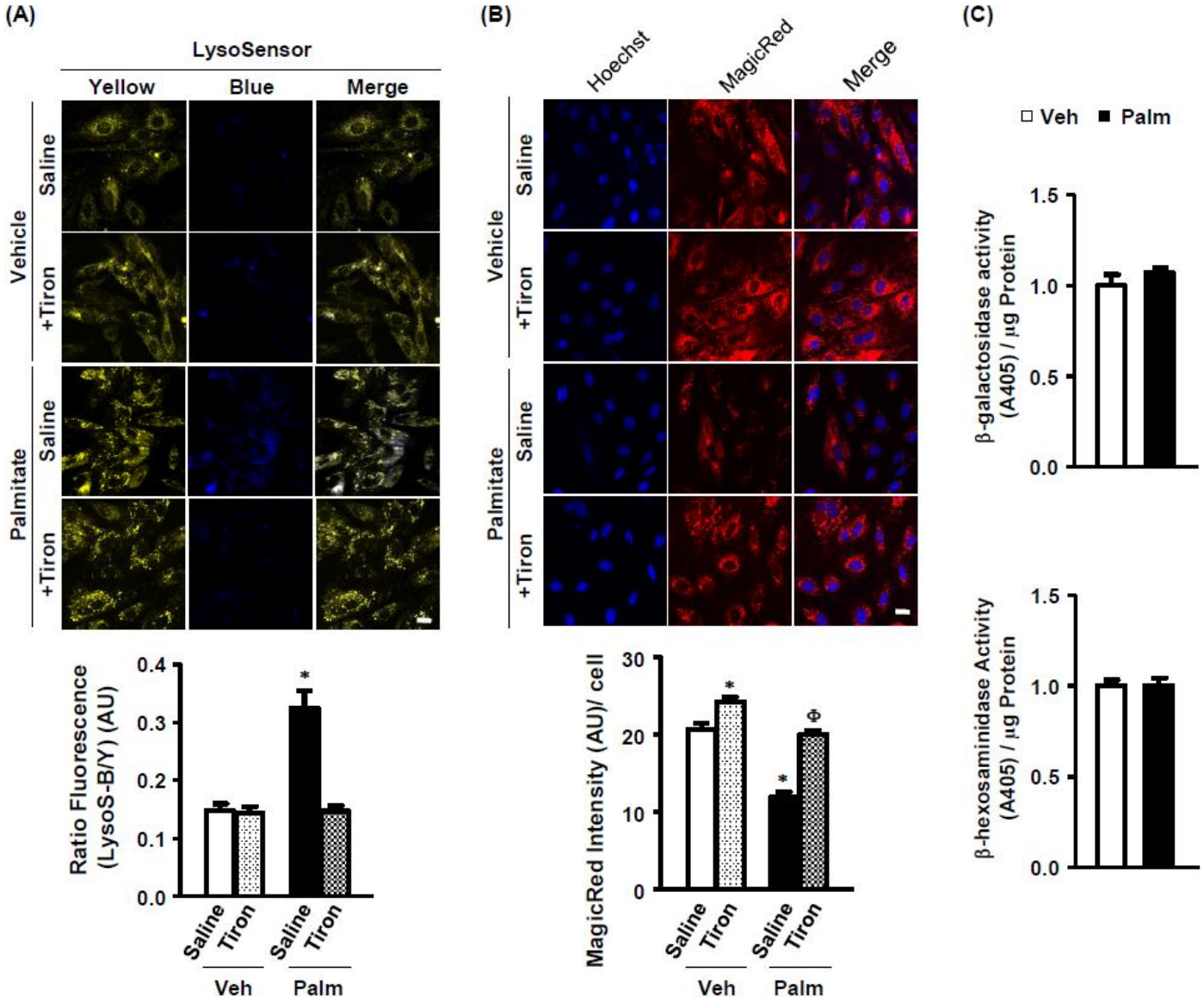
(A)
LysoSensor
Yellow
Blue
Merge
Vehicle
Palmitate
Saline
+Tiron
Ratio Fluorescence (LysoS-B/Y) (AU)
0.4
0.3
0.2
0.1
0.0
*
Saline
Tiron
Saline
Tiron
Veh
Palm
(B)
Hoechst
MagicRed
Merge
Vehicle
Palmitate
Saline
+Tiron
MagicRed Intensity (AU)/ cell
30
20
10
0
*
*
Φ
Saline
Tiron
Saline
Tiron
Veh
Palm
(C)
Veh
Palm
β-galactosidase activity (A405) / μg Protein
1.5
1.0
0.5
0.0
β-hexosaminidase Activity (A405) / μg Protein
1.5
1.0
0.5
0.0

contribute to their poor outcomes (Bugger and Abel, 2010; Sivitz, 2010). Numerous studies have recapitulated many of these features of mitochondria in cells overloaded with palmitate (Jheng et al., 2012; Yang et al., 2012; Yuzefovych et al., 2010). Growing evidence suggests that dysfunctional mitochondria are selectively cleared by mitophagy (mitochondria targeting autophagy) to protect cells from mitochondria-dependent oxidative stress and cell death (Gottlieb and Carreira, 2010; Kubli and Gustafsson, 2012). Therefore, we examined if palmitate-induced autophagy is mediated by mitochondrial superoxide. Mitochondrial superoxide was scavenged by transiently overexpressing mitochondria-targeted superoxide dismutase 2 (SOD2) in H9C2 CMs. Despite SOD2 overexpression, palmitate-induced autophagic abundance was not attenuated (Figure 3.10.A), suggesting a nonmitochondrial origin of superoxide mediating autophagy. Since the superoxide production from mitochondrial OXPHOS complexes requires substrate delivery to mitochondria, we inhibited carnitine palmitoyl transferase 1 (CPT1) with etomoxir to block the transfer of long-chain fatty acid substrates into the mitochondria. Surprisingly, etomoxir accentuated the palmitate-induced increase in LC3-II level in H9C2 CMs (Figure 3.10.B), ruling out a contribution of mitochondrial FAO to superoxide generation and palmitate-induced autophagy in H9C2 CMs. Finally, we evaluated for evidence for increased mitophagy in palmitate-treated CMs. If palmitate results in dysfunctional and depolarized mitochondria, mitophagy should be induced by palmitate. The phosphatase and tensin homolog-induced putative kinase 1 (PINK1)-Parkin interaction is required for stress-induced mitophagy. Both proteins are stabilized in depolarized mitochondria and their level is increased in mitophagy (Kubli and Gustafsson, 2012). Immunoblot analyses of mitochondrial fraction showed that PINK and

Figure 3.10. No evidence for mitochondrial superoxide production and mitophagy in palmitate-treated H9C2 CMs. (A) H9C2 CMs transfected with empty vector (pEmpty) or mitochondria-targeted SOD2 (pSOD2) were treated with vehicle or 500 μM palmitate for 4 h and were immunoblotted for SOD2 and LC3-I and II. (B) H9C2 CMs treated with vehicle or palmitate as described in (A) and with or without 50 μM etomoxir for 4 h were blotted for LC3-I and II. (C-D) H9C2 CMs treated with vehicle or palmitate for 4 h were immunoblotted for indicated proteins in the mitochondrial fraction (C) or in total cell lysate (D). Graph represents mean ± SEM. *****$p<0.05$ vs. vehicle, n=3. (B). Confocal microscopy of Ad GFP-LC3 (green) expressing H9C2 cells treated with vehicle or palmitate and subsequently incubated with anti-Tom20 antibody (red) and DAPI (blue). Scale bar is 10 μm.

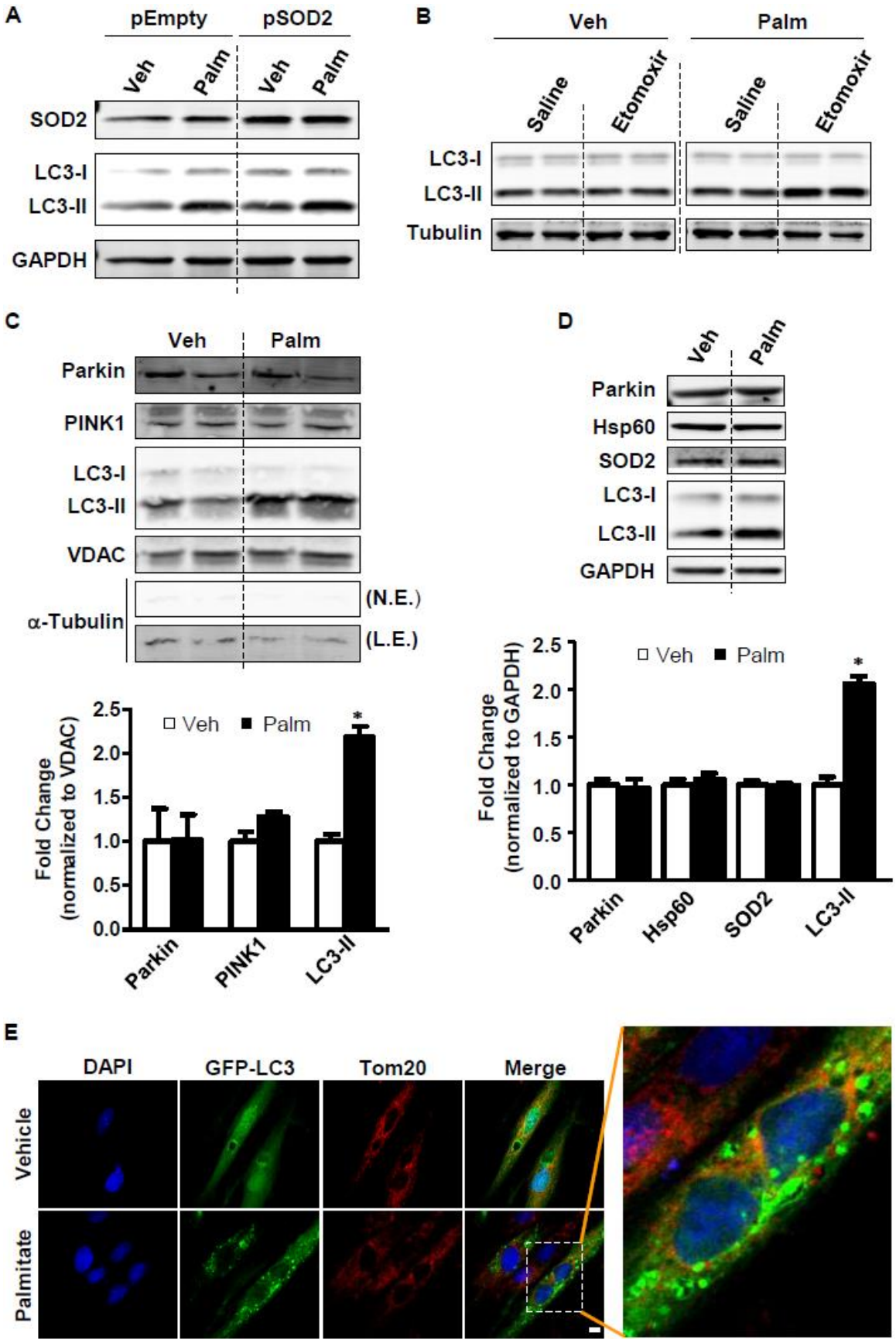
A
pEmpty
pSOD2
Veh
Palm
Veh
Palm
SOD2
LC3-I
LC3-II
GAPDH
B
Veh
Palm
Saline
Etomoxir
Saline
Etomoxir
LC3-I
LC3-II
Tubulin
C
Veh
Palm
Parkin
PINK1
LC3-I
LC3-II
VDAC
α-Tubulin
(N.E.)
(L.E.)
Fold Change (normalized to VDAC)
Veh
Palm
Parkin
PINK1
LC3-II
D
Veh
Palm
Parkin
Hsp60
SOD2
LC3-I
LC3-II
GAPDH
Fold Change (normalized to GAPDH)
Veh
Palm
Parkin
Hsp60
SOD2
LC3-II
E
DAPI
GFP-LC3
Tom20
Merge
Vehicle
Palmitate

Parkin levels were similar between vehicle and palmitate treated samples although LC3-II was significantly increased upon palmitate treatment (Figure 3.10.C). Moreover, the level of mitochondrial resident proteins Hsp60 and SOD2, which are degraded by mitophagy, remained unchanged in total cell lysates upon palmitate treatment (Figure 3.10.D). Lastly, when we immunostained H9C2 CMs expressing Ad-GFP-LC3 with the outer mitochondrial protein Tom20, we could not observe colocalization of autophagosomes (green punctae) with Tom20-positive mitochondria (red) upon palmitate treatment (Figure 3.10.E). Of note, we did not observe any changes in mitochondrial morphology in palmitate-treated CMs. Together, our data clearly showed that palmitate-induced autophagy is independent of mitochondria. Neither mitochondrial superoxide production nor mitophagy was altered by palmitate treatment.

3.3.10. Palmitate-induced autophagy is dependent on Nox2

Besides mitochondria, plasma membrane-bound NADPH oxidases (Noxs) are a major source of superoxide in cells. Nox2 and Nox4 are the major isoforms expressed in the heart (Zhang et al., 2013). Exposure to palmitate has been shown to induce Nox-derived superoxide production in cultured cells (Lambertucci et al., 2008; Maloney et al., 2009; Morgan et al., 2007). However, if Nox is involved autophagy induced by lipid-overload is not clear. Although previous studies relate ROS production to activation of autophagy, it is not clear if ROS is also involved in suppression of autophagic turnover as seen in our study. Therefore, we examined if increased superoxide production in palmitate-treated CMs is generated from Nox isoforms which could potentially be

involved in superoxide production, and if inhibiting Nox activity reverses palmitate-effect on autophagy.

Treatment with the Nox inhibitor Apocynin significantly reduced the accumulation of LC3-II in H9C2 CMs incubated with palmitate compared with untreated CMs (Figure 3.11.A). To test if apocynin reduces LC3-II levels by improving lysosomal function, we measured lysosomal enzyme CatL activity using MR substrate in live CMs. Supporting our hypothesis, apocynin significantly improved CatL activity in palmitate-treated cells (Figure 3.11.B). Surprisingly, in vehicle-treated CMs, we observed a slight increase in LC3-II level and a modest decrease in CatL activity. This effect could be due to inhibition of NOX activity below the physiological level required for acidification of endosomal vesicles that mature into lysosomes as suggested previously (Lamb et al., 2009). Although apocynin is primarily known to inhibit Nox2, it may also work as an antioxidant. To examine if Nox2 is specifically regulating palmitate-induced autophagy, we silenced Nox2 activity by siRNA mediated knockdown of its regulatory subunit p47phox. Consistent with apocynin data, silencing of Nox2 activity significantly lowered LC3-II level in palmitate-treated CMs (~31%) (Figure 3.11.C). Furthermore, knockdown of p47phox completely normalized the superoxide level in palmitate-treated CMs (Figure 3.3.D). Taken together, our data illustrate that palmitate-induced autophagosome accumulation is mediated by increased Nox2 activity which leads to increased superoxide generation and consequently impaired lysosomal function.

Figure 3.11. Palmitate-induced autophagy is dependent on Nox2 activity. (A) H9C2 CMs were incubated with vehicle or 500 μM palmitate for 4 h in presence or absence of 10 mM apocynin and immunoblotted for LC3-II. Graph represents mean ± SEM (n=3). (B) CMs treated as described in (A) were incubated with MR Cat L substrate during the last 1 h of incubation and visualized by confocal microscopy. Graphs represent MR intensity (AU) per cell. Data represent mean ± SEM, n=4. Number of cells/n=25-30. Scale bar is 20 μm. ⁎$p<0.05$ vs. vehicle-control #$p<0.05$ vs. palmitate-control. (C-D) CMs transfected with scramble (scr) or p47phox siRNA for 48 h were incubated with vehicle or palmitate for 4 h. (C) Immunoblot analyses of LC3-II and p47phox in total cell lysate, and (D) superoxide level in whole cell homogenate measured by ESR using CMH as a superoxide spin trap probe. ⁎$p<0.05$ vs. vehicle-scr #$p<0.05$ vs. palmitate-scr (n=3-6).

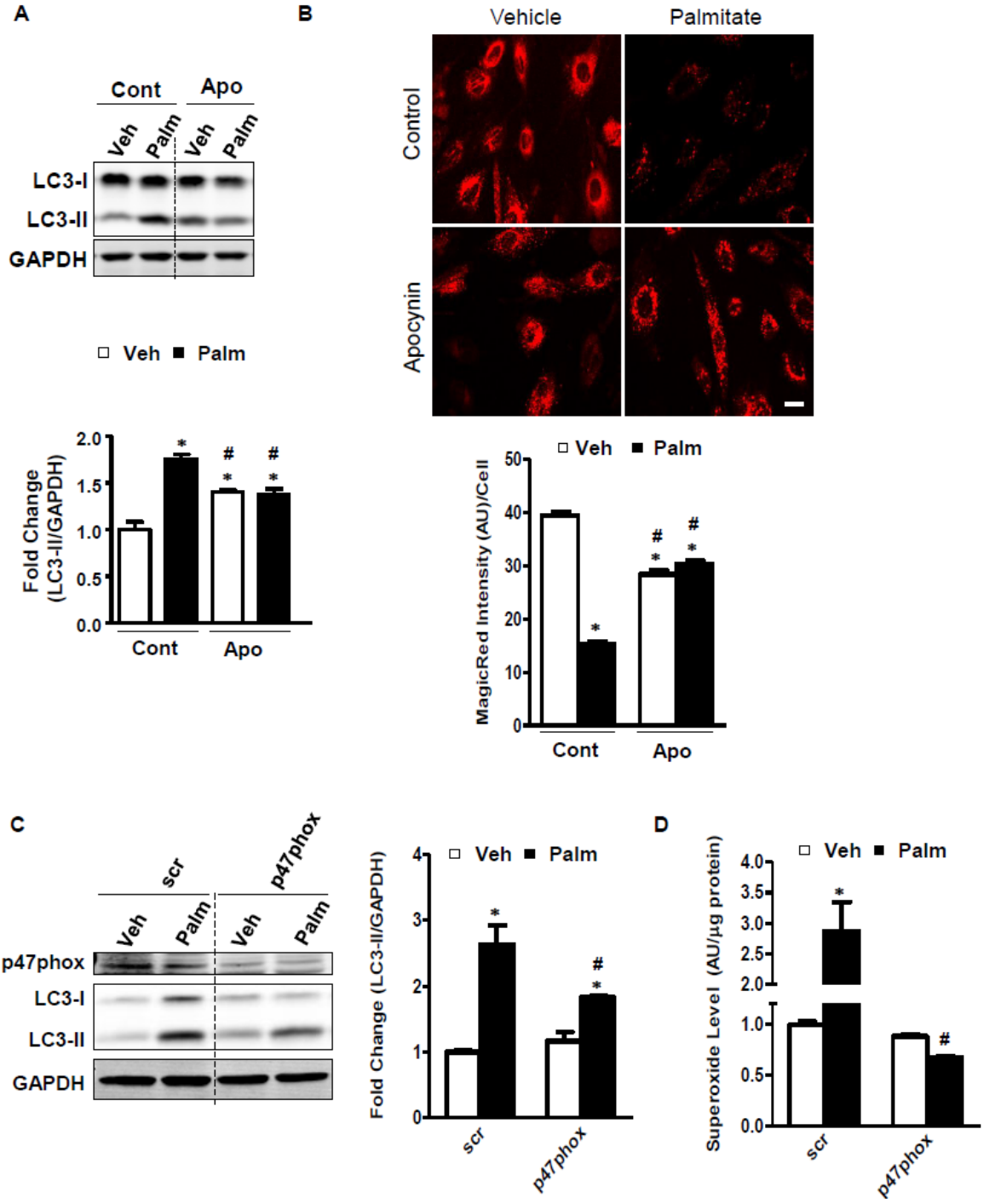
A
Cont
Apo
Veh
Palm
Veh
Palm
LC3-I
LC3-II
GAPDH
Veh
Palm
Fold Change (LC3-II/GAPDH)
2.0
1.5
1.0
0.5
0.0
Cont
Apo
B
Vehicle
Palmitate
Control
Apocynin
Veh
Palm
MagicRed Intensity (AU)/Cell
50
40
30
20
10
0
Cont
Apo
C
scr
p47phox
Veh
Palm
Veh
Palm
p47phox
LC3-I
LC3-II
GAPDH
Veh
Palm
Fold Change (LC3-II/GAPDH)
4
3
2
1
0
scr
p47phox
D
Veh
Palm
Superoxide Level (AU/µg protein)
4.0
3.5
3.0
2.5
2.0
1.0
0.5
0.0
scr
p47phox

3.3.11. Classical PKC isoforms link palmitate treatment to Nox2 activity and autophagy

To identify molecular signals that may link palmitate treatment to Nox2 activation, we examined different classes of protein kinase C (PKC). Justification for these experiments are based on a series of observations. First, palmitate has been shown to activate different PKC isoforms based on cell types (Alcazar et al., 1997; Kewalramani et al., 2011; Wang et al., 2010a). A similar activation of different PKCs have been reported in humans and animal models with obesity and diabetes (Farese and Sajan, 2012; Geraldes and King, 2010; Itani et al., 2000; Qu et al., 1999). Second, activation of PKCs was observed in parallel with activation of various Nox isoforms, and inhibition of PKCs led to inhibition of Nox activity (Gupte et al., 2009; Herrera et al., 2010; Raad et al., 2009; Siow et al., 2006). We incubated H9C2 CMs with different PKC inhibitors. GF109203x is a pan PKC inhibitor, whereas Gö6976 and rottlerin inhibit classical and novel classes of PKCs (Bynagari-Settipalli et al., 2012; Kontny et al., 2000). Immunoblot data show that generic inhibition of PKC had no significant effect on palmitate-induced autophagy (palm-control: 2.7 ± 0.124, palm-GF109203X: 2.3 ± 0.095) but led to an increase in LC3-II level in vehicle-treated CMs (veh-control: 1.0 ± 0.122, veh-GF109203X: 2.4 ± 0.199) (Figure 3.12.A). Interestingly, inhibition of novel PKCs resulted in a robust increase in LC3-II level in both vehicle and palmitate treated CMs (veh-rottlerin: 4.9 ± 0.811, palm-rottlerin: 4.1 ± 0.344). In contrast, inhibition of only classical PKCs significantly blunted palmitate-induced autophagic accumulation in CMs (palm- Gö6976: 1.7 ± 0.034). Consistent with a role of PKC in activating Nox-dependent superoxide production, inhibition of classical PKCs

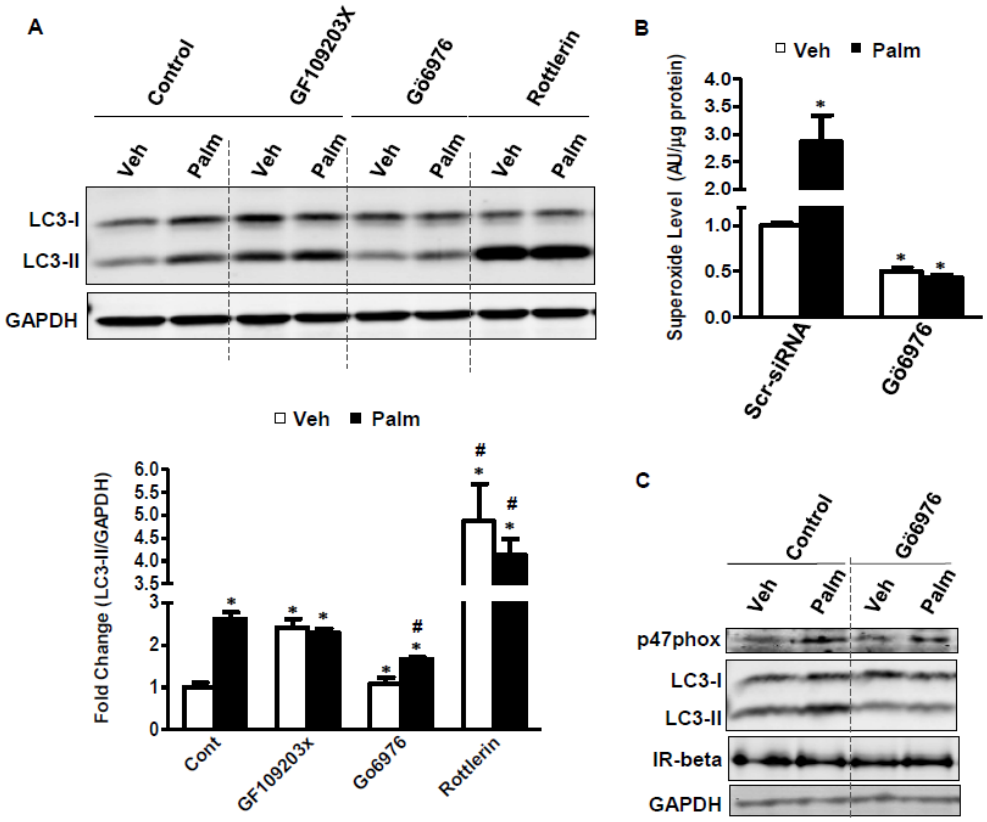

Figure 3.12. Classical PKC isoforms mediate palmitate-induced Nox2 activation and autophagy. (A) H9C2 CMs were incubated with vehicle or 500 µM palmitate for 4 h in the presence or absence of total (GF109203x), classical (Gö6976), and novel (rottlerin) PKC inhibitors and analyzed for LC3-II by immunoblotting. Graph represents mean ± SEM. ⁎p<0.05 vs. vehicle-control #p<0.05 vs. palmitate-control (n=6). (B) CMs transfected with or without scrambled siRNA for 48 h were incubated with vehicle or palmitate for 4 h in the presence or absence of Gö6976. Superoxide levels were measured by ESR using CMH as a spin probe. Graph represents normalized ESR peak intensity ± SEM (n=4-9). (C) CMs incubated with vehicle or palmitate and with or without Gö6976 for 4 h were analyzed for indicated proteins in the membrane fraction by western blot.

completely prevented palmitate-induced superoxide production in H9C2 CMs (Figure 3.12.B). Finally, immunoblot analyses of subcellular fractions showed that palmitate remarkably increased the translocation of p47phox subunit of Nox2 to the plasma membrane which is required for Nox2 activation (Figure 3.12.B). Treatment with Gö6976 partially blunted the p47phox membrane localization. These data support the involvement of classical PKCs in mediating palmitate-induced autophagosomal abundance probably by activating Nox2 and enhancing superoxide production.

3.4. Discussion

In this study, we demonstrated that lipid overload by palmitate increases cardiac autophagosome abundance primarily due to a defect in lysosomal function to degrade autophagic substrates. Studies on the regulation of cardiac autophagy in genetic and dietary models of obesity are limited. Accumulation of autophagic markers have been observed in models of DIO in parallel with hyperactivation of mTOR (Birse et al., 2010; Xu et al., 2012). However, the role of mTOR in regulating autophagy is not clear in these studies. In contrast, studies on insulin resistant T2DM mice have observed downregulated mTOR signaling in the heart while autophagy was induced (Mellor et al., 2013a). We explored the mechanisms whereby lipid overload regulates cardiac autophagy. Palmitate treatment for 4 h significantly increased both autophagy marker protein LC3-II and autophagosome number in H9C2 CMs confirming previous reports. However, signaling through Akt, AMPK, and mTOR was unaffected by palmitate treatment, indicating that pathways that activate autophagic initiation do not contribute to lipid-overload induced cardiac autophagy. Recent studies also observed an accumulation of autophagic markers

in palmitate-treated hepatocytes and pancreatic-β cells independently of pathways regulating autophagic initiation (Las et al., 2011; Tan et al., 2012). Autophagosome accumulation may also result from defective autophagic turnover as observed in Danon disease, Pompe disease, and several neurological disorders (Levine and Kroemer, 2008; Son et al., 2012). Upon blockade of autophagic turnover with CQ, we observed that the palmitate-induced increase in LC3-II level was secondary to impaired autophagosome degradation, which is supported by increased accumulation of the autophagic substrate p62 and of mCherry-GFP positive autophagosomes in palmitate-treated CMs.

In this study, we focused on the mechanism of palmitate-induced autophagy at the preclinical stage without the confounding effects of cell death. Several studies suggest a link between ER stress and autophagy in response to lipid overload (Choi et al., 2009; Yin et al., 2012). We found that acute palmitate treatment did not invoke ER-stress response at 4 h of treatment. The earliest evidence for ER stress was observed only at 8 h of treatment when the IRE1α-XBP1 axis of the UPR-pathway was activated, suggesting an ER-stress independent mechanism of autophagic regulation. As a major byproduct of palmitate metabolism, ceramide mediates a host of cytotoxic effects of lipid overload including autophagy (Pattingre et al., 2009b). We also observed an elevated ceramide level in palmitate-treated CMs. While blocking de novo ceramide biosynthesis by an SPT1 inhibitor lowered ceramide production, autophagy induced by palmitate was not altered, ruling out the role for ceramide in the autophagic process.

Elevated ROS production and ensuing oxidative stress are major hallmarks of obesity related pathologies. ROS induced cytotoxic effects have also been observed in palmitate-treated cells (Kim et al., 2010; Wen et al., 2011). Since ROS has been shown to

induce autophagy, we measured ROS production and explored its role in palmitate-induced autophagy. Palmitate incubation led to massive superoxide generation in H9C2 CMs and scavenging superoxide significantly lowered palmitate-induced autophagic accumulation. We also found that superoxide-dependent autophagy is specific to palmitate as monounsaturated FFA oleate failed to induce both superoxide production and autophagy. Oleate also reversed palmitate-induced autophagic accumulation. Our observations confirm previous reports suggesting that oleate induces different cellular response than palmitate and could antagonize various pathological effects of palmitate (Coll et al., 2008; Hu et al., 2011). Defective autophagic turnover results from various factors including reduced lysosomal content, impaired autolysosome formation, and defective lysosomal enzyme activity (Dehay et al., 2010; Koga et al., 2010; Las et al., 2011). Palmitate-treatment did not affect lysosomal protein content or autophagosome-lysosome fusion. However, we observed a defect in lysosomal enzyme activity in parallel with impaired lysosomal acidification in response to palmitate. Both lysosomal acidification and enzyme activity were normalized by scavenging superoxide, suggesting a pH-dependent defect in palmitate-treated CMs.

Mitochondria as a major source of ROS including superoxide is well documented in animal models of diabetes and in cultured cells with lipid overload (Bugger and Abel, 2008; Yang et al., 2012). We examined the role of mitochondria in palmitate-induced autophagy. Overexpression of mitochondrial superoxide dismutase (SOD2) had no effect on autophagy. Surprisingly, inhibition of CPT-1 to limit mitochondrial substrate delivery and superoxide production accentuated palmitate-induced autophagy. Moreover, features

of mitophagy were absent in palmitate-treated CMs. Therefore, our data excludes the possibility of mitochondrial involvement in palmitate-induced autophagy.

Our study has identified Nox2 as the major source of superoxide that regulates palmitate-induced autophagic abundance. Pharmacological inhibition of Nox2 activity significantly lowered autophagic abundance and enhanced lysosomal enzyme activity in palmitate-treated CMs. Likewise, RNAi mediated depletion of the Nox2 subunit p47phox blunted autophagic abundance and dramatically lowered superoxide level induced by palmitate. The activation of Nox2 in response to palmitate is mediated by classical PKC isoform, primarily PKCα. Inhibition of classical PKC attenuated palmitate-induced autophagy and prevented superoxide production in palmitate-treated CMs. More importantly, we observed increased membrane translocation of p47phox upon palmitate treatment. This translocation of p47phox, which is required for Nox2 activation, was partially blocked by inhibition of classical PKCs. In summary, our data support a model wherein palmitate activates classical PKCs which in turn promotes the formation and membrane localization of p47phox-bound Nox2 subcomplex potentially by phosphorylation of p47phox. The activated Nox2 increases superoxide production thereby impairing lysosomal acidification and pH-dependent lysosomal enzyme activity. Therefore, the increased autophagosome accumulation observed in palmitate-treated CMs could be secondary to an impairment in lysosomal function to degrade autophagic substrates.

In a mitochondria-centric world of oxidative stress and associated pathologies, the role of Nox is underappreciated. However, several studies have recognized that Nox-derived ROS contributes to numerous pathologic conditions including hypertension, I/R,

diabetes and CVD (Lassegue et al., 2012). Enhanced Nox activity and superoxide generation have been reported in experimental models of obesity and diabetes (Furukawa et al., 2004; Jiang et al., 2011), in patients with metabolic syndrome (Fortuno et al., 2006), and in diet-induced T2DM murine heart (Matsushima et al., 2009). Here, we uncovered a novel role for Nox2 in regulating autophagosome turnover by directly impacting lysosomal acidification and activity in response to lipid overload. Our study has identified a molecular regulator of autophagy in a mechanism highly relevant to obesity and can be exploited for the reactivation of autophagy as a potential therapeutic solution for obesity and metabolic syndrome (Sciarretta et al., 2012a).

CHAPTER 4

HIGH-FAT FEEDING ATTENUATES PRESSURE-OVERLOAD INDUCED CHANGES IN CARDIAC SIZE, FUNCTION, AND AUTOPHAGY

4.1. Introduction

Obesity is often accompanied by hypertension (>60%) and is probably the most common cause of left-ventricular (LV) hypertrophy. Sustained high systolic blood pressure in obese individuals is associated with concentric LV hypertrophy (Abel et al., 2008). Accumulating evidence indicates that autophagy is highly regulated in a variety of cardiac pathologies associated with obesity such as diabetes, I/R injury, hypertension and heart failure (discussed in section 1.5.2). However, the functional consequences of autophagy in obesity is unclear.

Our study in DIO mouse models revealed that HFF significantly increased autophagosome abundance in the heart without affecting cardiac contractile and hemodynamic functions. Therefore, the functional implications of such impairment in autophagic degradation is unclear. Since hypertension worsens cardiac function in many obesity-related heart diseases, we investigated how autophagy is regulated and what role it plays in pressure-overload induced hypertensive heart in HFD mice. Additionally, the regulation of autophagy and the associated changes in cardiac function in the presence of an additional stress such as pressure-overload in HFD animals may provide an insight into the functional consequence of autophagy in DIO.

4.2. Methods not described in Chapters 2 and 3

4.2.1. Transverse aortic constriction

After 8 weeks of NCD or HFD, cardiac pressure overload was introduced in a subset of WT mice by TAC by placing a 27-gauge (27-G) metal clip between the innominate

artery and the left common carotid artery. Control animals were subjected to sham surgery with no aortic constriction.

4.2.2. Cardiac contractile and hemodynamic function

Cardiac contractile function was assessed in TAC and sham operated animals every week for 4 weeks by transthoracic echocardiography using a 13 MHz linear probe (Vivid FiVe, GE Medical Systems, Milwaukee, WI). LV systolic and diastolic dimensions, wall thickness, fractional shortening, ejection fraction, and stroke volume were calculated as described previously (Riehle et al., 2011).

LV hemodynamic function was measured in mice by terminal cardiac catheterization prior to sacrificing the mice at the end of the diet regiment. These functional measurements were performed essentially as previously described (Riehle et al., 2011). Data were obtained and analyzed using LabChart7 Pro software (ADInstruments, Colorado Springs, CO).

4.3. Results

4.3.1. Body weight and heart weight measurements

Mice fed HFD for 12 weeks gained significant body weight (~29-46%) compared to NCD controls (Table 4.1). 4 weeks of TAC did not influence body weight in animals on either diet. However, TAC resulted in significant cardiac hypertrophy in NCD mice as evidenced by an increase in normalized heart weight (HW) and biventricular weight (BVW) compared to sham operated NCD mice. Most interestingly, TAC-induced cardiac

Table 4.1. Body weight, heart weight, and biventricular weight of WT mice fed with NCD or HFD for 12 weeks and subjected to sham or TAC surgery for the last 4 weeks of diet. *Effect of diet ($p<0.005$), #effect of surgery ($p<0.05$), and $interaction of diet and surgery ($p<0.05$) (n=3-5).

	NCD		HFD	
Parameters	**Sham**	**TAC**	**Sham**	**TAC**
Body Weight (g)*	27.8 ± 0.414	24.3 ± 1.716	35.9 ± 0.778	35.6 ± 3.14
Body weight/tibia length (g/mm)*	1.7 ± 0.029	1.5 ± 0.101	2.2 ± 0.044	2.2 ± 0.182
Heart weight (mg)*#$	134.2 ± 5.9	250.2 ± 40.3	133.4 ± 1.0	154.5 ± 17.4
Heart weight/tibia length (mg/mm)*#$	8.1 ± 0.337	15.2 ± 2.411	8.0 ± 0.064	9.4 ± 1.025
Biventricular weight/tibia length (mg/mm) *#$	7.3 ± 0.196	14.0 ± 2.208	7.1 ± 0.040	8.6 ± 0.985

hypertrophy was significantly blunted in HFD mice compared to TAC operated NCD mice (38% decrease in HW and BVW). These data indicate that HFF attenuates pressure overload-induced cardiac hypertrophy in mice.

4.3.2. Cardiac pressure-overload suppresses both basal and HFD-induced autophagic abundance

To understand how pressure overload by TAC may regulate cardiac autophagy in the setting of HFF, proteins involved in autophagy and its regulation were analyzed by immunoblotting in sham and TAC operated mice (Figure 4.1). Consistent with our earlier observation, HFF increased autophagic abundance in HFD mice compared with NCD controls. In contrast, TAC significantly reduced autophagy in both NCD (by 40%) and HFD (by 30%) animals as measured by LC3-II level (NCD-sham: 1.0 ± 0.082, NCD-TAC: 0.6 ± 0.109, HFD-sham: 1.34 ± 0.046, HFD-TAC: 1.0 ± 0.090). The adapter protein p62 was markedly increased in TAC-hearts than in sham-hearts on both diets (NCD-sham: 1.0 ± 0.082, NCD-TAC: 1.2 ± 0.011, HFD-sham: 0.87 ± 0.048, HFD-TAC: 0.98 ± 0.046), suggesting a suppression of autophagy upon TAC. Interestingly, Beclin1 was induced in response to TAC in NCD mice but not in HFD mice (NCD-sham: 1.0 ± 0.046, NCD-TAC: 1.4 ± 0.034, HFD-sham: 0.9 ± 0.022, HFD-TAC: 0.9 ± 0.014). However, the processing of lysosomal protein Cathepsin D (CSD) to its intermediate form (~46 kD) was significantly reduced in HFD animals and was not altered by TAC (NCD-sham: 1.0 ± 0.026, NCD-TAC: 1.0 ± 0.041, HFD-sham: 0.8 ± 0.015, HFD-TAC: 0.8 ± 0.027).

To elucidate the mechanism of TAC-induced alteration in autophagy, upstream

Figure 4.1. Reduced cardiac autophagy in response to pressure overload. Wildtype mice were fed with either a NCD or HFD for 12 weeks and analyzed for proteins involved in autophagy and its regulation in the heart. Representative immunoblots of proteins involved in the regulation of autophagy initiation (AKT, AMPK and Beclin1), mTOR signaling (S6), autophagic substrate targeting and vesicle formation (p62 and LC3), and lysosomal substrate degradation (CatD). *Effect of diet ($p<0.005$), $^{\#}$effect of surgery ($p<0.05$), and $^{\$}$interaction of diet and surgery ($p<0.05$) (n=3-5).

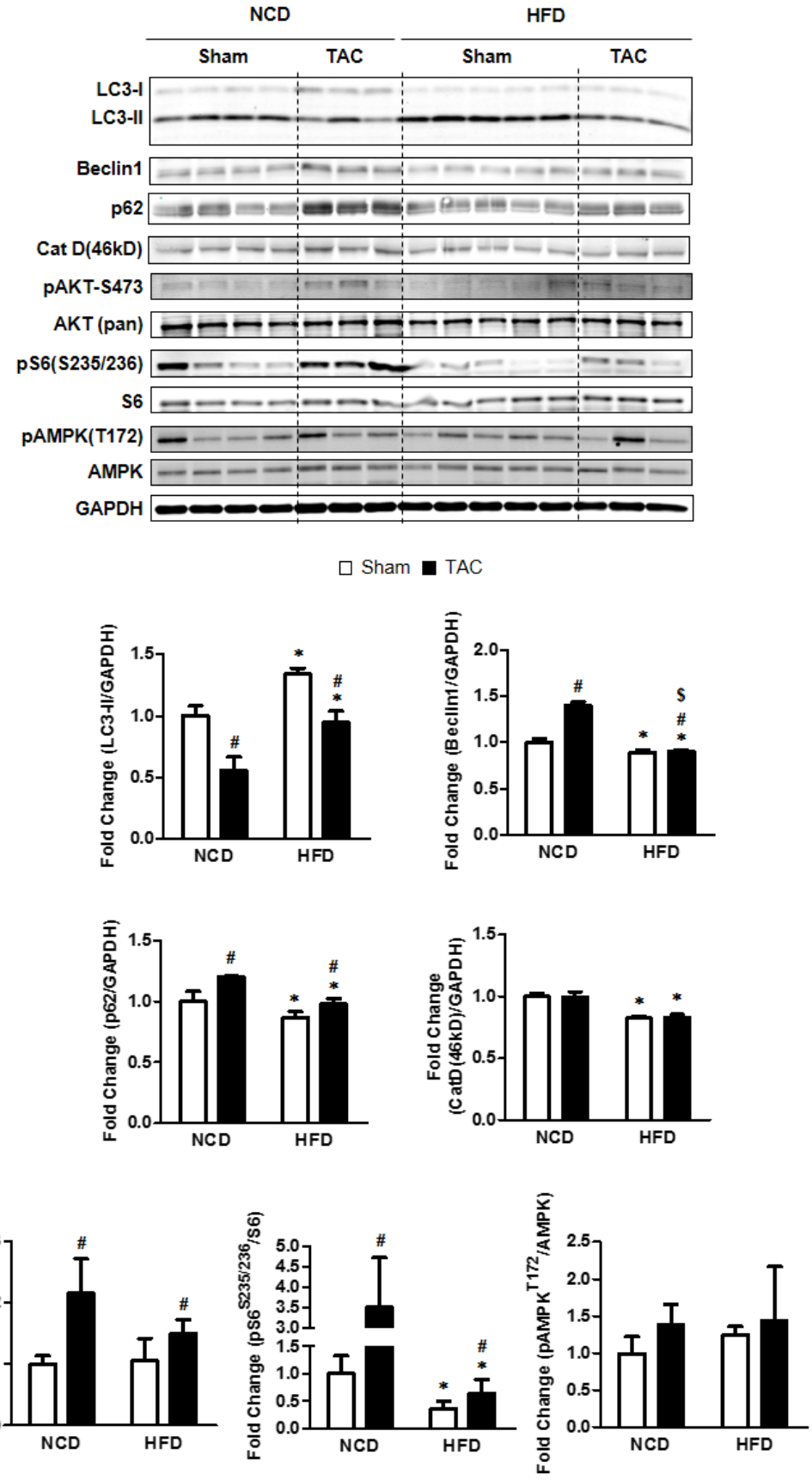
NCD
HFD
Sham
TAC
Sham
TAC
LC3-I
LC3-II
Beclin1
p62
Cat D(46kD)
pAKT-S473
AKT (pan)
pS6(S235/236)
S6
pAMPK(T172)
AMPK
GAPDH
Sham
TAC
Fold Change (LC3-II/GAPDH)
Fold Change (Beclin1/GAPDH)
Fold Change (p62/GAPDH)
Fold Change (CatD(46kD)/GAPDH)
Fold Change (pAKT S473 /AKT)
Fold Change (pS6 S235/236 /S6)
Fold Change (pAMPK T172 /AMPK)
NCD
HFD

regulatory pathways were assessed by immunoblotting. The data in Figure 4.1 show that TAC activates the AKT-mTOR signaling pathway in NCD and HFD hearts to different degrees. TAC resulted in a 2.2-fold increase in AKT-S473 phosphorylation in NCD hearts but only by 1.5-fold in HFD hearts (NCD-sham: 1.0 ± 0.137, NCD-TAC: 2.16 ±0.560, HFD-sham: 1.06 ± 0.367, HFD-TAC: 1.5 ± 0.232). Likewise, mTOR signaling measured by S6 phosphorylation was suppressed upon HFF, and TAC failed to induce S6 phosphorylation in HFD-hearts to the same extent as in NCD-hearts (NCD-sham: 1.0 ± 0.46, NCD-TAC: 3.52 ± 1.2, HFD-sham: 0.37 ± 0.18, HFD-TAC: 0.65 ± 0.25). The alternate upstream pathway regulating autophagy through AMPK was not altered at baseline or in response to TAC in both NCD and HFD mice.

4.3.3. High-fat feeding improves cardiac contractile function in mice subjected to pressure-overload

To study the impact of altered autophagy on cardiac structure and function, mice on NCD or HFD were examined by echocardiography 1, 2, 3 and 4 weeks following sham or TAC surgery. The data presented in Table 4.2 suggest that HFF per se did not alter LV dimensions in sham operated animals. However, TAC led to significant LV hypertrophy in NCD and HFD mice compared to respective sham controls. The LV diastolic dimensions measured by IVSd, LVIDd, and LVPWd were significantly increased as early as 1 week following TAC and remained higher at later time points. The TAC-induced changes in LV systolic dimensions were relatively subtle until 4 weeks of banding. Interestingly, TAC-induced LV hypertrophy was more pronounced in NCD mice than in HFD animals. For instance, IVSd, LVIDd, LVIDs and LVPWd were greater in NCD-

Table 4.2. Echocardiographic measurements in mice fed with NCD or HFD for 12 weeks and subjected to sham or TAC surgery for the last 4 weeks of diet. IVSd, interventricular septum thickness in diastole; IVSs, interventricular septum thickness in systole; LVIDd, left-ventricular internal diameter in diastole; LVIDs, left-ventricular internal diameter in systole; LVPWd, left-ventricular posterior wall thickness in diastole; LVPWs, left-ventricular posterior wall thickness in systole; EF, ejection fraction; FS, fractional shortening; HR, heart rate; SV, stroke volume. *Effect of diet ($p<0.005$), $^{\#}$effect of surgery ($p<0.05$), and $^{\$}$interaction of diet and surgery ($p<0.05$), same postsurgery time point (n=3-5).

Diet	**NCD**		**HFD**		**NCD**		**HFD**	
Surgery	**Sham**	**TAC**	**Sham**	**TAC**	**Sham**	**TAC**	**Sham**	**TAC**
Week(s) on surgery	**1**				**2**			
IVSd (cm)	0.079 ± 0.004	0.084 ± 0.011	0.074 ± 0.001	0.090 ± 0.004	0.084 ± 0.002	0.108 ± 0.003$^{\#}$	0.082 ± 0.004	0.105 ± 0.009$^{\#}$
IVSs (cm)	0.110 ± 0.002	0.117 ± 0.011	0.107 ± 0.003	0.13 ± 0.008	0.120 ± 0.007	0.136 ± 0.013$^{\#}$	0.116 ± 0.005	0.141 ± 0.012$^{\#}$
LVIDd (cm)	0.395 ± 0.013	0.417 ± 0.018	0.403 ± 0.016	0.423 ± 0.015	0.386 ± 0.004	0.417 ± 0.024	0.394 ± 0.011	0.389 ± 0.008
LVIDs (cm)	0.305 ± 0.014	0.331 ± 0.025	0.313 ± 0.015	0.331 ± 0.017	0.292 ± 0.010	0.336 ± 0.034	0.303 ± 0.009	0.301 ± 0.007
LVPWd (cm)	0.062 ± 0.002	0.076 ± 0.004	0.062 ± 0.003*	0.058 ± 0.001 $^{*\$}$	0.066 ± 0.002	0.070 ± 0.002$^{\#}$	0.062 ± 0.002	0.071 ± 0.003$^{\#}$
LVPWs (cm)	0.081 ± 0.001	0.091 ± 0.003	0.074 ± 0.008*	0.072 ± 0.003*	0.080 ± 0.005	0.085 ± 0.005	0.075 ± 0.004	0.085 ± 0.003
% EF	53.83 ± 2.248	49.94 ± 5.339	53.21 ± 1.795	52.13 ± 2.457	56.42 ± 3.327	47.47 ± 6.958	54.05 ± 1.394	53.48 ± 1.740
% FS	22.77 ± 1.227	20.79 ± 2.747	22.42 ± 0.993	21.82 ±1.331	24.34 ± 2.000	19.66 ± 3.756	22.87 ± 0.791	22.54 ± 0.977
HR (bpm)	520 ± 16	524 ± 21	543 ± 30	520 ± 40	534 ± 20	550 ± 60	532 ± 21	573 ± 56
SV(ml)	0.036 ± 0.002	0.035 ± 0.005	0.039 ± 0.003	0.041 ± 0.002	0.035 ± 0.002	0.039 ± 0.001	0.035 ± 0.003	0.034 ± 0.002

Table 4.2. (continued)

Diet	**NCD**		**HFD**		**NCD**		**HFD**	
Surgery	**Sham**	**TAC**	**Sham**	**TAC**	**Sham**	**TAC**	**Sham**	**TAC**
Week(s) on Surgery	**3**				**4**			
IVSd (cm)	0.087 ± 0.005	0.106 ± 0.009$^{\#}$	0.087 ± 0.005	0.103 ± 0.005$^{\#}$	0.089 ± 0.002	0.101 ± 0.001$^{\#}$	0.086 ± 0.004	0.097 ± 0.008$^{\#}$
IVSs (cm)	0.123 ± 0.007	0.139 ± 0.015$^{\#}$	0.117 ± 0.007	0.144 ± 0.004$^{\#}$	0.127 ± 0.003	0.131 ± 0.005	0.124 ± 0.008	0.136 ± 0.012
LVIDd (cm)	0.386 ± 0.007	0.439 ± 0.041	0.415 ± 0.011	0.407 ± 0.011	0.382 ± 0.003	0.465 ± 0.024$^{\#}$	0.407 ± 0.016	0.418 ± 0.023$^{\#}$
LVIDs (cm)	0.291 ± 0.006	0.355 ± 0.045	0.327 ± 0.012	0.313 ± 0.011	0.283 ± 0.003	0.388 ± 0.027$^{\#}$	0.314 ± 0.018	0.325 ± 0.023$^{\#\$}$
LVPWd (cm)	0.074 ± 0.008	0.069 ± 0.005	0.064 ± 0.004	0.064 ± 0.006	0.077 ± 0.002	0.071 ± 0.003	0.065 ± 0.004*	0.061 ± 0.004*
LVPWs (cm)	0.095 ± 0.007	0.086 ± 0.005	0.078 ± 0.004*	0.074 ± 0.004*	0.097 ± 0.005	0.083 ± 0.006	0.079 ± 0.003	0.078 ± 0.007
% EF	57.31 ± 0.651	47.51 ± 5.666	51.04 ± 2.025	54.27 ± 1.886$^{\$}$	58.88 ± 1.842	42.29 ± 3.666$^{\#}$	54.49 ± 2.742	53.25 ± 2.435$^{\#\$}$
% FS	24.71 ± 0.382	19.56 ± 3.028	21.24 ± 1.098	22.98 ± 1.049$^{\$}$	25.69 ± 1.095	16.82 ± 1.784$^{\#}$	23.21 ± 1.553	22.44 ± 1.369$^{\#\$}$
HR (bpm)	519 ± 18	566 ± 33	546 ± 24	563 ± 43	555 ± 43	529 ± 33	539 ± 23	567 ± 62
SV(ml)	0.037 ± 0.002	0.035 ± 0.002	0.036 ± 0.001	0.039 ± 0.003	0.035 ± 0.002	0.043 ± 0.001	0.037 ± 0.002	0.038 ± 0.003

TAC mice than in HFD-TAC mice by 4 weeks of TAC. Correspondingly, TAC resulted in impaired contractile function in NCD mice compared to NCD-sham controls as evidenced by a significant reduction in % EF and % FS after 3 weeks of banding. However, TAC- induced impairment in contractile function was blunted in mice fed with HFD. These data suggest that HFF attenuates cardiac hypertrophy and improves contractile function in mice subjected to pressure overload.

4.3.4. High-fat feeding does not alter pressure overload-induced changes in hemodynamic function

To examine the effect of cardiac pressure-overload on mice fed with HFD, hemodynamic function was measured after 4 weeks of TAC by LV catherization. TAC significantly increased LV pressure in both NCD and HFD mice evidenced by increased systolic and diastolic arterial pressure (APsys and APdia) and increased LV pressure (LVSP, LVEDP, and LVDevP) relative to sham controls (Table 4.3). More importantly, the HFD did not affect the hemodynamic profile of mice both at baseline (in sham animals) and in response to TAC-induced pressure overload.

4.4. Discussion

Hypertension is a common manifestation in obesity; it plays a causative role in hypertensive heart diseases commonly associated with obesity (Narkiewicz, 2006). Importantly, the risk for CVD is amplified only when obesity coexists with hypertension (Thomas et al., 2005), suggesting hypertension is a major contributing factor in obesity-

Table 4.3. Hemodynamic parameters obtained after LV catheterization of mice fed with NCD or HFD for 12 weeks and subjected to sham or TAC surgery for the last 4 weeks of diet. WT and Bec1-Tg mice fed with NCD or HFD. APsys, systolic arterial pressure; APdia, diastolic arterial pressure; LVSP, left-ventricular systolic pressure; LVDevP, left-ventricular developed pressure; HR, heart rate; +dP/dt, peak rate left-ventricular pressure increase; -dP/dt, peak rate of left-ventricular pressure decrease; LVEDP, left-ventricular end diastolic pressure. *Effect of diet ($p<0.005$), $^{\#}$effect of surgery ($p<0.05$), and $^{\$}$interaction of diet and surgery ($p<0.05$), same postsurgery time point (n=5-6).

Diet	**NCD**		**HFD**	
Surgery	**Sham**	**Band**	**Sham**	**Band**
APsys (mmHg)	88.32 ± 3.15	155.246 ± 13.871$^{\#}$	88.567 ± 6.442	163.671 ± 17.524$^{\#}$
APdia (mmHg)	52.11 ± 3.36	63.2128 ± 1.8882$^{\#}$	47.4658 ± 6.3555	59.2441 ± 6.3087$^{\#}$
LVSP (mmHg)	89.49± 2.83	159.25 ± 15.359$^{\#}$	85.916 ± 6.146	169.162 ± 17.104$^{\#}$
LVMP (mmHg)	-2.593 ± 0.841	3.3914 ± 3.3003	-2.2412 ± 2.0046	2.6744 ± 3.3998
LVDevP (mmHg)	92.08 ± 3.10	155.859 ± 18.462$^{\#}$	88.157 ± 4.847	166.488 ± 18.204$^{\#}$
HR (min^{-1})	477.8 ± 26.16	561.1 ± 12.847$^{\#}$	478.5 ± 24.206	485.4 ± 12.378$^{\#}$
+dP/dt (mm Hg/sec)	7600.1 ± 630.8	7984.9 ± 2112.7	6547.9 ± 589.6	7895.1 ± 1089
-dP/dt (mm Hg/sec)	-7651.7 ± 697.8	-8945.7 ± 2014.7	-8907.1 ± 2977.7	-9389.7 ± 1330.8
LVEDP (mm Hg)	3.35 ± 0.57	16.89 ± 5.33$^{\#}$	2.50 ± 2.19	10.3783 ± 2.96$^{\#}$

associated heart diseases.

Data presented in earlier chapters revealed that HFD-induced obesity is accompanied by increased autophagosome abundance in the heart. However, it is unclear whether such an increase in autophagic abundance is detrimental to the heart or is an attempt to protect heart from HFD-induced cardiac abnormalities. To understand the functional role of HFD-induced autophagy in the heart, we subjected the mice on HFD to cardiac pressure overload as an additional stress that may mimic conditions experienced by the heart in obesity; namely high-levels of circulating fatty acids and hypertension.

Both basal and HFD-induced cardiac autophagy were suppressed by TAC, albeit to different degrees. The suppression of autophagy paralleled with the activation of AKT and mTOR signaling, and accumulation of autophagic substrate protein p62, suggests that TAC inhibits the proximal arm of the autophagic induction pathway. Notably, the TAC-dependent activation of AKT and mTOR was significantly greater in NCD hearts compared with HFD hearts. Likewise, TAC-induced inhibition of autophagy was less pronounced in HFD-hearts. Furthermore, accumulation of p62 and processing of lysosomal protein CSD (~46kD) were simultaneously lower in HFD-TAC mice than in NCD-TAC mice. These data suggest that HFF partially alleviated the suppression of autophagy primarily by TAC (higher LC3-II level) primarily through the attenuation of AKT-mTOR signaling, which was sufficient to induce autophagosome turnover (low p62 level). However, the degree of autophagic turnover was still not enough to reduce autophagosomal abundance as p62 level in HFD-TAC mice was still higher than in HFD-sham mice, which was probably due to reduced lysosomal activity (lower CSD-46kD level) associated with HFF.

Phenotypic and echocardiographic measurements revealed a surprisingly beneficial affect HFF in TAC-operated hearts. HFF attenuated TAC-induced cardiac hypertrophy as HW and BVW in HFD mice was similar to sham animals and much lower than in NCD-TAC mice. Cardiac contractile function (% EF and % FS) remained preserved in TAC-operated HFD mice but worsened in NCD-TAC mice. Intriguingly, HFF had no apparent effect on changes LV hemodynamic induced by TAC as hemodynamic parameters remains similar in NCD and HFD mice.

In this study we observed that HFF partially reversed cardiac hypertrophy and impairment in contractile function induced by TAC in parallel with relatively maintained autophagic induction. Such improvement in cardiac function in HFD could be due to restoration of autophagy to normal level (similar to NCD-sham controls) by TAC, or it could an effect of HFF on pathways independent of autophagy. Moreover, it is not entirely clear from this study if TAC improved lysosomal function affecting autophagosome turnover, which may have improved cardiac function in HFD mice. Additional experiments such as fasting that induces autophagosome formation followed by cardiac function measurement may allow us to determine the directionality of changes in cardiac function in HFD-TAC animals compared to NCD-TAC controls and if such changes correlate with autophagy. Together, these results open an opportunity for further study examining a link between autophagy and HFD-induced improvement in cardiac function.

CHAPTER 5

CARDIAC AUTOPHAGY AND FUNCTION IN HIGH-FAT FED MICE ARE INDEPENDENT OF GENETIC ALTERATION IN AUTOPHAGY INDUCTION

5.1. Introduction

The role of autophagy as an adaptive or maladaptive response is context dependent (Nemchenko et al., 2011). For example, reduced autophagy in pressure overload-induced hypertrophy is considered an adaptive response since the excessive autophagy observed in chronic pressure-overload leads to heart failure. Furthermore, suppression of autophagy by genetic knockdown of Beclin1 delays the progression of pressure-overload induced heart failure (Zhu et al., 2007). In liver, 10 weeks of HFF has been shown to diminish autophagy in rat together with increased myocardial TG content. The authors suggest that reduced autophagy following 10-week HFF may be a cellular attempt to protect liver from the lipid-induced insulin resistance (Papackova et al., 2012). However, long-term HFF in mice for 20 weeks showed that defective autophagy contributes insulin resistance and restoration of autophagy improves hepatic insulin action (Yang et al., 2010). These data present a complex role of autophagy in hepatic insulin action which varies with the duration of HFF. It is important to note that autophagic response to HFF is also highly tissue dependent. The mechanism of HFD-induced autophagic regulation in the heart as observed in our study was different from hepatic autophagy as reported in previous studies. There is no data on whether the increased abundance of autophagosomes in HFD mice is protective or detrimental to the heart. In this study we tested our hypothesis that reduced autophagosomal turnover is an adaptive response of the heart to protect itself from lipid toxicity. We utilized Beclin1 heterozygous ($Bec1^{+/-}$) and cardiac-specific Beclin1 overexpressing (Bec1-Tg) mice to suppress or induce autophagic initiation, respectively, in the heart in the setting of HFF and examined the effect of these genetic alterations on autophagy and cardiac function.

5.2. Methods not described in Chapters 2, 3 and 4

5.2.1. Fasting animals

For fasting studies, mice were kept in empty cages without food for 20 h (for Beclin1$^{+/-}$ study) or 24 h (Bec1-Tg study) with free access to water and were sacrificed immediately after fasting.

5.2.2. Cardiac contractile and hemodynamic function

Cardiac contractile function was measured in wildtype (WT), Beclin1$^{+/-}$, and Bec1-Tg mice prior to and 4, 8, and 12 weeks following NCD or HFD as described in section 4.2.2. LV hemodynamic function was measured immediately prior to sacrificing the mice as described in section 4.2.2.

5.2.3. Glucose and insulin tolerance tests

Glucose tolerance test (GTT) was performed in mice following 10 weeks of NCD or HFD feeding. Mice were fasted for 6 h (6 AM -12 PM) before the test. A single bolus of glucose (1 mg/kg body weight in 0.9% saline) was administered by ip injection. Blood was drawn from tail vein and glucose levels were measured at 0, 5, 15, 30, 60, and 120 min using a standard glucometer (Bayer, IN).

Insulin tolerance test (ITT) was performed in mice following 11 weeks of NCD or HFD feeding. Random fed mice were given an ip injection of human regular insulin (Novolin R) (0.75 U/kg body weight in 0.9% saline) and blood glucose levels were measured as described for the GTT above.

5.3. Results

5.3.1. Morphometric and physiological data

Twelve weeks of HFF significantly increased body weight (BW) and heart weight (HW) in WT and $Bec1^{+/-}$ mice compared to NCD littermate controls (Table 5.1). Likewise, HFF significantly increased BW both in WT and Bec1-Tg mice but HW remained normal compared to NCD controls (Table 5.2). Fasting blood glucose levels were significantly higher in HFD mice across all genotypes compared to NCD controls.

5.3.2. Beclin1 regulates fasting induced cardiac autophagy

The $Bec1^{+/-}$ and Bec1-Tg mouse models used in this study have previously been shown to display altered autophagic activity with functional consequences in response to sTAB (Zhu et al., 2007). To revalidate the use of these models to suppress autophagy, we fasted mice and examined autophagy signaling in the heart. 15-week old WT or $Bec1^{+/-}$ male mice were fasted for 20 h (2 PM-10 AM) before harvesting the tissue. Immunoblot analyses show that autophagy in the heart, assessed by LC3-II level, was significantly induced in WT mice upon fasting relative to WT-fed mice (WT-fed: 1.0 ± 0.151, WT-fast: 1.5 ± 0.207) (Figure 5.1). The fasting-induced autophagy was blunted in $Bec1^{+/-}$ mice ($Bec1^{+/-}$-fed: 0.96 ± 0.048, $Bec1^{+/-}$-fast: 1.03 ± 0.091). Interestingly, Beclin1 level was unaltered by fasting in both WT and $Bec1^{+/-}$ mice (WT-fed: 1.0 ± 0.027, WT-fast: 0.9 ± 0.063, $Bec1^{+/-}$-fed: 1.0 ± 0.030, $Bec1^{+/-}$-fast: 0.9 ± 0.106). These data suggest that haploinsufficiency of Beclin1 plays a role in the suppression of fasting-induced autophagy in the murine heart, and validate $Bec1^{+/-}$ mouse as a relevant model to study the effect of suppression of autophagic initiation in response to a stress.

Table 5.1. Body weight, heart weight, and blood glucose level of WT and Bec1$^{+/-}$ mice fed with NCD or HFD for 12 weeks. ✱Effect of diet ($p<0.005$), $^{\#}$effect of genotype ($p<0.05$), and $^{\$}$interaction of diet and genotype ($p<0.05$) (n=10-12). †Pre- and postdiet differences in body weight.

	WT		Bec1$^{+/-}$	
Parameters	**NCD**	**HFD**	**NCD**	**HFD**
Body weight (g)✱	29.5 ± 0.7	40.0 ± 1.8	28.8 ± 0.8	40.0 ± 1.4
Body weight/tibia length (g/mm)✱	1.7 ± 0.04	2.3 ± 0.09	1.7 ± 0.04	2.3 ± 0.08
†Body weight gain (g)✱	5.9 ± 0.7	16.0 ± 1.6	5.9 ± 0.5	16.7 ± 1.0
Heart weight/tibia length (mg/mm)✱	7.8 ± 0.1	8.8 ± 0.3	8.0 ± 0.2	8.5 ± 0.2
Blood glucose (mg/dL)✱	142.9 ± 6.9	161.1 ± 13.6	135.4 ± 6.2	184.1 ± 9.8

Table 5.2. Body weight, heart weight, and blood glucose level of WT and Bec1-Tg mice fed with NCD or HFD for 12 weeks. ✱Effect of diet ($p<0.005$), $^{\#}$effect of genotype ($p<0.05$), and $^{\$}$interaction of diet and genotype ($p<0.05$) (n=12-16). †Pre- and postdiet differences in body weight.

	WT		Bec1-Tg	
Parameters	**NCD**	**HFD**	**NCD**	**HFD**
Body weight (g)✱	28.0 ± 0.5	36.5 ± 0.8	27.9 ± 0.5	35.6 ± 0.9
Body weight/tibia length (g/mm)✱	1.6 ± 0.03	2.1 ± 0.04	1.6 ± 0.03	2.1 ± 0.05
†Body weight gain (g)✱	3.4 ± 0.4	11.9 ± 0.6	3.2 ± 0.2	10.5 ± 0.9
Heart weight/tibia length (mg/mm)	7.7 ± 0.2	7.9 ± 0.2	7.8 ± 0.2	7.9 ± 0.2
Blood glucose (mg/dL)✱	131.5 ± 7.3	168.6 ± 7.6	140.1 ± 7.4	150.7 ± 7.6

Figure 5.1. Effect of altered Beclin1 expression on fasting-induced autophagy. (A) 15-week old WT and $Bec1^{+/-}$ mice were fasted for 20 h and immunblotted for indicated proteins in the heart. Densitometries of the indicated blots represent mean ± SEM (n=4-6). (B) 10-week old WT and Bec1-Tg mice were fasted for 24 h and immunblotted for indicated proteins in the heart. Densitometries of the indicated blots represent mean ± SEM (n=3). *Effect of fasting ($p<0.005$), $^{\#}$effect of genotype ($p<0.05$), and $^{\$}$interaction of fasting and genotype ($p<0.05$). See text for details.

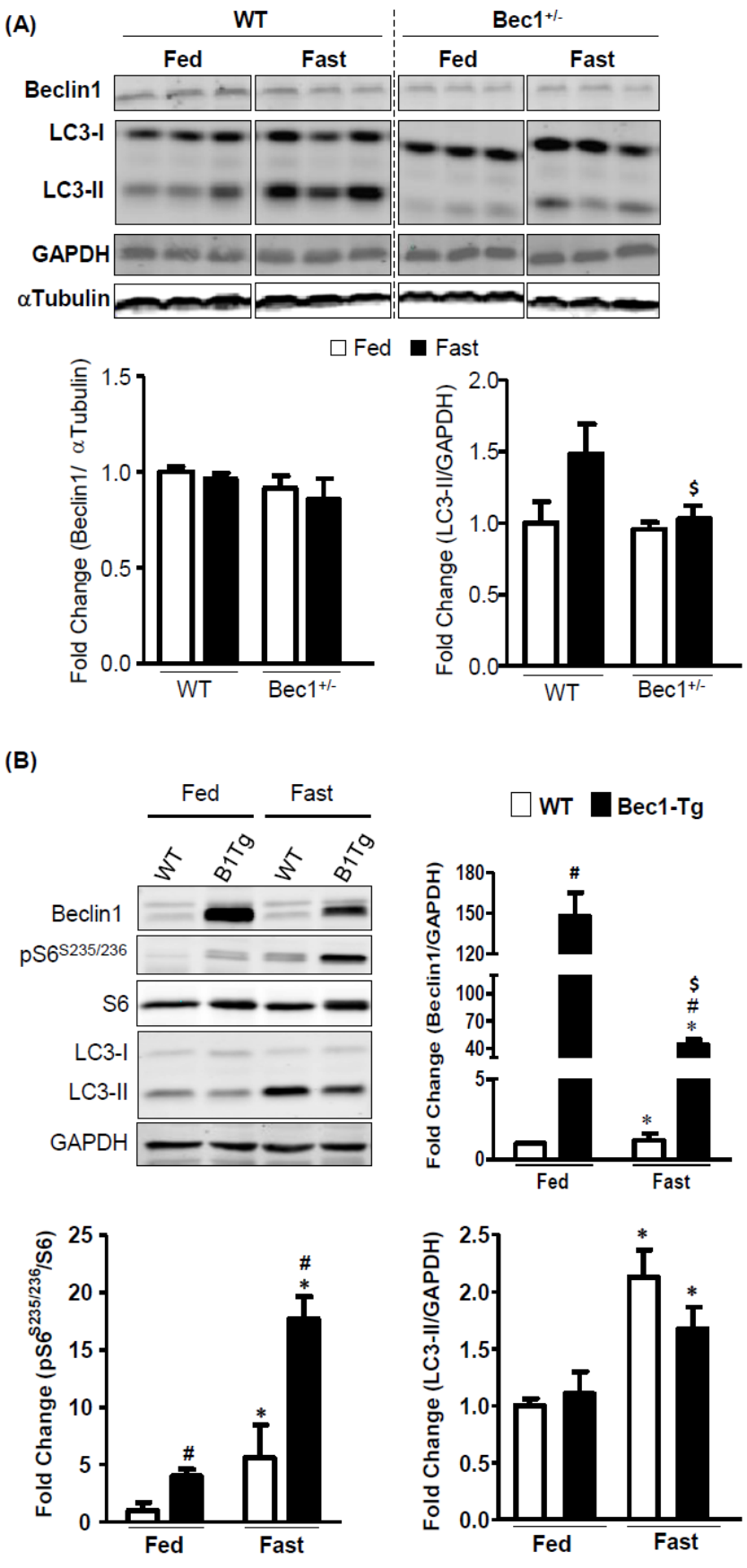
(A)
WT
Bec1+/-
Fed
Fast
Fed
Fast
Beclin1
LC3-I
LC3-II
GAPDH
αTubulin
Fed
Fast
Fold Change (Beclin1/ αTubulin)
1.5
1.0
0.5
0.0
WT
Bec1+/-
Fold Change (LC3-II/GAPDH)
2.0
1.5
1.0
0.5
0.0
$
WT
Bec1+/-
(B)
Fed
Fast
WT
B1Tg
WT
B1Tg
Beclin1
pS6S235/236
S6
LC3-I
LC3-II
GAPDH
WT
Bec1-Tg
Fold Change (Beclin1/GAPDH)
180
150
120
100
70
40
5
0
#
$
#
*
*
Fed
Fast
Fold Change (pS6S235/236/S6)
25
20
15
10
5
0
#
*
*
Fed
Fast
Fold Change (LC3-II/GAPDH)
2.5
2.0
1.5
1.0
0.5
0.0
*
*
Fed
Fast

We next examined if the cardiac overexpression Beclin1 would induce basal and fasting-induced autophagy. 10-week old WT and Bec1-Tg mice were fasted for 24 h (9 AM-9 AM) and analyzed for proteins involved in autophagy in the whole heart homogenate. The Beclin1 level was significantly higher in both fed and fasted Bec1-Tg mice compared to WT controls (WT-fed: 1.0 ± 0.02, Bec1-Tg-fed: 147.8 ± 17.40, WT-fast: 1.2 ± 0.25, Bec1-Tg-fast: 44.0 ± 5.59 (Figure 5.1). Surprisingly, Beclin1 level was significantly reduced by ~70% upon fasting in Bec1-Tg mice compared to Bec1-Tg-fed animals, which is in contrast with the general notion that Beclin1 is upregulated by fasting. Nonetheless, fasting significantly induced autophagy in both genotypes as assessed by LC3-II level (WT-fed: 1.0 ± 0.06, Bec1-Tg-fed: 1.1 ± 0.20, WT-fast: 2.1 ± 0.24, Bec1-Tg-fast: 1.7 ± 5.59). Additionally, there was a modest (~20%) decrease in LC3-II level in fasted Bec1-Tg hearts compared to fasted WT-hearts. Interestingly, phosphorylation of the mTOR target protein S6 was significantly upregulated upon fasting in mice in both genotypes (WT-fed: 1.0 ± 0.73, Bec1-Tg-fed: 4.0 ± 0.58, WT-fast: 5.6 ± 2.88, Bec1-Tg-fast: 17.7 ± 1.91). The S6 phosphorylation was more pronounced in Bec1-Tg mice than in WT mice under both fed and fasted conditions. The induction of mTOR signaling in parallel with an induction in autophagy in fasted animals is currently unclear and requires further study.

5.3.3. High-fat diet-induced autophagic abundance is unaffected by altered Beclin1 expression.

Beclin1 is known to promote autophagic initiation as downregulation of Beclin1 suppressed fasting-induced autophagy in our study as well as in others (Kang et al.,

2011). To test if knockdown of Beclin1 attenuates HFD-induced autophagic abundance, core autophagic proteins and upstream regulators of autophagy were analyzed by western blot (Figure 5.2). Consistent with our previous data, 12 weeks of HFF significantly increased cardiac autophagosome abundance as evidenced by increased LC3-II level in HFD mice than in NCD controls (WT-NCD: 1.0 ± 0.112, WT-HFD: 1.23 ± 0.025). Contrary to the role of Beclin1, autophagy in $Bec1^{+/-}$-NCD mice was higher than in WT-NCD mice. Furthermore, HFF did not cause any additional increase in autophagy in $Bec1^{+/-}$ mice above the basal level ($Bec1^{+/-}$-NCD: 1.3 ± 1.354, $Bec1^{+/-}$-HFD: 1.3 ± 0.110). Interestingly, Beclin1 protein level was not reduced in $Bec1^{+/-}$-mice compared WT controls (WT-NCD: 1.0 ± 0.056, $Bec1^{+/-}$-NCD: 1.2 ± 0.032). However, HFF led to a significant increase in Beclin1 level in either genotype (WT-HFD: 1.38 ± 0.149, $Bec1^{+/-}$-HFD: 1.45 ± 0.134). To determine if heterozygosity of Beclin1 regulates autophagic initiation pathway independent of its protein level, we examine upstream signaling molecules and autophagy proteins involved in autophagic induction. Insulin signaling through AKT trended downward in HFD animals independently of genotypes. However, mTOR signaling assessed by S6 phosphorylation remained unchanged in HFD mice. Likewise, AMPK phosphorylation also remained preserved in WT and $Bec1^{+/-}$ mice on HFD. The autophagy protein Atg7, which is upregulated upon autophagic induction, was slightly higher following HFF in WT and $Bec1^{+/-}$ mice. These data suggest that despite a trend towards an increase in some autophagic markers in HFD hearts, upstream signaling and autophagic initiation pathway essentially remained unchanged upon HFF and Beclin1 heterozygosity.

Since heterozygous Beclin1 has no apparent effect on autophagy associated with

Figure 5.2. Regulation of autophagy by high-fat feeding is unaffected by Beclin1 heterozygosity. Wildtype and $Bec1^{+/-}$ mice were fed with NCD or HFD for 12 weeks and analyzed for proteins involved in autophagy and its regulation. (A) Representative western blots of proteins involved in mTOR signaling (S6), autophagic induction (Beclin1), and autophagosome formation (LC3). (B) Representative immunoblots of proteins regulating initiation of autophagy (AKT and AMPK) and formation of LC3-II (Atg7). Densitometries of the indicated immunoblots presented as mean ± SEM. *Effect of diet ($p<0.005$), $^{\#}$effect of genotype ($p<0.05$), and $^{\$}$interaction of diet and genotype ($p<0.05$) (n=4-6). See text for details.

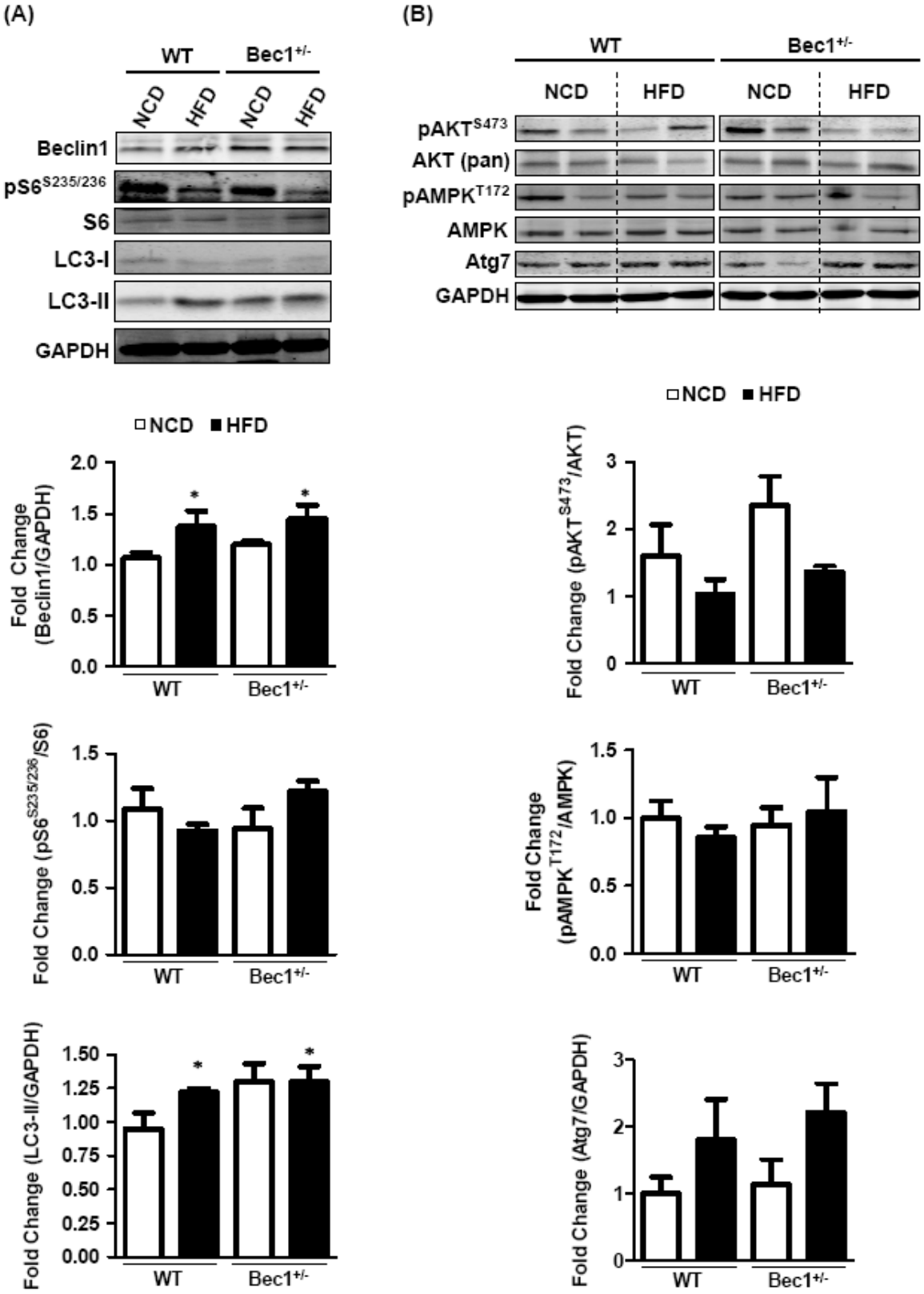
(A)
WT
Bec1+/-
NCD
HFD
NCD
HFD
Beclin1
pS6S235/236
S6
LC3-I
LC3-II
GAPDH
NCD HFD
Fold Change (Beclin1/GAPDH)
2.0
1.5
1.0
0.5
0.0
*
*
WT
Bec1+/-
Fold Change (pS6S235/236/S6)
1.5
1.0
0.5
0.0
WT
Bec1+/-
Fold Change (LC3-II/GAPDH)
1.50
1.25
1.00
0.75
0.50
0.25
0.00
*
*
WT
Bec1+/-
(B)
WT
Bec1+/-
NCD
HFD
NCD
HFD
pAKTS473
AKT (pan)
pAMPKT172
AMPK
Atg7
GAPDH
NCD HFD
Fold Change (pAKTS473/AKT)
3
2
1
0
WT
Bec1+/-
Fold Change (pAMPKT172/AMPK)
1.5
1.0
0.5
0.0
WT
Bec1+/-
Fold Change (Atg7/GAPDH)
3
2
1
0
WT
Bec1+/-

HFF, we examined if cardiac-specific Beclin1 overexpression regulates HFD-dependent autophagy. The Beclin1 level in the heart was 25-27 fold higher in transgenic animals compared to WT controls (WT-NCD: 1.0 ± 0.097, WT-HFD: 1.4 ± 0.083, Bec1-Tg-NCD (25.4 ± 2.259, Bec1-Tg-HFD: 27.5 ± 2.859) (Figure 5.3). 12 weeks of feeding significantly induced levels of the autophagy marker LC3-II in HFD mice in both genotypes compared to NCD controls (WT-NCD: 1.0 ± 0.089, WT-HFD: 1.8 ± 0.215, Bec1-Tg-NCD: 1.1 ± 0.589, Bec1-Tg-HFD: 1.9 ± 0.244), which supports our previous observation of HFD-induced autophagosomal abundance. However, the Beclin1 overexpression could not alter autophagy in both NCD and HFD mice. Although insulin signaling through AKT and mTOR signaling through ribosomal protein S6 were partially reduced, the data were highly variable and no significant difference was observed between NCD and HFD mice across both genotypes. The hyperphosphorylated form of 4E-BP1 (4E-BP1γ) has been shown to be a consequence of signaling via AKT and mTOR kinases (Gingras et al., 1998). Interestingly, the level of 4E-BP1γ was slightly upregulated in HFD mice compared to NCD controls in both genotypes (WT-NCD: 1.0 ± 0.102, WT-HFD: 1.5 ± 0.248, Bec1-Tg-NCD: 1.3 ± 0.234, Bec1-Tg-HFD: 1.5 ± 0.146, p-values = not significant), implying that AKT and mTOR signaling was maintained in HFD mice.

5.3.4. HFD-induced changes in cardiac dimension and function are independent of Beclin1 expression

To examine if genetic suppression of Beclin1 level alters cardiac function upon HFF, cardiac dimension and function were assessed by echocardiography in WT and $Bec1^{+/-}$

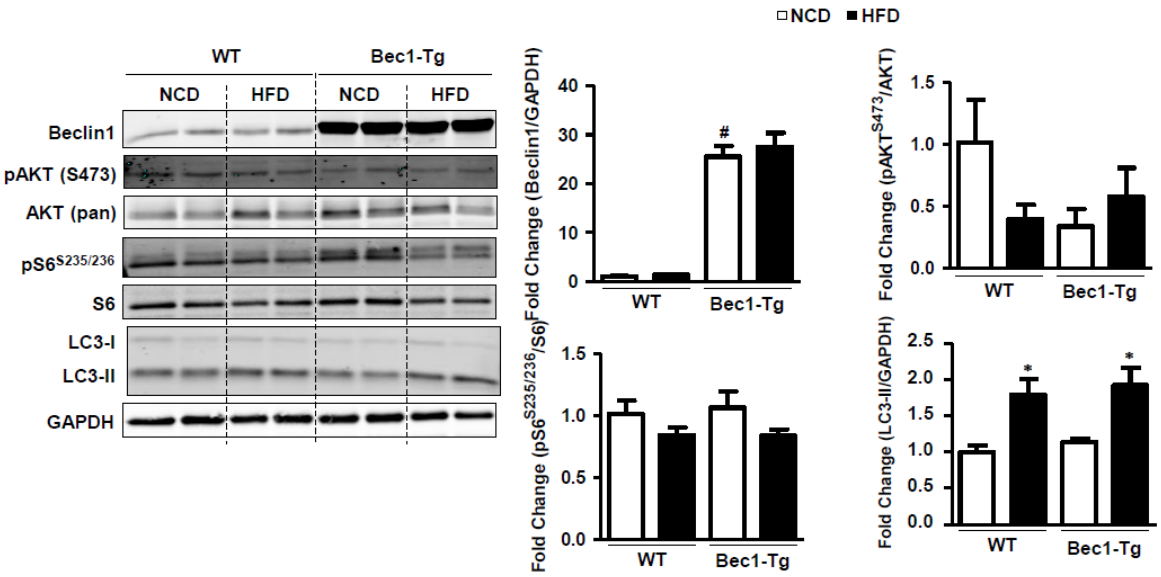

Figure 5.3. Cardiac-specific transgene expression of Beclin1 does not impact high-fat diet-induced autophagy. Wildtype and Bec1-Tg mice were fed with NCD or HFD for 12 weeks and analyzed for proteins involved in autophagy and its regulation. Representative western blots of proteins involved in mTOR signaling (S6), in the regulation of autophagic initiation (AKT and Beclin1), and in autophagosome formation (LC3). Densitometries of the indicated immunoblots presented as mean ± SEM. *Effect of diet ($p<0.005$), $^{\#}$effect of genotype ($p<0.05$), and $^{\$}$interaction of diet and genotype ($p<0.05$) (n=6-9). See text for details.

mice prior to and 4, 8, and 12 weeks following HFD or NCD feeding. HFF resulted in mild LV hypertrophy as evidenced by a significant increase in LV- wall thickness as early as 4 weeks (Table 5.3). Both IVS and LVPW were significantly higher in HFD hearts compared to NCD hearts upon 4, 8, and 12 weeks of HFF. These changes in LV-wall thickness remain preserved in $Bec1^{+/-}$ mice. More importantly, HFD mice had no impairment in cardiac contractile function. Both %EF and %FS were similar in HFD and NCD mice in both genotypes.

In contrast to $Bec1^{+/-}$ mice, Bec1-Tg mice express high level of Beclin1 in the heart compared to WT mice which enhances autophagic activity (Zhu et al., 2007). We tested if the heart-specific overexpression of Beclin1 alters cardiac structure and function in NCD and HFD mice. Cardiac dimension and contractile function were assessed before and 4, 8, 12 weeks following NCD or HFD. The data presented in Table 5.4 show that HFF leads to mild cardiac hypertrophy in both WT and Bec1-Tg mice. The LV wall thickness (IVSd, IVSs, LVPWd, and LVPWs) and systolic internal diameter (IVIDs) were slightly increased in HFD mice as early as 4 weeks of HFD and remained statistically significant at later time points. Although % EF and %FS are slightly higher in HFD mice in both genotypes compared to NCD controls, cardiac function was essentially remained within the normal range in HFD and NCD mice. The echocardiographic data suggest that HFD induces mild compensatory changes in LV-dimension without affecting contractile function. Moreover, Beclin1 heterozygosity did not impact cardiac dimension and function in both NCD and HFD animals.

Table 5.3. Echocardiographic measurements in WT and Bec1$^{+/-}$ mice fed with NCD or HFD. IVSd, interventricular septum thickness in diastole; IVSs, interventricular septum thickness in systole; LVIDd, left-ventricular internal diameter in diastole; LVIDs, left-ventricular internal diameter in systole; LVPWd, left-ventricular posterior wall thickness in diastole; LVPWs, left-ventricular posterior wall thickness in systole; EF, ejection fraction; FS, fractional shortening; HR, heart rate; SV, stroke volume. *Effect of diet ($p<0.005$), $^{\#}$effect of genotype ($p<0.05$), and $^{\$}$interaction of diet and genotype ($p<0.05$) (n=10-12).

Genotype	**WT**		**Bec1$^{+/-}$**		**WT**		**Bec1$^{+/-}$**	
Diet	**NCD**	**HFD**	**NCD**	**HFD**	**NCD**	**HFD**	**NCD**	**HFD**
Weeks on diet	**0**				**4**			
IVSd (cm)	0.07 ± 0.002	0.08 ± 0.002	0.08 ± 0.003	0.07 ± 0.002	0.077 ± 0.002	0.082 ± 0.002*	0.077 ± 0.002	0.085 ± 0.002*
IVSs (cm)	0.10 ± 0.003	0.11 ± 0.003	0.11 ± 0.003	0.10 ± 0.005	0.106 ± 0.004	0.120 ± 0.004*	0.108 ± 0.004	0.121 ± 0.003*
LVIDd (cm)	0.40 ± 0.009	0.40 ± 0.008	0.40 ± 0.007	0.39 ± 0.004	0.407 ± 0.010	0.406 ± 0.006	0.396 ± 0.005	0.400 ± 0.005
LVIDs (cm)	0.30 ± 0.012	0.28 ± 0.010	0.29 ± 0.008	0.29 ± 0.005	0.294 ± 0.012	0.282 ± 0.007	0.281 ± 0.008	0.280 ± 0.005
LVPWd (cm)	0.06 ± 0.002	0.07 ± 0.002	0.06 ± 0.002	0.07 ± 0.002	0.0645 ± 0.003	0.070 ± 0.002	0.065 ± 0.003	0.067 ± 0.002
LVPWs (cm)	0.09 ± 0.003	0.10 ± 0.004	0.09± 0.003	0.09 ± 0.004	0.090 ± 0.004	0.101 ± 0.002*	0.092 ± 0.004	0.098 ± 0.003*
% EF	59.1 ± 2.804	63.2 ± 2.178	60.3 ± 1.405	60.1 ± 1.954	62.432 ± 2.16	66.355 ± 1.57	64.254 ± 1.78	65.42 ± 1.71
% FS	26.1 ± 1.722	28.7 ± 1.457	26.6 ± 0.867	26.5 ± 1.240	28.08 ± 1.384	30.63 ± 1.078	29.23 ± 1.273	29.99 ± 1.183
HR (bpm)	532 ± 16.43	540 ± 10.93	511 ± 15.84	534 ± 11.40	499 ± 11.85	524 ± 15.79*	511 ± 20.17	547 ± 11.22*
SV(ml)	0.04 ± 0.002	0.04 ± 0.001	0.04 ± 0.001	0.04 ± 0.001	0.0411 ± 0.002	0.042 ± 0.002	0.041 ± 0.041	0.041 ± 0.001

Table 5.3. (continued)

Genotype	**WT**		**Bec1$^{+/-}$**		**WT**		**Bec1$^{+/-}$**	
Diet	**NCD**	**HFD**	**NCD**	**HFD**	**NCD**	**HFD**	**NCD**	**HFD**
Weeks on diet	**8**				**12**			
IVSd (cm)	0.075 ± 0.001	0.084 ± 0.002*	0.078 ± 0.002	0.081 ± 0.002*	0.076 ± 0.003	0.084 ± 0.003*	0.080 ± 0.001	0.0853 ± 0.003*
IVSs (cm)	0.109 ± 0.003	0.120 ± 0.004*	0.109 ± 0.004	0.116 ± 0.004*	0.109 ± 0.003	0.117 ± 0.004*	0.112 ± 0.003	0.121 ± 0.004*
LVIDd (cm)	0.414 ± 0.009	0.407 ± 0.007	0.392 ± 0.007#	0.388 ± 0.005#	0.406 ± 0.014	0.412 ± 0.011	0.406 ± 0.009	0.401 ± 0.005
LVIDs (cm)	0.291 ± 0.010	0.283 ± 0.007	0.272 ± 0.009#	0.264 ± 0.007#	0.283 ± 0.015	0.283 ± 0.011	0.277 ± 0.010	0.272 ± 0.009
LVPWd (cm)	0.068 ± 0.001	0.074 ± 0.002*	0.068 ± 0.001	0.074 ± 0.001*	0.070 ± 0.002	0.076 ± 0.002*	0.068 ± 0.003	0.075 ± 0.001*
LVPWs (cm)	0.098 ± 0.002	0.105 ± 0.003*	0.095 ± 0.003	0.103 ± 0.002*	0.097 ± 0.005	0.105 ± 0.004*	0.096 ± 0.004	0.106 ± 0.004*
% EF	65.15 ± 1.728	66.14 ± 1.243	66.45 ± 1.586	68.34 ± 1.608	65.84 ± 2.897	67.57 ± 1.623	68.15 ± 1.518	68.602 ± 2.341
% FS	29.82 ± 1.203	30.40 ± 0.834	30.67 ± 1.099	32.02 ± 1.138	30.38 ± 1.982	31.45 ± 1.150	31.813 ± 1.087	32.230 ± 1.643
HR (bpm)	519 ± 10.14	536 ± 17.01	549 ± 14.89	561 ± 16.36	512 ± 6.31	554 ± 10.65	538 ± 18.76	536 ± 19.23
SV(ml)	0.045 ± 0.002	0.042 ± 0.001	0.039 ± 0.002	0.040 ± 0.001	0.044 ± 0.004	0.044 ± 0.001	0.046 ± 0.002	0.041 ± 0.002

Table 5.4. Echocardiographic measurements in WT and Bec1-Tg mice fed with NCD or HFD. IVSd, interventricular septum thickness in diastole; IVSs, interventricular septum thickness in systole; LVIDd, left-ventricular internal diameter in diastole; LVIDs, left-ventricular internal diameter in systole; LVPWd, left-ventricular posterior wall thickness in diastole; LVPWs, left-ventricular posterior wall thickness in systole; EF, ejection fraction; FS, fractional shortening; HR, heart rate; SV, stroke volume. *Effect of diet ($p<0.005$), $^{\#}$effect of genotype ($p<0.05$), and $^{\$}$interaction of diet and genotype ($p<0.05$) (n=13-14).

Genotype	**WT**		**Bec1-Tg**		**WT**		**Bec1-Tg**	
Diet	**NCD**	**HFD**	**NCD**	**HFD**	**NCD**	**HFD**	**NCD**	**HFD**
Weeks on diet	**0**				**4**			
IVSd (cm)	0.08 ± 0.002	0.08 ± 0.002	0.76 ± 0.004	0.08 ± 0.0024	0.07 ± 0.002	0.08 ± 0.002*	0.07 ± 0.003	0.08 ± 0.003*
IVSs (cm)	0.11 ± 0.002	0.11 ± 0.003	0.10 ± 0.003	0.11 ± 0.004	0.10 ± 0.002	0.11 ± 0.004	0.11 ± 0.005	0.11 ± 0.005
LVIDd (cm)	0.39 ± .006	0.40 ± 0.010	0.40 ± 0.005	0.39 ± 0.005	0.41 ± 0.011	0.40 ± 0.006	0.41 ± 0.008	0.40 ± 0.007
LVIDs (cm)	0.27 ± 0.003	0.29 ± 0.013	0.30 ± 0.003	0.28 ± 0.007$^{\$}$	0.29 ± 0.011	0.28 ± 0.007	0.29 ± 0.009	0.29 ± 0.008
LVPWd (cm)	0.07 ± 0.004	0.06 ± 0.001	0.06 ± 0.002	0.07 ± 0.003	0.07 ± 0.003	0.07 ± 0.002	0.07 ± 0.002	0.07 ± 0.002
LVPWs (cm)	0.10 ± 0.005	0.09 ± 0.003	0.09 ± 0.004	0.09 ± 0.004	0.09 ± 0.002	0.10 ± 0.004	0.09 ± 0.003	0.10 ± 0.003
% EF	67.8 ± 1.709	62.4 ± 2.577	59.5 ± 1.556	63.9 ± 2.070	63.6 ± 1.846	66.1 ± 1.621	62.9 ± 2.678	62.3 ± 1.818
% FS	31.6 ± 1.206	28.0 ± 1.647	26.0 ± 0.942	28.9 ± 1.391	28.8 ± 1.223	30.4 ± 1.119	28.4 ± 1.755	27.9 ± 1.160
HR (bpm)	532 ± 6.073	536 ± 12.155	516 ± 8.519	532 ± 21.207	525 ± 22.482	540 ± 15.123	484 ± 16.644$^{\#}$	504 ± 13.712$^{\#}$
SV(ml)	0.04 ± 0.002	0.04 ± 0.002	0.04 ± 0.002	0.04 ± 0.001	0.04 ± 0.003	0.04 ± 0.002	0.04 ± 0.002	0.04 ± 0.002

Table 5.4. (continued)

Genotype	**WT**		**Bec1-Tg**		**WT**		**Bec1-Tg**	
Diet	**NCD**	**HFD**	**NCD**	**HFD**	**NCD**	**HFD**	**NCD**	**HFD**
Weeks on diet	**8**				**12**			
IVSd (cm)	0.08 ± 0.002	0.08 ± 0.003*	0.08 ± 0.002	0.09 ± 0.003*	0.08 ± 0.001	0.08 ± 0.001*	0.08 ± 0.002	0.08 ± 0.001*
IVSs (cm)	0.11 ± 0.003	0.11 ± 0.005*	0.11 ± 0.004	0.12 ± 0.006*	0.11 ± 0.002	0.12 ± 0.002*	0.11 ± 0.002	0.12 ± 0.003*
LVIDd (cm)	0.42 ± 0.008	0.41 ± 0.009	0.41 ± 0.004	0.40 ± 0.008	0.42 ± 0.007	0.41 ± 0.009	0.42 ± 0.007	0.40 ± 0.009
LVIDs (cm)	0.29 ± 0.008	0.28 ± 0.013	0.29 ± 0.005	0.27 ± 0.011	0.29 ± 0.007	0.28 ± 0.010*	0.29 ± 0.008	0.28 ± 0.009*
LVPWd (cm)	0.06 ± 0.002	0.07 ± 0.002*	0.06 ± 0.002	0.07 ± 0.003*	0.06 ± 0.004	0.07 ± 0.003*	0.06 ± 0.002	0.08 ± 0.001*
LVPWs (cm)	0.09 ± 0.002	0.10 ± 0.004*	0.09 ± 0.003	0.10 ± 0.004*	0.09 ± 0.004	0.10 ± 0.003*	0.09 ± 0.002	0.10 ± 0.003*
% EF	65.0 ± 0.990	66.6 ± 2.590	67.1 ± 0.856	69.5 ± 1.902	65.6 ± 1.538	68.3 ± 1.608*	64.8 ± 1.536	67.1 ± 1.876*
% FS	29.6 ± 0.654	31.0 ± 1.617*	31.0 ± 0.611	32.9 ± 1.488*	30.0 ± 1.061	32.1 ± 1.277*	29.5 ± 1.109	31.2 ± 1.292*
HR (bpm)	506 ± 19.908	518 ± 8.458	518 ± 20.295	554 ± 29.613	521 ± 19.833	531 ± 14.836	515 ± 28.005	544 ± 19.569
SV(ml)	0.05 ± 0.001	0.04 ± 0.002	0.05 ± 0.001	0.05 ± 0.001	0.05 ± 0.002	0.05 ± 0.002	0.05 ± 0.001	0.05 ± 0.002

5.3.5. LV hemodynamic functions are preserved in Bec1$^{+/-}$ mice and partially improved in Bec1-Tg mice on HFD

Following 12 weeks of HFF, LV hemodynamic function was measured in WT and Beclin1$^{+/-}$ mice by terminal LV-catheterization. The data show that both WT and Beclin1$^{+/-}$ mice have similar LV hemodynamic profiles regardless of diet (Table 5.5). These results indicate that HFF and Beclin1 heterozygosity have no effect on hemodynamic outcomes of the heart following short-term HFF. This is consistent with echocardiographic data which indicate that both WT and Beclin1$^{+/-}$ have normal cardiac contractile function.

LV hemodynamic function was also measured in Bec1-Tg and control mice following 12 weeks of NCD or HFD. HFF resulted in mild hypertension as evidenced by significant increases in systolic and diastolic arterial pressure and left ventricular systolic pressure in HFD mice (Table 5.6). Interestingly, these changes are slightly attenuated in Bec1-Tg HFD mice compared to WT-HFD mice.

5.3.6. Bec1$^{+/-}$ mice show impaired glucose tolerance but maintain insulin sensitivity upon high-fat feeding

DIO is often accompanied by systemic insulin resistance and impaired glucose tolerance. To determine if HFF impaired systemic glucose disposal and insulin sensitivity, GTT and ITT were performed on WT and Bec1$^{+/-}$ mice fed with NCD or HFD. As shown in Figure 5.4.A, mice on HFD developed significant glucose intolerance compared to NCD mice. However, glucose intolerance was remarkably higher in Bec1$^{+/-}$ mice than in WT mice HFD. These data suggest that Beclin heterozygosity worsens the

Table 5.5. Hemodynamic parameters obtained after LV catheterization of WT and Bec1$^{+/-}$ mice fed with NCD or HFD. LVSP, left-ventricular systolic pressure; LVMP, left-ventricular mean pressure; LVDevP, left-ventricular developed pressure; +dP/dt, peak rate left-ventricular pressure increase; -dP/dt, peak rate of left-ventricular pressure decrease; LVEDP, left-ventricular end diastolic pressure; Tau weiss, the time constant for left-ventricular isovolumic relaxation. *Effect of diet ($p<0.005$), $^{\#}$effect of genotype ($p<0.05$), and $^{\$}$interaction of diet and genotype ($p<0.05$) (n=4-6).

Group	**WT**		**Bec1$^{+/-}$**	
Diet	**NCD**	**HFD**	**NCD**	**HFD**
LVSP (mmHg)	94.70 ± 3.8	109.16 ± 7.148	101.01 ± 2.467	101.65 ± 5.034
LVMP (mmHg)	0.204 ± 0.9	-0.966 ± 0.369	-0.477± 0.635	-1.028 ± 0.470
LVDevP (mmHg)	94.49 ± 4.2	110.13 ± 7.271	101.48 ± 2.606	102.68 ± 5.258
HR (min-1)$^{\#}$	417.3 ± 10.1	408.4 ± 31.208	468.5 ± 24.919	468.6 ± 17.598
+dP/dt (mm Hg/sec)	6433 ± 647.0	8134 ± 711.93	8000 ± 786.40	7931 ± 566.33
-dP/dt (mm Hg/sec)	-6769 ± 1012.4	-8048.3 ± 1108.0	-7562 ± 1177.1	-8218 ± 421.0
LVEDP (mm Hg)	9.745 ± 2.6	8.238 ± 1.627	10.568 ± 1.926	7.924 ± 1.000
Tau weiss (sec)	0.022 ± 0.01	0.014 ± 0.0	0.016 ± 0.004	0.012 ± 0.001

Table 5.6. Hemodynamic parameters obtained after LV catheterization of WT and Bec1-Tg mice fed with NCD or HFD. APsys, systolic arterial pressure; APdia, diastolic arterial pressure; LVSP, left-ventricular systolic pressure; LVDevP, left-ventricular developed pressure; HR, heart rate; +dP/dt, peak rate left-ventricular pressure increase; -dP/dt, peak rate of left-ventricular pressure decrease; LVEDP, left-ventricular end diastolic pressure; Tau weiss, the time constant for left-ventricular isovolumic relaxation. *Effect of diet ($p<0.005$), $^{\#}$effect of genotype ($p<0.05$), and $^{\$}$interaction of diet and genotype ($p<0.05$) (n=5-8).

Genotype	**WT**		**Bec1-Tg**	
Diet	**NCD**	**HFD**	**NCD**	**HFD**
APsys (mmHg)$^{* \$}$	95.35 ± 2.907	110.28 ± 2.319	98.31 ± 1.157	100.47 ± 2.842
APdia (mmHg)*	64.01 ± 1.843	74.52 ± 1.913	63.66 ± 1.837	68.62 ± 1.221
LVSP (mmHg)$^{* \$}$	97.96 ± 4.061	111.2 ± 2.691	99.39 ± 1.661	100.53 ± 2.779
LV Dev P (mmHg)	96.90 ± 5.406	110.18 ± 3.390	100.61 ± 2.083	98.94 ± 3.150
HR (min-1)	454.2 ± 28.318	478.5 ± 7.991	475.3 ± 17.268	451.1 ± 23.847
+dP/dt (mm Hg/sec)	7325 ± 1019	8543 ± 801.8	8914 ± 597.9	7406 ± 542
-dP/dt (mm Hg/sec)	-7433 ± 1385.6	-7959 ± 904.2	-8586 ± 977.8	-6240 ± 735.1
LVEDP (mm Hg)	15.691 ± 4.223	15.398 ± 3.420	9.259 ± 1.797	16.366 ± 1.029
Tau weiss (sec)	0.018 ± 0.005	0.023 ± 0.007	0.013 ± 0.002	0.023 ± 0.004

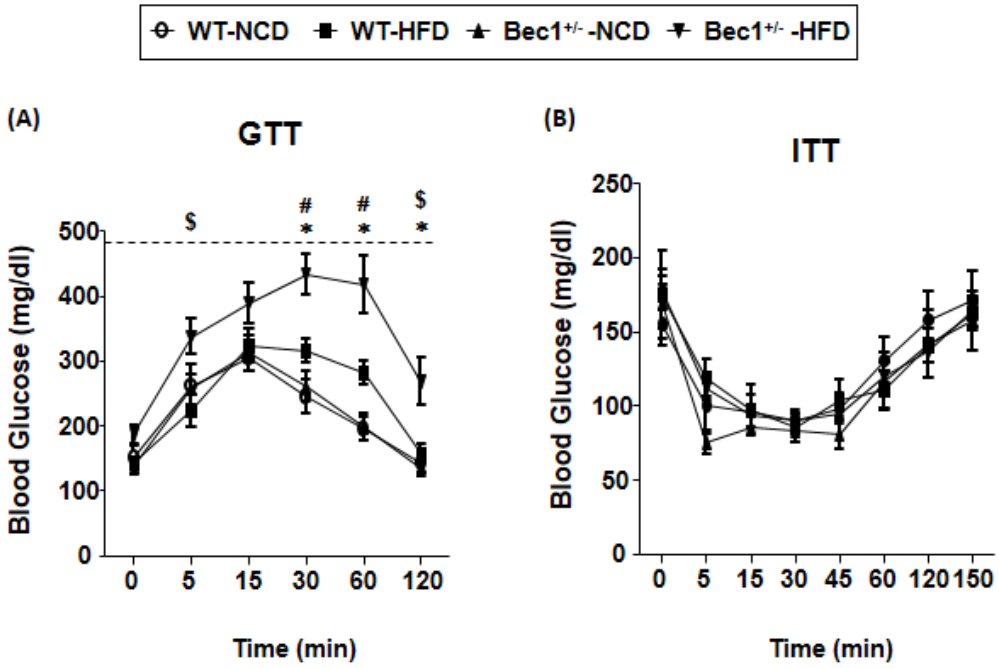

Figure 5.4. Glucose and insulin tolerance tests in NCD or HFD fed WT and Bec1$^{+/-}$ mice. (A) Glucose tolerance tests (GTTs) performed in WT and Bec1$^{+/-}$ mice following 12 weeks of NCD or HFD. The graphs represent levels of blood glucose at indicated time points following a single ip glucose injection. All mice were fasted for 6 h prior to GTTs. *Effect of diet ($p<0.005$), $^{\#}$effect of genotype ($p<0.05$), and $^{\$}$interaction of diet and genotype ($p<0.05$), same time point (n=6-9). (B) Insulin tolerance tests (ITTs) performed in WT and Beclin1$^{+/-}$ mice fed ad libitum with NCD or HFD for 12 weeks. The graphs represent blood glucose levels at indicated time points following a single ip insulin injection (n=4-7). See text for details.

impairment in systemic glucose disposal in HFD animals. Despite impaired glucose tolerance, $Bec1^{+/-}$-HFD mice showed normal insulin sensitivity in ITTs (Figure 5.4.B). The WT-HFD mice also maintained normal insulin sensitivity.

5.4. Discussion

Altered autophagic activity has been observed under various conditions affecting cardiac function such as IR, hypertension, cardiac hypertrophy and heart failure. The induction of autophagy could be both beneficial as in ischemia and compensatory cardiac hypertrophy and detrimental as in reperfusion and heart failure. Mouse models of altered Beclin1expression have been used to modulate autophagy and to define its role in response to hemodynamic stress in the heart (Gottlieb and Mentzer, 2012; Zhu et al., 2007). In this study, we utilized the same genetic models to understand if the increased autophagic abundance in the murine heart is an adaptive or maladaptive response to HFF.

We initially tested whether Beclin1 plays a role in autophagy in presence of a known stressor such a starvation to validate the use of $Bec1^{+/-}$ and Bec1-Tg mouse models for the regulation of autophagy initiation. As expected, $Bec1^{+/-}$ mice have blunted response to starvation-induced autophagy. Intriguingly, we did not observe induction of autophagy in Bec1-Tg mice in both fed and fasted states. Of note, Beclin1 expression was similar in $Bec1^{+/-}$ mice and WT mice but significantly upregulated in Bec1-Tg mice in both fed and fasted states.

Modulation of autophagic response by altering gene expression is a means to understand the mechanism and function of autophagy. In this study, utilizing mouse models of differential Beclin1 expression, we sought to understand the role of increased

autophagic abundance in response to HFF. HFD significantly elevated autophagosomal abundance in WT murine hearts. However, autophagy was not suppressed in HFD-fed $Bec1^{+/-}$ mice. Moreover, overexpression of Beclin1 did not augment HFD-induced autophagosomal abundance in Bec1-Tg hearts. These data suggest that Beclin1-dependent autophagic regulation plays no major role in HFD-induced autophagy.

Examination of cardiac function in the heart revealed that 12 weeks of HFD induced mild cardiac hypertrophy with increased LV wall thickness but preserved contractile function. The HFD induced changes in cardiac hypertrophy are not corrected by heterozygous deletion of Beclin1 or by CM-specific Beclin1 overexpression. Moreover, we observed minor changes in LV systolic and diastolic functions in HFD animals, which are unaffected by Beclin1 knockdown. Although, Bec1-Tg mice exhibit slightly better hemodynamic function (higher %EF and %FS) than WT mice on HFD, it is difficult to interpret it as an improvement since WT HFD mice did not have impaired hemodynamic function. It seems reasonable from these observations to assume that the HFF protocol used in this study did not present sufficient or appropriate stress to invoke marked changes in cardiac and hemodynamic functions. Previous studies showed that Beclin1 plays a role in autophagy only in presence of severe stress but not under basal conditions (He et al., 2012; Zhu et al., 2007). Our HFD regimen might not reach the threshold of stress necessary to induce Beclin1 signaling. Thus alterations in Beclin1 gene expression in either direction had no obvious impact on contractile and hemodynamic function of the heart in our model of DIO. However, it is important to note that $Bec1^{+/-}$ and Bec1-Tg mice used in this study have previously been shown to regulate autophagy in heart failure induced by sTAB as well as in response to 48-h fasting (Zhu et al., 2007).

Although alteration of Beclin1 expression showed no impairment in cardiac function, at the systemic level heterozygous Beclin1 worsens glucose intolerance induced by HFF. However, $Bec1^{+/-}$ mice fed with NCD showed normal glucose tolerance. This is consistent with a previous study showing that Beclin1 signaling is required to maintain normal glucose tolerance only when presented with a stress such as exercise and HFF but not under basal conditions (He et al., 2012). Since $Beclin1^{+/-}$ mice used in our study are heterozygous for the whole body, it is likely that HFD induced glucose intolerance is worsened in these mice due to lack of adequate Beclin1 signaling in tissues maintaining blood glucose such as liver, skeletal muscles and pancreatic beta cells. Since ITT profiles of both WT and $Bec1^{+/-}$ mice were normal on NCD or HFD, glucose intolerance in $Bec1^{+/-}$ HFD mice implies a defect pancreatic β cells in these mice upon HFF.

In summary, this study demonstrates that HFD-induced autophagy may be independent of autophagic initiation and particularly Beclin1 expression or activity. The differential effect of Beclin1 on autophagy induced by starvation versus HFD suggests that the regulation of autophagy by Beclin1 may depend on factors other than its protein level alone. In fact, recent studies showed that Beclin1 activity is regulated by PTMs such as phosphorylation and K-63 linked ubiquitination (Kang et al., 2011). It might be possible that Beclin1 undergoes different degrees or types of PTMs in response to starvation compared to HFF. Further study is required to define which aspects of these changes contribute to Beclin1 function under a given set of autophagic stress.

CHAPTER 6

IMPLICATIONS AND FUTURE DIRECTIONS

6.1. Restoration of autophagic turnover

Obesity is a complex metabolic condition that adversely affects proper sensing and utilization of nutrients at cellular and organismic levels. Derangement of the metabolic and energetic homeostatic apparatus leads to the emergence of insulin resistance, lipotoxicity and other metabolic disturbances in obese and diabetic hearts (Boudina and Abel, 2007). Autophagy has emerged as a prosurvival pathway protecting the heart against various metabolic and mechanical stressors (Nishida et al., 2009). Conceivably, deregulation of autophagic activity is associated with several cardiac pathologies including I/R, MI, hypertension, and heart failure (Chiong et al., 2011). Relevant to obesity and diabetes, an animal model of DIO has shown impaired autophagic turnover in the heart (Xu et al., 2012). However, whether defective turnover was due to impaired autolysosome formation or impaired lysosomal enzyme activity was unclear. In this study, we showed that HFF increased autophagic abundance in the murine heart, and, using an in vitro model of lipid overload, provided evidence for a pH-dependent impairment in lysosomal enzyme activity as a primary mechanism of defective autophagic turnover leading to increased autophagosome abundance.

ROS mediated oxidative stress plays a central role in several metabolic diseases such as CVD, atherosclerosis, and diabetes. However, antioxidant therapy to treat such diseases has produced limited success, which warrants the need for targeting pathways that have evolved to eliminate the sources of ROS and limit ROS-induced cellular damage. Strong evidence suggests the role of autophagy in mitigating ROS-induced oxidative injury and improving cell survival. Conversely, impaired autophagic activity

sensitizes cells to oxidative injury (Dutta et al., 2013; Kiffin et al., 2006; Lee et al., 2012).

Mitochondrial ROS has long been known as a primary contributor of oxidative stress. However, in a more clinically relevant model of DIO and diabetes, membrane bound Noxs seemed to be an important determinant of oxidative stress (Feillet-Coudray et al., 2009; Jiang et al., 2011; Roberts et al., 2006; Wong et al., 2011). In the heart, Nox-derived ROS has been implicated in I/R injury, MI, cardiac hypertrophy and heart failure (Bedard and Krause, 2007). Here, we have identified a novel role for Nox2-derived superoxide anion in the impairment of lysosomal enzyme activity that blunted autophagosome turnover. The Nox2 activation was directly regulated by classical PKCs in response to lipid overload. Nox2 has previously been shown to regulate autophagy in phagocytes and endothelial cells (Buroker et al., 2012; Teng et al., 2012). Several studies showed that Nox2 is directly activated by various PKCs (Raad et al., 2009; Serpillon et al., 2009). However, the role of the PKC-Nox2 pathway in the regulation of autophagy is unknown. Despite the activation of this pathway in experimental models of obesity and diabetes, little is known about its role in the important homeostatic process of autophagy.

For strategies focusing on the "reactivation of autophagy as a therapeutic solution to obesity and metabolic syndrome" (Sciarretta et al., 2012a), our study provides a promising target. Given the role of Nox-derived ROS in multiple cardiac pathologies, it is not unreasonable to assume that Nox-induced inhibition of autophagic turnover may contribute to the pathogenesis of these diseases. Therefore, pharmacological inhibition of Nox carries the prospect of not only restoring the normal autophagic turnover but also having beneficial effect on pathologies associated with Nox activation. In fact, the

interest for the identification and development of small molecule Nox inhibitors has greatly increased in the past decade (Jaquet et al., 2009). However, the generation of a Nox inhibitor may be particularly challenging for its specificity. There are multiple isoforms of Nox which are highly tissue-specific and which possess different tissue-specific physiological functions (Streeter et al., 2013). A specific inhibitor should act on only its intended target without affecting other isoform-specific functions. At present relatively few Nox-inhibitors have been successfully used in experimental models, and the next challenge is to translate this success into developing a drug-like, specific Nox inhibitor for in vivo and clinical uses.

6.2 Future directions

The major finding of the present study is that the impairments in lysosomal acidification and pH-dependent lysosomal enzyme activity led to increased autophagosome accumulation in H9C2 CMs in response to palmitate. The impaired autophagic turnover was also observed in high-fat fed mouse hearts, suggesting it to be a common phenomenon in response to lipid overload. We identified PKC-induced Nox2 activation the key mechanism mediating the effect of lipid overload on lysosomal acidification and enzyme activity. Together with a previously reported role in oxidative stress and its implication in various cardiac pathologies, the findings of the present study suggest that Nox2 may play a key role in the activation of multiple pathophysiological pathways by impairing normal autophagic flux in CMs and possibly in other tissues.

The present study raises several questions that require further investigation. First, we explored the role of Nox2 in lipid-induced autophagy. However, Nox4 is another Nox

isoform highly expressed in the heart. It has been shown to mediate oxidative stress in multiple cardiac pathologies (Kuroda et al., 2010; Matsushima et al., 2013). A recent report has implicated Nox4 in starvation-induced autophagy in CMs (Sciarretta et al., 2012c). Whether Nox4 also plays a role in lipid-induced autophagic regulation needs further study.

Second, we showed that palmitate-induced activation of Nox2 was mediated by classical PKCs. However, how palmitate activates PKC was not explored in our study. This is particularly important since coincubation with oleate normalized palmitate-induced autophagic abundance. Recent studies have shown that palmitate but not oleate impairs mitochondrial function, induces apoptosis, and activates pathways generating toxic lipid intermediates which collectively contribute to insulin resistance (Hu et al., 2011; Yuzefovych et al., 2010). Long-chain acyl-CoA, ceramide, and diacylglycerol have constantly been cited as major toxic lipid intermediates linked to lipotoxic cardiomyopathy (Wende and Abel, 2010). In our study, ceramide did not seem to play a role in palmitate-induced autophagy. Instead, a recent study has found increased DAG accumulation in parallel with increased autophagic induction in palmitate-treated hepatocytes (Tan et al., 2012). Given the role of DAG in PKC activation and our own observation of the PKC-dependent effect of palmiate on autophagy, it is likely that palmitate treatment resulted in DAG accumulation in H9C2 CMs which leads to PKC activation. Additional experiments are required to test this hypothesis and to examine if oleate prevents palmitate-induced accumulation of DAG and of autophagosomes.

Third, most of our experiments exploring the mechanism of lipid overload-induced autophagy were performed in vitro in cell culture. Therefore, to validate the

pathophysiological relevance of this mechanism, additional experiments need to be performed in our animal model of DIO. It is important to realize that observations made with acute palmitate-treatment may not be the representative of the effect of relatively long HFD feeding.

Fourth and most important, our in vivo data did not show any deleterious effect of reduced autophagosome turnover in HFD mice on cardiac function at baseline or in response to TAC. It is be possible that our HFD regimen and TAC-induced pressure overload do not present sufficient stress to induce cardiac dysfunction. Future experiments should focus on introducing sufficient, appropriate, and relevant stress to invoke cardiac dysfunction in mouse model of DIO. One such stress could be subjecting HFD mice to ischemia and reperfusion. In fact, studies suggest that HFD increases susceptibility to I/R injury but the role of autophagy in this process is not well understood (Liu and Lloyd, 2013; Mozaffari and Schaffer, 2008). Prolonging the duration of HFF or increasing the fat content in the diet have been used previously to study effect of obesity in animal models of DIO (Bagnol et al., 2012; Buettner et al., 2007). Once a cardiac dysfunction phenotype is established in DIO model, additional experiments are required to determine the role impaired autophagosome turnover in cardiac dysfunction. The presence of an appropriate stress may also allow us to re-evaluate the effect of altering autophagic initiation on HFD-induced autophagy and on cardiac function using $Bec1^{+/-}$ and Becl-Tg mouse models described in Chapter 5.

Finally, we have not assessed Nox2 expression and activity in the hearts of DIO mice. A cardiac-specific Nox2 knockout mouse would be an ideal model in which to test the relevancy of the enzyme in the regulation of autophagic turnover in DIO and diabetes.

With the availability of global Nox2 knockout mice (Pollock et al., 1995), it is now possible to examine the role of Nox2 in cardiac autophagic turnover in animal models of obesity with cardiac dysfunction.

6.3. Final conclusions

Our studies have identified a novel role for PKC-Nox signaling pathway in linking lipid overload to impairment in autophagic turnover. To our knowledge, this is the first report demonstrating that Nox2-borne superoxide anion directly impairs lysosomal acidification and consequently lysosomal enzyme activity leading to the accumulation of autophagic substrates. Together with its role as an important mediator of oxidative stress, our current findings suggest that Nox2 may exert its pathological effect in part by inhibiting normal autophagic flux. Our study provides a platform for future research in which to test the role of Nox2 in autophagic regulation in animal models of obesity and associated pathologies and to examine if restoring autophagic flux by targeted inhibition of Nox2 could provide therapeutic solution to some obesity related abnormalities.

REFERENCES

1998. Clinical Guidelines on the Identification, Evaluation, and Treatment of Overweight and Obesity in Adults--The Evidence Report. National Institutes of Health. *Obesity Research*. 6 Suppl 2:51S-209S.

Abel, E.D., S.E. Litwin, and G. Sweeney. 2008. Cardiac remodeling in obesity. *Physiological Reviews*. 88:389-419.

Abel, E.D., K.M. O'Shea, and R. Ramasamy. 2012. Insulin resistance: metabolic mechanisms and consequences in the heart. *Arteriosclerosis, Thrombosis, and Vascular Biology*. 32:2068-2076.

Alcazar, O., Z. Qiu-yue, E. Gine, and J. Tamarit-Rodriguez. 1997. Stimulation of islet protein kinase C translocation by palmitate requires metabolism of the fatty acid. *Diabetes*. 46:1153-1158.

An, D., and B. Rodrigues. 2006. Role of changes in cardiac metabolism in development of diabetic cardiomyopathy. *American Journal of Physiology. Heart and Circulatory Physiology*. 291:H1489-1506.

Anderson, E.J., A.P. Kypson, E. Rodriguez, C.A. Anderson, E.J. Lehr, and P.D. Neufer. 2009. Substrate-specific derangements in mitochondrial metabolism and redox balance in the atrium of the type 2 diabetic human heart. *Journal of the American College of Cardiology*. 54:1891-1898.

Avelar, E., T.V. Cloward, J.M. Walker, R.J. Farney, M. Strong, R.C. Pendleton, N. Segerson, T.D. Adams, R.E. Gress, S.C. Hunt, and S.E. Litwin. 2007. Left ventricular hypertrophy in severe obesity: interactions among blood pressure, nocturnal hypoxemia, and body mass. *Hypertension*. 49:34-39.

Azad, M.B., Y. Chen, and S.B. Gibson. 2009. Regulation of autophagy by reactive oxygen species (ROS): implications for cancer progression and treatment. *Antioxidants & Redox Signaling*. 11:777-790.

Baerga, R., Y. Zhang, P.H. Chen, S. Goldman, and S. Jin. 2009. Targeted deletion of autophagy-related 5 (atg5) impairs adipogenesis in a cellular model and in mice. *Autophagy*. 5:1118-1130.

Bagnol, D., H.A. Al-Shamma, D. Behan, K. Whelan, and A.J. Grottick. 2012. Diet-induced models of obesity (DIO) in rodents. *Current protocols in neuroscience / editorial board, Jacqueline N. Crawley ... [et al.]*. Chapter 9:Unit 9 38 31-13.

Bedard, K., and K.H. Krause. 2007. The NOX family of ROS-generating NADPH oxidases: physiology and pathophysiology. *Physiological Reviews*. 87:245-313.

Bellot, G., R. Garcia-Medina, P. Gounon, J. Chiche, D. Roux, J. Pouyssegur, and N.M. Mazure. 2009. Hypoxia-induced autophagy is mediated through hypoxia-inducible factor induction of BNIP3 and BNIP3L via their BH3 domains. *Molecular and Cellular Biology*. 29:2570-2581.

Bensaad, K., E.C. Cheung, and K.H. Vousden. 2009. Modulation of intracellular ROS levels by TIGAR controls autophagy. *The EMBO Journal*. 28:3015-3026.

Birnie, D.H., L.E. Vickers, W.S. Hillis, J. Norrie, and S.M. Cobbe. 2005. Increased titres of anti-human heat shock protein 60 predict an adverse one year prognosis in patients with acute cardiac chest pain. *Heart*. 91:1148-1153.

Birse, R.T., J. Choi, K. Reardon, J. Rodriguez, S. Graham, S. Diop, K. Ocorr, R. Bodmer, and S. Oldham. 2010. High-fat-diet-induced obesity and heart dysfunction are regulated by the TOR pathway in Drosophila. *Cell Metabolism*. 12:533-544.

Bjorkoy, G., T. Lamark, A. Brech, H. Outzen, M. Perander, A. Overvatn, H. Stenmark, and T. Johansen. 2005. p62/SQSTM1 forms protein aggregates degraded by autophagy and has a protective effect on huntingtin-induced cell death. *The Journal of Cell Biology*. 171:603-614.

Boden, G. 2011. Obesity, insulin resistance and free fatty acids. *Curr Opin Endocrinol Diabetes Obes*. 18:139-143.

Boden, G., X. Duan, C. Homko, E.J. Molina, W. Song, O. Perez, P. Cheung, and S. Merali. 2008. Increase in endoplasmic reticulum stress-related proteins and genes in adipose tissue of obese, insulin-resistant individuals. *Diabetes*. 57:2438-2444.

Bodine, S.C., E. Latres, S. Baumhueter, V.K. Lai, L. Nunez, B.A. Clarke, W.T. Poueymirou, F.J. Panaro, E. Na, K. Dharmarajan, Z.Q. Pan, D.M. Valenzuela, T.M. DeChiara, T.N. Stitt, G.D. Yancopoulos, and D.J. Glass. 2001. Identification of ubiquitin ligases required for skeletal muscle atrophy. *Science*. 294:1704-1708.

Boudina, S., and E.D. Abel. 2007. Diabetic cardiomyopathy revisited. *Circulation*. 115:3213-3223.

Bova, M.P., O. Yaron, Q. Huang, L. Ding, D.A. Haley, P.L. Stewart, and J. Horwitz. 1999. Mutation R120G in alphaB-crystallin, which is linked to a desmin-related myopathy, results in an irregular structure and defective chaperone-like function. *Proceedings of the National Academy of Sciences of the United States of America*. 96:6137-6142.

Buettner, R., J. Scholmerich, and L.C. Bollheimer. 2007. High-fat diets: modeling the metabolic disorders of human obesity in rodents. *Obesity*. 15:798-808.

Bugger, H., and E.D. Abel. 2008. Molecular mechanisms for myocardial mitochondrial dysfunction in the metabolic syndrome. *Clinical Science*. 114:195-210.

Bugger, H., and E.D. Abel. 2010. Mitochondria in the diabetic heart. *Cardiovascular Research*. 88:229-240.

Bukau, B., J. Weissman, and A. Horwich. 2006. Molecular chaperones and protein quality control. *Cell*. 125:443-451.

Buroker, N.E., J.Y. Huang, J. Barboza, D.R. Ledee, R.J. Eastman, Jr., H. Reinecke, X.H. Ning, J.A. Bassuk, and M.A. Portman. 2012. The adaptor-related protein complex 2, alpha 2 subunit (AP2alpha2) gene is a peroxisome proliferator-activated receptor cardiac target gene. *Protein J*. 31:75-83.

Bursch, W. 2004. Multiple cell death programs: Charon's lifts to Hades. *FEMS Yeast Res*. 5:101-110.

Bynagari-Settipalli, Y.S., P. Lakhani, J. Jin, K. Bhavaraju, M.C. Rico, S. Kim, D. Woulfe, and S.P. Kunapuli. 2012. Protein kinase C isoform epsilon negatively regulates ADP-induced calcium mobilization and thromboxane generation in platelets. *Arteriosclerosis, Thrombosis, and Vascular Biology*. 32:1211-1219.

Chan, E.Y. 2009. mTORC1 phosphorylates the ULK1-mAtg13-FIP200 autophagy regulatory complex. *Science Signaling*. 2:pe51.

Chen, Y., M.B. Azad, and S.B. Gibson. 2009. Superoxide is the major reactive oxygen species regulating autophagy. *Cell Death and Differentiation*. 16:1040-1052.

Chen, Z.J., and L.J. Sun. 2009. Nonproteolytic functions of ubiquitin in cell signaling. *Molecular Cell*. 33:275-286.

Chess, D.J., and W.C. Stanley. 2008. Role of diet and fuel overabundance in the development and progression of heart failure. *Cardiovascular Research*. 79:269-278.

Chiong, M., Z.V. Wang, Z. Pedrozo, D.J. Cao, R. Troncoso, M. Ibacache, A. Criollo, A. Nemchenko, J.A. Hill, and S. Lavandero. 2011. Cardiomyocyte death: mechanisms and translational implications. *Cell Death & Disease*. 2:e244.

Chiu, H.C., A. Kovacs, D.A. Ford, F.F. Hsu, R. Garcia, P. Herrero, J.E. Saffitz, and J.E. Schaffer. 2001. A novel mouse model of lipotoxic cardiomyopathy. *The Journal of Clinical Investigation*. 107:813-822.

Choi, S.E., S.M. Lee, Y.J. Lee, L.J. Li, S.J. Lee, J.H. Lee, Y. Kim, H.S. Jun, K.W. Lee, and Y. Kang. 2009. Protective role of autophagy in palmitate-induced INS-1 beta-cell death. *Endocrinology*. 150:126-134.

Clague, M.J., and S. Urbe. 2010. Ubiquitin: same molecule, different degradation pathways. *Cell*. 143:682-685.

Cnop, M., F. Foufelle, and L.A. Velloso. 2012. Endoplasmic reticulum stress, obesity and diabetes. *Trends in Molecular Medicine*. 18:59-68.

Codogno, P., and A.J. Meijer. 2010. Autophagy: a potential link between obesity and insulin resistance. *Cell Metabolism*. 11:449-451.

Coll, T., E. Eyre, R. Rodriguez-Calvo, X. Palomer, R.M. Sanchez, M. Merlos, J.C. Laguna, and M. Vazquez-Carrera. 2008. Oleate reverses palmitate-induced insulin resistance and inflammation in skeletal muscle cells. *The Journal of Biological Chemistry*. 283:11107-11116.

Cousin, S.P., S.R. Hugl, C.E. Wrede, H. Kajio, M.G. Myers, Jr., and C.J. Rhodes. 2001. Free fatty acid-induced inhibition of glucose and insulin-like growth factor I-induced deoxyribonucleic acid synthesis in the pancreatic beta-cell line INS-1. *Endocrinology*. 142:229-240.

Cox, B.E., E.E. Griffin, J.C. Ullery, and W.G. Jerome. 2007. Effects of cellular cholesterol loading on macrophage foam cell lysosome acidification. *Journal of Lipid Research*. 48:1012-1021.

Crighton, D., S. Wilkinson, J. O'Prey, N. Syed, P. Smith, P.R. Harrison, M. Gasco, O. Garrone, T. Crook, and K.M. Ryan. 2006. DRAM, a p53-induced modulator of autophagy, is critical for apoptosis. *Cell*. 126:121-134.

Czaja, M.J. 2010. Autophagy in health and disease. 2. Regulation of lipid metabolism and storage by autophagy: pathophysiological implications. *American Journal of Physiology. Cell Physiology*. 298:C973-978.

Daido, S., T. Kanzawa, A. Yamamoto, H. Takeuchi, Y. Kondo, and S. Kondo. 2004. Pivotal role of the cell death factor BNIP3 in ceramide-induced autophagic cell death in malignant glioma cells. *Cancer Research*. 64:4286-4293.

Dalakas, M.C., K.Y. Park, C. Semino-Mora, H.S. Lee, K. Sivakumar, and L.G. Goldfarb. 2000. Desmin myopathy, a skeletal myopathy with cardiomyopathy caused by mutations in the desmin gene. *The New England Journal of Medicine*. 342:770-780.

Dehay, B., J. Bove, N. Rodriguez-Muela, C. Perier, A. Recasens, P. Boya, and M. Vila. 2010. Pathogenic lysosomal depletion in Parkinson's disease. *The Journal of Neuroscience: The Official Journal of the Society for Neuroscience*. 30:12535-12544.

Deretic, V. 2006. Autophagy as an immune defense mechanism. *Curr Opin Immunol*. 18:375-382.

Dong, F., Q. Li, N. Sreejayan, J.M. Nunn, and J. Ren. 2007. Metallothionein prevents high-fat diet induced cardiac contractile dysfunction: role of peroxisome proliferator activated receptor gamma coactivator 1alpha and mitochondrial biogenesis. *Diabetes*. 56:2201-2212.

Dutta, D., J. Xu, J.S. Kim, W.A. Dunn, Jr., and C. Leeuwenburgh. 2013. Upregulated autophagy protects cardiomyocytes from oxidative stress-induced toxicity. *Autophagy*. 9:328-344.

Ebato, C., T. Uchida, M. Arakawa, M. Komatsu, T. Ueno, K. Komiya, K. Azuma, T. Hirose, K. Tanaka, E. Kominami, R. Kawamori, Y. Fujitani, and H. Watada. 2008. Autophagy is important in islet homeostasis and compensatory increase of beta cell mass in response to high-fat diet. *Cell Metabolism*. 8:325-332.

Edwards, J.M., Z.P. Neeb, M.A. Alloosh, X. Long, I.N. Bratz, C.R. Peller, J.P. Byrd, S. Kumar, A.G. Obukhov, and M. Sturek. 2010. Exercise training decreases store-operated Ca2+entry associated with metabolic syndrome and coronary atherosclerosis. *Cardiovascular Research*. 85:631-640.

Eguchi, Y., S. Shimizu, and Y. Tsujimoto. 1997. Intracellular ATP levels determine cell death fate by apoptosis or necrosis. *Cancer Research*. 57:1835-1840.

Elmore, S.P., T. Qian, S.F. Grissom, and J.J. Lemasters. 2001. The mitochondrial permeability transition initiates autophagy in rat hepatocytes. *FASEB Journal: Official Publication of the Federation of American Societies for Experimental Biology*. 15:2286-2287.

Ezaki, J., N. Matsumoto, M. Takeda-Ezaki, M. Komatsu, K. Takahashi, Y. Hiraoka, H. Taka, T. Fujimura, K. Takehana, M. Yoshida, J. Iwata, I. Tanida, N. Furuya, D.M. Zheng, N. Tada, K. Tanaka, E. Kominami, and T. Ueno. 2011. Liver autophagy contributes to the maintenance of blood glucose and amino acid levels. *Autophagy*. 7:727-736.

Farese, R.V., and M.P. Sajan. 2012. Atypical protein kinase C in cardiometabolic abnormalities. *Current Opinion in Lipidology*. 23:175-181.

Farre, J.C., and S. Subramani. 2004. Peroxisome turnover by micropexophagy: an autophagy-related process. *Trends in Cell Biology*. 14:515-523.

Feillet-Coudray, C., T. Sutra, G. Fouret, J. Ramos, C. Wrutniak-Cabello, G. Cabello, J.P. Cristol, and C. Coudray. 2009. Oxidative stress in rats fed a high-fat high-sucrose diet and preventive effect of polyphenols: Involvement of mitochondrial and NAD(P)H oxidase systems. *Free Radical Biology & Medicine*. 46:624-632.

Finkelstein, E.A., J.G. Trogdon, J.W. Cohen, and W. Dietz. 2009. Annual medical spending attributable to obesity: payer-and service-specific estimates. *Health Aff (Millwood)*. 28:w822-831.

Fortunato, F., and G. Kroemer. 2009. Impaired autophagosome-lysosome fusion in the pathogenesis of pancreatitis. *Autophagy*. 5:850-853.

Fortuno, A., G. San Jose, M.U. Moreno, O. Beloqui, J. Diez, and G. Zalba. 2006. Phagocytic NADPH oxidase overactivity underlies oxidative stress in metabolic syndrome. *Diabetes*. 55:209-215.

Fujitani, Y., R. Kawamori, and H. Watada. 2009. The role of autophagy in pancreatic beta-cell and diabetes. *Autophagy*. 5:280-282.

Furukawa, S., T. Fujita, M. Shimabukuro, M. Iwaki, Y. Yamada, Y. Nakajima, O. Nakayama, M. Makishima, M. Matsuda, and I. Shimomura. 2004. Increased oxidative stress in obesity and its impact on metabolic syndrome. *The Journal of Clinical Investigation*. 114:1752-1761.

Gal, J., A.L. Strom, R. Kilty, F. Zhang, and H. Zhu. 2007. p62 accumulates and enhances aggregate formation in model systems of familial amyotrophic lateral sclerosis. *The Journal of Biological Chemistry*. 282:11068-11077.

Garcia-Mata, R., Y.S. Gao, and E. Sztul. 2002. Hassles with taking out the garbage: aggravating aggresomes. *Traffic*. 3:388-396.

Geraldes, P., and G.L. King. 2010. Activation of protein kinase C isoforms and its impact on diabetic complications. *Circulation Research*. 106:1319-1331.

Gertz, E.W., J.A. Wisneski, W.C. Stanley, and R.A. Neese. 1988. Myocardial substrate utilization during exercise in humans. Dual carbon-labeled carbohydrate isotope experiments. *The Journal of Clinical Investigation*. 82:2017-2025.

Gingras, A.C., S.G. Kennedy, M.A. O'Leary, N. Sonenberg, and N. Hay. 1998. 4E-BP1, a repressor of mRNA translation, is phosphorylated and inactivated by the Akt(PKB) signaling pathway. *Genes & Development*. 12:502-513.

Glatz, J.F., J.J. Luiken, and A. Bonen. 2010. Membrane fatty acid transporters as regulators of lipid metabolism: implications for metabolic disease. *Physiological Reviews*. 90:367-417.

Goldberg, I.J., C.M. Trent, and P.C. Schulze. 2012. Lipid metabolism and toxicity in the heart. *Cell Metabolism*. 15:805-812.

Gottlieb, R.A., and R.S. Carreira. 2010. Autophagy in health and disease. 5. Mitophagy as a way of life. *American Journal of Physiology. Cell Physiology*. 299:C203-210.

Gottlieb, R.A., and R.M. Mentzer, Jr. 2012. Autophagy: an affair of the heart. *Heart Failure Reviews*. DOI 10.1007/s10741-012-9367-2, Springer, US.

Graves, A.R., P.K. Curran, C.L. Smith, and J.A. Mindell. 2008. The Cl-/H+ antiporter ClC-7 is the primary chloride permeation pathway in lysosomes. *Nature*. 453:788-792.

Gupte, S.A., P.M. Kaminski, S. George, L. Kouznestova, S.C. Olson, R. Mathew, T.H. Hintze, and M.S. Wolin. 2009. Peroxide generation by p47phox-Src activation of Nox2 has a key role in protein kinase C-induced arterial smooth muscle contraction. *American Journal of Physiology. Heart and Circulatory Physiology*. 296:H1048-1057.

Gustafsson, A.B., and R.A. Gottlieb. 2008. Recycle or die: the role of autophagy in cardioprotection. *Journal of Molecular and Cellular Cardiology*. 44:654-661.

Gustafsson, A.B., and R.A. Gottlieb. 2009. Autophagy in ischemic heart disease. *Circulation Research*. 104:150-158.

Ha, T., Y. Li, X. Gao, J.R. McMullen, T. Shioi, S. Izumo, J.L. Kelley, A. Zhao, G.E. Haddad, D.L. Williams, I.W. Browder, R.L. Kao, and C. Li. 2005. Attenuation of cardiac hypertrophy by inhibiting both mTOR and NFkappaB activation in vivo. *Free Radical Biology & Medicine*. 39:1570-1580.

He, C., M.C. Bassik, V. Moresi, K. Sun, Y. Wei, Z. Zou, Z. An, J. Loh, J. Fisher, Q. Sun, S. Korsmeyer, M. Packer, H.I. May, J.A. Hill, H.W. Virgin, C. Gilpin, G. Xiao, R. Bassel-Duby, P.E. Scherer, and B. Levine. 2012. Exercise-induced BCL2-regulated autophagy is required for muscle glucose homeostasis. *Nature*. 481:511-515.

He, C., and D.J. Klionsky. 2009. Regulation mechanisms and signaling pathways of autophagy. *Annual Review of Genetics*. 43:67-93.

Hein, S., E. Arnon, S. Kostin, M. Schonburg, A. Elsasser, V. Polyakova, E.P. Bauer, W.P. Klovekorn, and J. Schaper. 2003. Progression from compensated hypertrophy to failure in the pressure-overloaded human heart: structural deterioration and compensatory mechanisms. *Circulation*. 107:984-991.

Herrera, M., G.B. Silva, and J.L. Garvin. 2010. Angiotensin II stimulates thick ascending limb superoxide production via protein kinase C(alpha)-dependent NADPH oxidase activation. *The Journal of Biological Chemistry*. 285:21323-21328.

Hu, W., J. Ross, T. Geng, S.E. Brice, and L.A. Cowart. 2011. Differential regulation of dihydroceramide desaturase by palmitate versus monounsaturated fatty acids: implications for insulin resistance. *The Journal of Biological Chemistry*. 286:16596-16605.

Huang, C., W. Liu, C.N. Perry, S. Yitzhaki, Y. Lee, H. Yuan, Y.T. Tsukada, A. Hamacher-Brady, R.M. Mentzer, Jr., and R.A. Gottlieb. 2010. Autophagy and protein kinase C are required for cardioprotection by sulfaphenazole. *American Journal of Physiology. Heart and Circulatory Physiology*. 298:H570-579.

Huang, J., V. Canadien, G.Y. Lam, B.E. Steinberg, M.C. Dinauer, M.A. Magalhaes, M. Glogauer, S. Grinstein, and J.H. Brumell. 2009. Activation of antibacterial autophagy by NADPH oxidases. *Proceedings of the National Academy of Sciences of the United States of America*. 106:6226-6231.

Hubert, H.B., M. Feinleib, P.M. McNamara, and W.P. Castelli. 1983. Obesity as an independent risk factor for cardiovascular disease: a 26-year follow-up of participants in the Framingham Heart Study. *Circulation*. 67:968-977.

Hue, L., and H. Taegtmeyer. 2009. The Randle cycle revisited: a new head for an old hat. *American Journal of Physiology. Endocrinology and Metabolism*. 297:E578-591.

Hur, K.Y., H.S. Jung, and M.S. Lee. 2010. Role of autophagy in beta-cell function and mass. *Diabetes, Obesity & Metabolism*. 12 Suppl 2:20-26.

Ichimura, Y., T. Kumanomidou, Y.S. Sou, T. Mizushima, J. Ezaki, T. Ueno, E. Kominami, T. Yamane, K. Tanaka, and M. Komatsu. 2008. Structural basis for sorting mechanism of p62 in selective autophagy. *The Journal of Biological Chemistry*. 283:22847-22857.

Itani, S.I., Q. Zhou, W.J. Pories, K.G. MacDonald, and G.L. Dohm. 2000. Involvement of protein kinase C in human skeletal muscle insulin resistance and obesity. *Diabetes*. 49:1353-1358.

Itoh, K., T. Chiba, S. Takahashi, T. Ishii, K. Igarashi, Y. Katoh, T. Oyake, N. Hayashi, K. Satoh, I. Hatayama, M. Yamamoto, and Y. Nabeshima. 1997. An Nrf2/small Maf heterodimer mediates the induction of phase II detoxifying enzyme genes through antioxidant response elements. *Biochemical and Biophysical Research Communications*. 236:313-322.

Jager, S., C. Bucci, I. Tanida, T. Ueno, E. Kominami, P. Saftig, and E.L. Eskelinen. 2004. Role for Rab7 in maturation of late autophagic vacuoles. *Journal of Cell Science*. 117:4837-4848.

Jain, A., T. Lamark, E. Sjottem, K.B. Larsen, J.A. Awuh, A. Overvatn, M. McMahon, J.D. Hayes, and T. Johansen. 2010. p62/SQSTM1 is a target gene for transcription factor NRF2 and creates a positive feedback loop by inducing antioxidant response element-driven gene transcription. *The Journal of Biological Chemistry*. 285:22576-22591.

Jaquet, V., L. Scapozza, R.A. Clark, K.H. Krause, and J.D. Lambeth. 2009. Small-molecule NOX inhibitors: ROS-generating NADPH oxidases as therapeutic targets. *Antioxidants & Redox Signaling*. 11:2535-2552.

Jheng, H.F., P.J. Tsai, S.M. Guo, L.H. Kuo, C.S. Chang, I.J. Su, C.R. Chang, and Y.S. Tsai. 2012. Mitochondrial fission contributes to mitochondrial dysfunction and insulin resistance in skeletal muscle. *Molecular and Cellular Biology*. 32:309-319.

Jiang, F., H.K. Lim, M.J. Morris, L. Prior, E. Velkoska, X. Wu, and G.J. Dusting. 2011. Systemic upregulation of NADPH oxidase in diet-induced obesity in rats. *Redox Report: Communications in Free Radical Research*. 16:223-229.

Kanazawa, T., I. Taneike, R. Akaishi, F. Yoshizawa, N. Furuya, S. Fujimura, and M. Kadowaki. 2004. Amino acids and insulin control autophagic proteolysis through different signaling pathways in relation to mTOR in isolated rat hepatocytes. *The Journal of Biological Chemistry*. 279:8452-8459.

Kang, R., H.J. Zeh, M.T. Lotze, and D. Tang. 2011. The Beclin 1 network regulates autophagy and apoptosis. *Cell Death and Differentiation*. 18:571-580.

Kaushik, S., A.C. Massey, N. Mizushima, and A.M. Cuervo. 2008. Constitutive activation of chaperone-mediated autophagy in cells with impaired macroautophagy. *Molecular Biology of the Cell*. 19:2179-2192.

Kaushik, S., J.A. Rodriguez-Navarro, E. Arias, R. Kiffin, S. Sahu, G.J. Schwartz, A.M. Cuervo, and R. Singh. 2011. Autophagy in hypothalamic AgRP neurons regulates food intake and energy balance. *Cell Metabolism*. 14:173-183.

Kenchaiah, S., J.C. Evans, D. Levy, P.W. Wilson, E.J. Benjamin, M.G. Larson, W.B. Kannel, and R.S. Vasan. 2002. Obesity and the risk of heart failure. *The New England Journal of Medicine*. 347:305-313.

Kerner, J., and C. Hoppel. 2000. Fatty acid import into mitochondria. *Biochimica et biophysica acta*. 1486:1-17.

Kewalramani, G., L.N. Fink, F. Asadi, and A. Klip. 2011. Palmitate-activated macrophages confer insulin resistance to muscle cells by a mechanism involving protein kinase C theta and epsilon. *PloS one*. 6:e26947.

Kiffin, R., U. Bandyopadhyay, and A.M. Cuervo. 2006. Oxidative stress and autophagy. *Antioxidants & Redox Signaling*. 8:152-162.

Kiffin, R., C. Christian, E. Knecht, and A.M. Cuervo. 2004. Activation of chaperone-mediated autophagy during oxidative stress. *Molecular Biology of the Cell*. 15:4829-4840.

Kim, J., W.P. Huang, and D.J. Klionsky. 2001. Membrane recruitment of Aut7p in the autophagy and cytoplasm to vacuole targeting pathways requires Aut1p, Aut2p, and the autophagy conjugation complex. *The Journal of Cell Biology*. 152:51-64.

Kim, J., A.R. Wende, S. Sena, H.A. Theobald, J. Soto, C. Sloan, B.E. Wayment, S.E. Litwin, M. Holzenberger, D. LeRoith, and E.D. Abel. 2008. Insulin-like growth factor I receptor signaling is required for exercise-induced cardiac hypertrophy. *Mol Endocrinol*. 22:2531-2543.

Kim, J.E., S.E. Song, Y.W. Kim, J.Y. Kim, S.C. Park, Y.K. Park, S.H. Baek, I.K. Lee, and S.Y. Park. 2010. Adiponectin inhibits palmitate-induced apoptosis through suppression of reactive oxygen species in endothelial cells: involvement of cAMP/protein kinase A and AMP-activated protein kinase. *The Journal of Endocrinology*. 207:35-44.

Kirisako, T., Y. Ichimura, H. Okada, Y. Kabeya, N. Mizushima, T. Yoshimori, M. Ohsumi, T. Takao, T. Noda, and Y. Ohsumi. 2000. The reversible modification regulates the membrane-binding state of Apg8/Aut7 essential for autophagy and the cytoplasm to vacuole targeting pathway. *The Journal of Cell Biology*. 151:263-276.

Kissova, I., B. Salin, J. Schaeffer, S. Bhatia, S. Manon, and N. Camougrand. 2007. Selective and non-selective autophagic degradation of mitochondria in yeast. *Autophagy*. 3:329-336.

Klionsky, D.J., A.M. Cuervo, and P.O. Seglen. 2007. Methods for monitoring autophagy from yeast to human. *Autophagy*. 3:181-206.

Koga, H., S. Kaushik, and A.M. Cuervo. 2010. Altered lipid content inhibits autophagic vesicular fusion. *FASEB Journal: Official Publication of the Federation of American Societies for Experimental Biology*. 24:3052-3065.

Komiya, K., T. Uchida, T. Ueno, M. Koike, H. Abe, T. Hirose, R. Kawamori, Y. Uchiyama, E. Kominami, Y. Fujitani, and H. Watada. 2010. Free fatty acids stimulate autophagy in pancreatic beta-cells via JNK pathway. *Biochemical and Biophysical Research Communications*. 401:561-567.

Kontny, E., M. Kurowska, K. Szczepanska, and W. Maslinski. 2000. Rottlerin, a PKC isozyme-selective inhibitor, affects signaling events and cytokine production in human monocytes. *Journal of Leukocyte Biology*. 67:249-258.

Kornak, U., D. Kasper, M.R. Bosl, E. Kaiser, M. Schweizer, A. Schulz, W. Friedrich, G. Delling, and T.J. Jentsch. 2001. Loss of the ClC-7 chloride channel leads to osteopetrosis in mice and man. *Cell*. 104:205-215.

Kostin, S., L. Pool, A. Elsasser, S. Hein, H.C. Drexler, E. Arnon, Y. Hayakawa, R. Zimmermann, E. Bauer, W.P. Klovekorn, and J. Schaper. 2003. Myocytes die by multiple mechanisms in failing human hearts. *Circulation Research*. 92:715-724.

Kovsan, J., M. Bluher, T. Tarnovscki, N. Kloting, B. Kirshtein, L. Madar, I. Shai, R. Golan, I. Harman-Boehm, M.R. Schon, A.S. Greenberg, Z. Elazar, N. Bashan,

and A. Rudich. 2011. Altered autophagy in human adipose tissues in obesity. *The Journal of Clinical Endocrinology and Metabolism*. 96:E268-277.

Kubli, D.A., and A.B. Gustafsson. 2012. Mitochondria and mitophagy: the yin and yang of cell death control. *Circulation Research*. 111:1208-1221.

Kuroda, J., T. Ago, S. Matsushima, P. Zhai, M.D. Schneider, and J. Sadoshima. 2010. NADPH oxidase 4 (Nox4) is a major source of oxidative stress in the failing heart. *Proceedings of the National Academy of Sciences of the United States of America*. 107:15565-15570.

Kurz, T., A. Terman, B. Gustafsson, and U.T. Brunk. 2008. Lysosomes and oxidative stress in aging and apoptosis. *Biochimica et biophysica acta*. 1780:1291-1303.

Kuzman, J.A., T.D. O'Connell, and A.M. Gerdes. 2007. Rapamycin prevents thyroid hormone-induced cardiac hypertrophy. *Endocrinology*. 148:3477-3484.

Lamb, F.S., J.G. Moreland, and F.J. Miller, Jr. 2009. Electrophysiology of reactive oxygen production in signaling endosomes. *Antioxidants & Redox Signaling*. 11:1335-1347.

Lambertucci, R.H., S.M. Hirabara, R. Silveira Ldos, A.C. Levada-Pires, R. Curi, and T.C. Pithon-Curi. 2008. Palmitate increases superoxide production through mitochondrial electron transport chain and NADPH oxidase activity in skeletal muscle cells. *Journal of Cellular Physiology*. 216:796-804.

Las, G., S.B. Serada, J.D. Wikstrom, G. Twig, and O.S. Shirihai. 2011. Fatty acids suppress autophagic turnover in beta-cells. *The Journal of Biological Chemistry*. 286:42534-42544.

Lassegue, B., A. San Martin, and K.K. Griendling. 2012. Biochemistry, physiology, and pathophysiology of NADPH oxidases in the cardiovascular system. *Circulation Research*. 110:1364-1390.

Lavallard, V.J., A.J. Meijer, P. Codogno, and P. Gual. 2012. Autophagy, signaling and obesity. *Pharmacological Research: The Official Journal of the Italian Pharmacological Society*. 66:513-525.

Lavie, C.J., R.V. Milani, and H.O. Ventura. 2009. Obesity and cardiovascular disease: risk factor, paradox, and impact of weight loss. *Journal of the American College of Cardiology*. 53:1925-1932.

Lee, D.Y., and E.J. Brown. 2012. Ubiquilins in the crosstalk among proteolytic pathways. *Biological Chemistry*. 393:441-447.

Lee, J., S. Giordano, and J. Zhang. 2012. Autophagy, mitochondria and oxidative stress: cross-talk and redox signalling. *The Biochemical Journal*. 441:523-540.

Levine, B., and G. Kroemer. 2008. Autophagy in the pathogenesis of disease. *Cell*. 132:27-42.

Li, Z.L., J.R. Woollard, B. Ebrahimi, J.A. Crane, K.L. Jordan, A. Lerman, S.M. Wang, and L.O. Lerman. 2012. Transition from obesity to metabolic syndrome is associated with altered myocardial autophagy and apoptosis. *Arteriosclerosis, Thrombosis, and Vascular Biology*. 32:1132-1141.

Liu, H.Y., J. Han, S.Y. Cao, T. Hong, D. Zhuo, J. Shi, Z. Liu, and W. Cao. 2009. Hepatic autophagy is suppressed in the presence of insulin resistance and hyperinsulinemia: inhibition of FoxO1-dependent expression of key autophagy genes by insulin. *The Journal of Biological Chemistry*. 284:31484-31492.

Liu, J., and S.G. Lloyd. 2013. High-fat, low-carbohydrate diet alters myocardial oxidative stress and impairs recovery of cardiac function after ischemia and reperfusion in obese rats. *Nutrition Research*. 33:311-321.

Lopaschuk, G.D., and D.P. Kelly. 2008. Signalling in cardiac metabolism. *Cardiovascular Research*. 79:205-207.

Lopaschuk, G.D., J.R. Ussher, C.D. Folmes, J.S. Jaswal, and W.C. Stanley. 2010. Myocardial fatty acid metabolism in health and disease. *Physiological Reviews*. 90:207-258.

Luiken, J.J., D.J. Dyck, X.X. Han, N.N. Tandon, Y. Arumugam, J.F. Glatz, and A. Bonen. 2002. Insulin induces the translocation of the fatty acid transporter FAT/CD36 to the plasma membrane. *American Journal of Physiology. Endocrinology and Metabolism*. 282:E491-495.

Lum, J.J., D.E. Bauer, M. Kong, M.H. Harris, C. Li, T. Lindsten, and C.B. Thompson. 2005. Growth factor regulation of autophagy and cell survival in the absence of apoptosis. *Cell*. 120:237-248.

Ma, X., H. Liu, S.R. Foyil, R.J. Godar, C.J. Weinheimer, J.A. Hill, and A. Diwan. 2012. Impaired autophagosome clearance contributes to cardiomyocyte death in ischemia/reperfusion injury. *Circulation*. 125:3170-3181.

Madaro, L., V. Marrocco, S. Carnio, M. Sandri, and M. Bouche. 2013. Intracellular signaling in ER stress-induced autophagy in skeletal muscle cells. *FASEB Journal: Official Publication of the Federation of American Societies for Experimental Biology*.

Majeski, A.E., and J.F. Dice. 2004. Mechanisms of chaperone-mediated autophagy. *The International Journal of Biochemistry & Cell Biology*. 36:2435-2444.

Malnick, S.D., and H. Knobler. 2006. The medical complications of obesity. *QJM : Monthly Journal of the Association of Physicians*. 99:565-579.

Maloney, E., I.R. Sweet, D.M. Hockenbery, M. Pham, N.O. Rizzo, S. Tateya, P. Handa, M.W. Schwartz, and F. Kim. 2009. Activation of NF-kappaB by palmitate in endothelial cells: a key role for NADPH oxidase-derived superoxide in response to TLR4 activation. *Arteriosclerosis, Thrombosis, and Vascular Biology*. 29:1370-1375.

Mandarim-de-Lacerda, C.A. 2003. Stereological tools in biomedical research. *Anais da Academia Brasileira de Ciencias*. 75:469-486.

Manente, A.G., G. Pinton, D. Tavian, G. Lopez-Rodas, E. Brunelli, and L. Moro. 2011. Coordinated sumoylation and ubiquitination modulate EGF induced EGR1 expression and stability. *PloS One*. 6:e25676.

Marchi, E.D., F. Baldassari, A. Bononi, M.R. Wieckowski, and P. Pinton. 2013. Oxidative Stress in Cardiovascular Diseases and Obesity: Role of p66Shc and Protein Kinase C. *Oxidative Medicine and Cellular Longevity*. 2013.

Mari, M., S.A. Tooze, and F. Reggiori. 2011. The puzzling origin of the autophagosomal membrane. *F1000 Biol Rep*. 3:25.

Martinet, W., M.W. Knaapen, M.M. Kockx, and G.R. De Meyer. 2007. Autophagy in cardiovascular disease. *Trends in Molecular Medicine*. 13:482-491.

Massey, A.C., S. Kaushik, G. Sovak, R. Kiffin, and A.M. Cuervo. 2006. Consequences of the selective blockage of chaperone-mediated autophagy. *Proceedings of the National Academy of Sciences of the United States of America*. 103:5805-5810.

Matsui, Y., H. Takagi, X. Qu, M. Abdellatif, H. Sakoda, T. Asano, B. Levine, and J. Sadoshima. 2007. Distinct roles of autophagy in the heart during ischemia and reperfusion: roles of AMP-activated protein kinase and Beclin 1 in mediating autophagy. *Circulation Research*. 100:914-922.

Matsushima, S., S. Kinugawa, T. Yokota, N. Inoue, Y. Ohta, S. Hamaguchi, and H. Tsutsui. 2009. Increased myocardial NAD(P)H oxidase-derived superoxide causes the exacerbation of postinfarct heart failure in type 2 diabetes. *American Journal of Physiology. Heart and Circulatory Physiology*. 297:H409-416.

Matsushima, S., J. Kuroda, T. Ago, P. Zhai, J.Y. Park, L.H. Xie, B. Tian, and J. Sadoshima. 2013. Increased oxidative stress in the nucleus caused by Nox4 mediates oxidation of HDAC4 and cardiac hypertrophy. *Circulation Research*. 112:651-663.

McMullen, J.R., M.C. Sherwood, O. Tarnavski, L. Zhang, A.L. Dorfman, T. Shioi, and S. Izumo. 2004. Inhibition of mTOR signaling with rapamycin regresses established cardiac hypertrophy induced by pressure overload. *Circulation*. 109:3050-3055.

Mei, S., H.M. Ni, S. Manley, A. Bockus, K.M. Kassel, J.P. Luyendyk, B.L. Copple, and W.X. Ding. 2011. Differential roles of unsaturated and saturated fatty acids on

autophagy and apoptosis in hepatocytes. *The Journal of Pharmacology and Experimental Therapeutics*. 339:487-498.

Mellor, K.M., J.R. Bell, R.H. Ritchie, and L.M. Delbridge. 2013a. Myocardial insulin resistance, metabolic stress and autophagy in diabetes. *Clinical and Experimental Pharmacology & Physiology*. 40:56-61.

Mellor, K.M., M.E. Reichelt, and L.M. Delbridge. 2013b. Autophagic predisposition in the insulin resistant diabetic heart. *Life Sciences*. 92:616-620.

Menon, M.B., A. Kotlyarov, and M. Gaestel. 2011. SB202190-induced cell type-specific vacuole formation and defective autophagy do not depend on p38 MAP kinase inhibition. *PloS One*. 6:e23054.

Mijaljica, D., M. Prescott, and R.J. Devenish. 2011. Microautophagy in mammalian cells: revisiting a 40-year-old conundrum. *Autophagy*. 7:673-682.

Mindell, J.A. 2012. Lysosomal acidification mechanisms. *Annual Review of Physiology*. 74:69-86.

Mizushima, N., A. Kuma, Y. Kobayashi, A. Yamamoto, M. Matsubae, T. Takao, T. Natsume, Y. Ohsumi, and T. Yoshimori. 2003. Mouse Apg16L, a novel WD-repeat protein, targets to the autophagic isolation membrane with the Apg12-Apg5 conjugate. *Journal of Cell Science*. 116:1679-1688.

Mizushima, N., A. Yamamoto, M. Hatano, Y. Kobayashi, Y. Kabeya, K. Suzuki, T. Tokuhisa, Y. Ohsumi, and T. Yoshimori. 2001. Dissection of autophagosome formation using Apg5-deficient mouse embryonic stem cells. *The Journal of Cell Biology*. 152:657-668.

Mizushima, N., A. Yamamoto, M. Matsui, T. Yoshimori, and Y. Ohsumi. 2004. In vivo analysis of autophagy in response to nutrient starvation using transgenic mice expressing a fluorescent autophagosome marker. *Molecular Biology of the Cell*. 15:1101-1111.

Morgan, D., H.R. Oliveira-Emilio, D. Keane, A.E. Hirata, M. Santos da Rocha, S. Bordin, R. Curi, P. Newsholme, and A.R. Carpinelli. 2007. Glucose, palmitate and pro-inflammatory cytokines modulate production and activity of a phagocyte-like NADPH oxidase in rat pancreatic islets and a clonal beta cell line. *Diabetologia*. 50:359-369.

Mozaffari, M.S., and S.W. Schaffer. 2008. Myocardial ischemic-reperfusion injury in a rat model of metabolic syndrome. *Obesity*. 16:2253-2258.

Murphy, S.L., J. Xu, and K.D. Kochanek. 2012. Deaths- Preliminary Data for 2010. *National Vital Statistics Reports*. 60:1-68.

Nakai, A., O. Yamaguchi, T. Takeda, Y. Higuchi, S. Hikoso, M. Taniike, S. Omiya, I. Mizote, Y. Matsumura, M. Asahi, K. Nishida, M. Hori, N. Mizushima, and K. Otsu. 2007. The role of autophagy in cardiomyocytes in the basal state and in response to hemodynamic stress. *Nature Medicine*. 13:619-624.

Narkiewicz, K. 2006. Obesity and hypertension--the issue is more complex than we thought. *Nephrology, Dialysis, Transplantation: Official Publication of the European Dialysis and Transplant Association - European Renal Association*. 21:264-267.

Nemchenko, A., M. Chiong, A. Turer, S. Lavandero, and J.A. Hill. 2011. Autophagy as a therapeutic target in cardiovascular disease. *Journal of Molecular and Cellular Cardiology*. 51:584-593.

Nijholt, D.A., T.R. de Graaf, E.S. van Haastert, A.O. Oliveira, C.R. Berkers, R. Zwart, H. Ovaa, F. Baas, J.J. Hoozemans, and W. Scheper. 2011. Endoplasmic reticulum stress activates autophagy but not the proteasome in neuronal cells: implications for Alzheimer's disease. *Cell Death and Differentiation*. 18:1071-1081.

Nishida, K., S. Kyoi, O. Yamaguchi, J. Sadoshima, and K. Otsu. 2009. The role of autophagy in the heart. *Cell Death and Differentiation*. 16:31-38.

Nishino, I., J. Fu, K. Tanji, T. Yamada, S. Shimojo, T. Koori, M. Mora, J.E. Riggs, S.J. Oh, Y. Koga, C.M. Sue, A. Yamamoto, N. Murakami, S. Shanske, E. Byrne, E. Bonilla, I. Nonaka, S. DiMauro, and M. Hirano. 2000. Primary LAMP-2 deficiency causes X-linked vacuolar cardiomyopathy and myopathy (Danon disease). *Nature*. 406:906-910.

Novak, I., V. Kirkin, D.G. McEwan, J. Zhang, P. Wild, A. Rozenknop, V. Rogov, F. Lohr, D. Popovic, A. Occhipinti, A.S. Reichert, J. Terzic, V. Dotsch, P.A. Ney, and I. Dikic. 2010. Nix is a selective autophagy receptor for mitochondrial clearance. *EMBO Reports*. 11:45-51.

Ogata, M., S. Hino, A. Saito, K. Morikawa, S. Kondo, S. Kanemoto, T. Murakami, M. Taniguchi, I. Tanii, K. Yoshinaga, S. Shiosaka, J.A. Hammarback, F. Urano, and K. Imaizumi. 2006. Autophagy is activated for cell survival after endoplasmic reticulum stress. *Molecular and Cellular Biology*. 26:9220-9231.

Ogden, C.L., M.E. Carroll, B.K. Kit, and K.M. Flegal. 2012. Prevalence of obesity in the United States, 2009-2010. *NCHS Data Brief*:1-8.

Palmieri, M., S. Impey, H. Kang, A. di Ronza, C. Pelz, M. Sardiello, and A. Ballabio. 2011. Characterization of the CLEAR network reveals an integrated control of cellular clearance pathways. *Human Molecular Genetics*. 20:3852-3866.

Pankiv, S., E.A. Alemu, A. Brech, J.A. Bruun, T. Lamark, A. Overvatn, G. Bjorkoy, and T. Johansen. 2010. FYCO1 is a Rab7 effector that binds to LC3 and PI3P to

mediate microtubule plus end-directed vesicle transport. *The Journal of Cell Biology*. 188:253-269.

Pankiv, S., T.H. Clausen, T. Lamark, A. Brech, J.A. Bruun, H. Outzen, A. Overvatn, G. Bjorkoy, and T. Johansen. 2007. p62/SQSTM1 binds directly to Atg8/LC3 to facilitate degradation of ubiquitinated protein aggregates by autophagy. *The Journal of Biological Chemistry*. 282:24131-24145.

Pantos, C., V. Malliopoulou, I. Mourouzis, A. Thempeyioti, I. Paizis, A. Dimopoulos, T. Saranteas, C. Xinaris, and D.V. Cokkinos. 2006. Hyperthyroid hearts display a phenotype of cardioprotection against ischemic stress: a possible involvement of heat shock protein 70. *Hormone and metabolic research = Hormon- und Stoffwechselforschung = Hormones et metabolisme*. 38:308-313.

Papackova, Z., H. Dankova, E. Palenickova, L. Kazdova, and M. Cahova. 2012. Effect of short- and long-term high-fat feeding on autophagy flux and lysosomal activity in rat liver. *Physiological Research / Academia Scientiarum Bohemoslovaca*. 61 Suppl 2:S67-76.

Parent, N., E. Winstall, M. Beauchemin, C. Paquet, G.G. Poirier, and R. Bertrand. 2009. Proteomic analysis of enriched lysosomes at early phase of camptothecin-induced apoptosis in human U-937 cells. *Journal of Proteomics*. 72:960-973.

Patschan, S., J. Chen, A. Polotskaia, N. Mendelev, J. Cheng, D. Patschan, and M.S. Goligorsky. 2008. Lipid mediators of autophagy in stress-induced premature senescence of endothelial cells. *American Journal of Physiology. Heart and Circulatory Physiology*. 294:H1119-1129.

Patterson, C. 2006. Search and destroy: the role of protein quality control in maintaining cardiac function. *Journal of Molecular and Cellular Cardiology*. 40:438-441.

Pattingre, S., C. Bauvy, S. Carpentier, T. Levade, B. Levine, and P. Codogno. 2009a. Role of JNK1-dependent Bcl-2 phosphorylation in ceramide-induced macroautophagy. *The Journal of Biological Chemistry*. 284:2719-2728.

Pattingre, S., C. Bauvy, T. Levade, B. Levine, and P. Codogno. 2009b. Ceramide-induced autophagy: to junk or to protect cells? *Autophagy*. 5:558-560.

Perry, C.N., S. Kyoi, N. Hariharan, H. Takagi, J. Sadoshima, and R.A. Gottlieb. 2009. Novel methods for measuring cardiac autophagy in vivo. *Methods in Enzymology*. 453:325-342.

Pollock, J.D., D.A. Williams, M.A. Gifford, L.L. Li, X. Du, J. Fisherman, S.H. Orkin, C.M. Doerschuk, and M.C. Dinauer. 1995. Mouse model of X-linked chronic granulomatous disease, an inherited defect in phagocyte superoxide production. *Nature Genetics*. 9:202-209.

Qu, X., J.P. Seale, and R. Donnelly. 1999. Tissue and isoform-selective activation of protein kinase C in insulin-resistant obese Zucker rats - effects of feeding. *The Journal of Endocrinology*. 162:207-214.

Raad, H., M.H. Paclet, T. Boussetta, Y. Kroviarski, F. Morel, M.T. Quinn, M.A. Gougerot-Pocidalo, P.M. Dang, and J. El-Benna. 2009. Regulation of the phagocyte NADPH oxidase activity: phosphorylation of gp91phox/NOX2 by protein kinase C enhances its diaphorase activity and binding to Rac2, p67phox, and p47phox. *FASEB Journal: Official Publication of the Federation of American Societies for Experimental Biology*. 23:1011-1022.

Rabinowitz, J.D., and E. White. 2010. Autophagy and metabolism. *Science*. 330:1344-1348.

Randle, P.J., P.B. Garland, C.N. Hales, and E.A. Newsholme. 1963. The glucose fatty-acid cycle. Its role in insulin sensitivity and the metabolic disturbances of diabetes mellitus. *Lancet*. 1:785-789.

Ravikumar, B., A. Acevedo-Arozena, S. Imarisio, Z. Berger, C. Vacher, C.J. O'Kane, S.D. Brown, and D.C. Rubinsztein. 2005. Dynein mutations impair autophagic clearance of aggregate-prone proteins. *Nature Genetics*. 37:771-776.

Rider, O.J., J.M. Francis, M.K. Ali, J. Byrne, K. Clarke, S. Neubauer, and S.E. Petersen. 2009. Determinants of left ventricular mass in obesity; a cardiovascular magnetic resonance study. *J Cardiovasc Magn Reson*. 11:9.

Riehle, C., A.R. Wende, V.G. Zaha, K.M. Pires, B. Wayment, C. Olsen, H. Bugger, J. Buchanan, X. Wang, A.B. Moreira, T. Doenst, G. Medina-Gomez, S.E. Litwin, C.J. Lelliott, A. Vidal-Puig, and E.D. Abel. 2011. PGC-1beta deficiency accelerates the transition to heart failure in pressure overload hypertrophy. *Circulation Research*. 109:783-793.

Roberts, C.K., R.J. Barnard, R.K. Sindhu, M. Jurczak, A. Ehdaie, and N.D. Vaziri. 2006. Oxidative stress and dysregulation of NAD(P)H oxidase and antioxidant enzymes in diet-induced metabolic syndrome. *Metabolism: Clinical and Experimental*. 55:928-934.

Roberts, P., S. Moshitch-Moshkovitz, E. Kvam, E. O'Toole, M. Winey, and D.S. Goldfarb. 2003. Piecemeal microautophagy of nucleus in Saccharomyces cerevisiae. *Molecular Biology of the Cell*. 14:129-141.

Saftig, P., and J. Klumperman. 2009. Lysosome biogenesis and lysosomal membrane proteins: trafficking meets function. *Nature Reviews. Molecular Cell Biology*. 10:623-635.

Sandri, M. 2010. Autophagy in skeletal muscle. *FEBS Letters*. 584:1411-1416.

Sardiello, M., M. Palmieri, A. di Ronza, D.L. Medina, M. Valenza, V.A. Gennarino, C. Di Malta, F. Donaudy, V. Embrione, R.S. Polishchuk, S. Banfi, G. Parenti, E. Cattaneo, and A. Ballabio. 2009. A gene network regulating lysosomal biogenesis and function. *Science*. 325:473-477.

Sarkar, S., B. Ravikumar, R.A. Floto, and D.C. Rubinsztein. 2009. Rapamycin and mTOR-independent autophagy inducers ameliorate toxicity of polyglutamine-expanded huntingtin and related proteinopathies. *Cell Death and Differentiation*. 16:46-56.

Sautin, Y.Y., M. Lu, A. Gaugler, L. Zhang, and S.L. Gluck. 2005. Phosphatidylinositol 3-kinase-mediated effects of glucose on vacuolar H+-ATPase assembly, translocation, and acidification of intracellular compartments in renal epithelial cells. *Molecular and Cellular Biology*. 25:575-589.

Scarlatti, F., C. Bauvy, A. Ventruti, G. Sala, F. Cluzeaud, A. Vandewalle, R. Ghidoni, and P. Codogno. 2004. Ceramide-mediated macroautophagy involves inhibition of protein kinase B and up-regulation of beclin 1. *The Journal of Biological Chemistry*. 279:18384-18391.

Scherz-Shouval, R., and Z. Elazar. 2011. Regulation of autophagy by ROS: physiology and pathology. *Trends in Biochemical Sciences*. 36:30-38.

Scherz-Shouval, R., E. Shvets, E. Fass, H. Shorer, L. Gil, and Z. Elazar. 2007. Reactive oxygen species are essential for autophagy and specifically regulate the activity of Atg4. *The EMBO Journal*. 26:1749-1760.

Sciarretta, S., M. Volpe, and J. Sadoshima. 2012a. Is reactivation of autophagy a possible therapeutic solution for obesity and metabolic syndrome? *Autophagy*. 8:1252-1254.

Sciarretta, S., P. Zhai, D. Shao, Y. Maejima, J. Robbins, M. Volpe, G. Condorelli, and J. Sadoshima. 2012b. Rheb is a critical regulator of autophagy during myocardial ischemia: pathophysiological implications in obesity and metabolic syndrome. *Circulation*. 125:1134-1146.

Sciarretta, S., P. Zhai, M. Volpe, and J. Sadoshima. 2012c. Activation of Nox4 Promotes Cardiomyocyte Autophagy and Survival During Nutrient Starvation. *Circulation*. 126.

Sengupta, A., J.D. Molkentin, and K.E. Yutzey. 2009. FoxO transcription factors promote autophagy in cardiomyocytes. *The Journal of Biological Chemistry*. 284:28319-28331.

Serpillon, S., B.C. Floyd, R.S. Gupte, S. George, M. Kozicky, V. Neito, F. Recchia, W. Stanley, M.S. Wolin, and S.A. Gupte. 2009. Superoxide production by NAD(P)H oxidase and mitochondria is increased in genetically obese and hyperglycemic rat heart and aorta before the development of cardiac dysfunction. The role of

glucose-6-phosphate dehydrogenase-derived NADPH. *American Journal of Physiology. Heart and Circulatory Physiology*. 297:H153-162.

Settembre, C., C. Di Malta, V.A. Polito, M. Garcia Arencibia, F. Vetrini, S. Erdin, S.U. Erdin, T. Huynh, D. Medina, P. Colella, M. Sardiello, D.C. Rubinsztein, and A. Ballabio. 2011. TFEB links autophagy to lysosomal biogenesis. *Science*. 332:1429-1433.

Settembre, C., A. Fraldi, L. Jahreiss, C. Spampanato, C. Venturi, D. Medina, R. de Pablo, C. Tacchetti, D.C. Rubinsztein, and A. Ballabio. 2008. A block of autophagy in lysosomal storage disorders. *Human Molecular Genetics*. 17:119-129.

Shibata, M., K. Yoshimura, N. Furuya, M. Koike, T. Ueno, M. Komatsu, H. Arai, K. Tanaka, E. Kominami, and Y. Uchiyama. 2009. The MAP1-LC3 conjugation system is involved in lipid droplet formation. *Biochemical and Biophysical Research Communications*. 382:419-423.

Singh, R., and A.M. Cuervo. 2012. Lipophagy: connecting autophagy and lipid metabolism. *International Journal of Cell Biology*. 2012:282041.

Singh, R., S. Kaushik, Y. Wang, Y. Xiang, I. Novak, M. Komatsu, K. Tanaka, A.M. Cuervo, and M.J. Czaja. 2009a. Autophagy regulates lipid metabolism. *Nature*. 458:1131-1135.

Singh, R., Y. Xiang, Y. Wang, K. Baikati, A.M. Cuervo, Y.K. Luu, Y. Tang, J.E. Pessin, G.J. Schwartz, and M.J. Czaja. 2009b. Autophagy regulates adipose mass and differentiation in mice. *The Journal of Clinical Investigation*. 119:3329-3339.

Siow, Y.L., K.K. Au-Yeung, C.W. Woo, and K. O. 2006. Homocysteine stimulates phosphorylation of NADPH oxidase p47phox and p67phox subunits in monocytes via protein kinase Cbeta activation. *The Biochemical Journal*. 398:73-82.

Sivitz, W.I. 2010. Mitochondrial dysfunction in obesity and diabetes. *US Endocrinology*. 6:20-27.

Son, J.H., J.H. Shim, K.H. Kim, J.Y. Ha, and J.Y. Han. 2012. Neuronal autophagy and neurodegenerative diseases. *Experimental & Molecular Medicine*. 44:89-98.

Sowa, M.E., E.J. Bennett, S.P. Gygi, and J.W. Harper. 2009. Defining the human deubiquitinating enzyme interaction landscape. *Cell*. 138:389-403.

Stanley, W.C., F.A. Recchia, and G.D. Lopaschuk. 2005. Myocardial substrate metabolism in the normal and failing heart. *Physiological Reviews*. 85:1093-1129.

Streeter, J., W. Thiel, K. Brieger, and F.J. Miller, Jr. 2013. Opportunity nox: the future of NADPH oxidases as therapeutic targets in cardiovascular disease. *Cardiovascular Therapeutics*. 31:125-137.

Summers, S.A. 2006. Ceramides in insulin resistance and lipotoxicity. *Progress in Lipid Research*. 45:42-72.

Sumner, J.P., J.A. Dow, F.G. Earley, U. Klein, D. Jager, and H. Wieczorek. 1995. Regulation of plasma membrane V-ATPase activity by dissociation of peripheral subunits. *The Journal of Biological Chemistry*. 270:5649-5653.

Tan, S.H., G. Shui, J. Zhou, J.J. Li, B.H. Bay, M.R. Wenk, and H.M. Shen. 2012. Induction of autophagy by palmitic acid via protein kinase C-mediated signaling pathway independent of mTOR (mammalian target of rapamycin). *The Journal of Biological Chemistry*. 287:14364-14376.

Tanaka, Y., G. Guhde, A. Suter, E.L. Eskelinen, D. Hartmann, R. Lullmann-Rauch, P.M. Janssen, J. Blanz, K. von Figura, and P. Saftig. 2000. Accumulation of autophagic vacuoles and cardiomyopathy in LAMP-2-deficient mice. *Nature*. 406:902-906.

Taniguchi, T., S. Kido, E. Yamauchi, M. Abe, T. Matsumoto, and H. Taniguchi. 2010. Induction of endosomal/lysosomal pathways in differentiating osteoblasts as revealed by combined proteomic and transcriptomic analyses. *FEBS Letters*. 584:3969-3974.

Tanner, J.M., D.T. Kearns, B.J. Kim, C. Sloan, Z. Jia, T. Yang, E.D. Abel, and J.D. Symons. 2010. Fasting-induced reductions in cardiovascular and metabolic variables occur sooner in obese versus lean mice. *Exp Biol Med (Maywood)*. 235:1489-1497.

Teng, R.J., J. Du, S. Welak, T. Guan, A. Eis, Y. Shi, and G.G. Konduri. 2012. Cross talk between NADPH oxidase and autophagy in pulmonary artery endothelial cells with intrauterine persistent pulmonary hypertension. *American Journal of Physiology. Lung Cellular and Molecular Physiology*. 302:L651-663.

Thomas, F., K. Bean, B. Pannier, J.M. Oppert, L. Guize, and A. Benetos. 2005. Cardiovascular mortality in overweight subjects: the key role of associated risk factors. *Hypertension*. 46:654-659.

Tsujimoto, Y. 1997. Apoptosis and necrosis: intracellular ATP level as a determinant for cell death modes. *Cell Death and Differentiation*. 4:429-434.

Turdi, S., M.R. Kandadi, J. Zhao, A.F. Huff, M. Du, and J. Ren. 2011. Deficiency in AMP-activated protein kinase exaggerates high fat diet-induced cardiac hypertrophy and contractile dysfunction. *Journal of Molecular and Cellular Cardiology*. 50:712-722.

Unger, R.H., and L. Orci. 2002. Lipoapoptosis: its mechanism and its diseases. *Biochimica et biophysica acta*. 1585:202-212.

Vaidyanathan, V.V., N. Puri, and P.A. Roche. 2001. The last exon of SNAP-23 regulates granule exocytosis from mast cells. *The Journal of Biological Chemistry*. 276:25101-25106.

von Herrath, M.G., S. Guerder, H. Lewicki, R.A. Flavell, and M.B. Oldstone. 1995. Coexpression of B7-1 and viral ("self") transgenes in pancreatic beta cells can break peripheral ignorance and lead to spontaneous autoimmune diabetes. *Immunity*. 3:727-738.

Wang, X., H. Osinska, R. Klevitsky, A.M. Gerdes, M. Nieman, J. Lorenz, T. Hewett, and J. Robbins. 2001. Expression of R120G-alphaB-crystallin causes aberrant desmin and alphaB-crystallin aggregation and cardiomyopathy in mice. *Circulation Research*. 89:84-91.

Wang, X., and E.J. Terpstra. 2012. Ubiquitin receptors and protein quality control. *Journal of Molecular and Cellular Cardiology*.

Wang, X., W. Yu, A. Nawaz, F. Guan, S. Sun, and C. Wang. 2010a. Palmitate induced insulin resistance by PKCtheta-dependent activation of mTOR/S6K pathway in C2C12 myotubes. *Experimental and Clinical Endocrinology & Diabetes: Official Journal, German Society of Endocrinology [and] German Diabetes Association*. 118:657-661.

Wang, Y., M.A. Beydoun, L. Liang, B. Caballero, and S.K. Kumanyika. 2008. Will all Americans become overweight or obese? estimating the progression and cost of the US obesity epidemic. *Obesity*. 16:2323-2330.

Wang, Z.V., B.A. Rothermel, and J.A. Hill. 2010b. Autophagy in hypertensive heart disease. *The Journal of Biological Chemistry*. 285:8509-8514.

Weidberg, H., E. Shvets, and Z. Elazar. 2011. Biogenesis and cargo selectivity of autophagosomes. *Annual Review of Biochemistry*. 80:125-156.

Wellman, N.S., and B. Friedberg. 2002. Causes and consequences of adult obesity: health, social and economic impacts in the United States. *Asia Pacific Journal of Clinical Nutrition*. 11 Suppl 8:S705-709.

Wellnitz, K.A., R.Lombardi, R.L.Salazar, H.Taegtmeyer. 2009. Markers and mediators of autophagy are increased in the hearts of two murine models of type 2 diabetes irrespective of cardiac function. *Circulation*. 240:S490.

Wen, H., D. Gris, Y. Lei, S. Jha, L. Zhang, M.T. Huang, W.J. Brickey, and J.P. Ting. 2011. Fatty acid-induced NLRP3-ASC inflammasome activation interferes with insulin signaling. *Nature Immunology*. 12:408-415.

Wende, A.R., and E.D. Abel. 2010. Lipotoxicity in the heart. *Biochimica et biophysica acta*. 1801:311-319.

Williams, A., S. Sarkar, P. Cuddon, E.K. Ttofi, S. Saiki, F.H. Siddiqi, L. Jahreiss, A. Fleming, D. Pask, P. Goldsmith, C.J. O'Kane, R.A. Floto, and D.C. Rubinsztein. 2008. Novel targets for Huntington's disease in an mTOR-independent autophagy pathway. *Nat Chem Biol*. 4:295-305.

Willis, M.S., J.C. Schisler, A.L. Portbury, and C. Patterson. 2009. Build it up-Tear it down: protein quality control in the cardiac sarcomere. *Cardiovascular Research*. 81:439-448.

Wilson, P.W., R.B. D'Agostino, L. Sullivan, H. Parise, and W.B. Kannel. 2002. Overweight and obesity as determinants of cardiovascular risk: the Framingham experience. *Arch Intern Med*. 162:1867-1872.

Wisneski, J.A., W.C. Stanley, R.A. Neese, and E.W. Gertz. 1990. Effects of acute hyperglycemia on myocardial glycolytic activity in humans. *The Journal of Clinical Investigation*. 85:1648-1656.

Wong, Y.C., M.K. Sim, and K.O. Lee. 2011. Des-aspartate-angiotensin-I and angiotensin IV improve glucose tolerance and insulin signalling in diet-induced hyperglycaemic mice. *Biochemical Pharmacology*. 82:1198-1208.

Wright, J.J., J. Kim, J. Buchanan, S. Boudina, S. Sena, K. Bakirtzi, O. Ilkun, H.A. Theobald, R.C. Cooksey, K.V. Kandror, and E.D. Abel. 2009. Mechanisms for increased myocardial fatty acid utilization following short-term high-fat feeding. *Cardiovascular Research*. 82:351-360.

Xie, Z., C. He, and M.H. Zou. 2011a. AMP-activated protein kinase modulates cardiac autophagy in diabetic cardiomyopathy. *Autophagy*. 7:1254-1255.

Xie, Z., K. Lau, B. Eby, P. Lozano, C. He, B. Pennington, H. Li, S. Rathi, Y. Dong, R. Tian, D. Kem, and M.H. Zou. 2011b. Improvement of cardiac functions by chronic metformin treatment is associated with enhanced cardiac autophagy in diabetic OVE26 mice. *Diabetes*. 60:1770-1778.

Xu, X., Y. Hua, N. Sreejayan, Y. Zhang, and J. Ren. 2012. Akt2 knockout preserves cardiac function in high-fat diet-induced obesity by rescuing cardiac autophagosome maturation. *Journal of Molecular Cell Biology*.

Xu, X., Y. Hua, N. Sreejayan, Y. Zhang, and J. Ren. 2013. Akt2 knockout preserves cardiac function in high-fat diet-induced obesity by rescuing cardiac autophagosome maturation. *Journal of Molecular Cell Biology*. 5:61-63.

Xu, X., and J. Ren. 2012. Unmasking the janus faces of autophagy in obesity-associated insulin resistance and cardiac dysfunction. *Clinical and Experimental Pharmacology & Physiology*. 39:200-208.

Yamaguchi, O., Y. Higuchi, S. Hirotani, K. Kashiwase, H. Nakayama, S. Hikoso, T. Takeda, T. Watanabe, M. Asahi, M. Taniike, Y. Matsumura, I. Tsujimoto, K.

Hongo, Y. Kusakari, S. Kurihara, K. Nishida, H. Ichijo, M. Hori, and K. Otsu. 2003. Targeted deletion of apoptosis signal-regulating kinase 1 attenuates left ventricular remodeling. *Proceedings of the National Academy of Sciences of the United States of America*. 100:15883-15888.

Yan, L., D.E. Vatner, S.J. Kim, H. Ge, M. Masurekar, W.H. Massover, G. Yang, Y. Matsui, J. Sadoshima, and S.F. Vatner. 2005. Autophagy in chronically ischemic myocardium. *Proceedings of the National Academy of Sciences of the United States of America*. 102:13807-13812.

Yang, C., C.C. Aye, X. Li, A. Diaz Ramos, A. Zorzano, and S. Mora. 2012. Mitochondrial dysfunction in insulin resistance: differential contributions of chronic insulin and saturated fatty acid exposure in muscle cells. *Bioscience Reports*. 32:465-478.

Yang, L., P. Li, S. Fu, E.S. Calay, and G.S. Hotamisligil. 2010. Defective hepatic autophagy in obesity promotes ER stress and causes insulin resistance. *Cell Metabolism*. 11:467-478.

Yin, J.J., Y.B. Li, Y. Wang, G.D. Liu, J. Wang, X.O. Zhu, and S.H. Pan. 2012. The role of autophagy in endoplasmic reticulum stress-induced pancreatic beta cell death. *Autophagy*. 8:158-164.

Yorimitsu, T., and D.J. Klionsky. 2005. Autophagy: molecular machinery for self-eating. *Cell Death and Differentiation*. 12 Suppl 2:1542-1552.

Youle, R.J., and D.P. Narendra. 2011. Mechanisms of mitophagy. *Nature reviews. Molecular Cell Biology*. 12:9-14.

Yuzefovych, L., G. Wilson, and L. Rachek. 2010. Different effects of oleate vs. palmitate on mitochondrial function, apoptosis, and insulin signaling in L6 skeletal muscle cells: role of oxidative stress. *American Journal of Physiology. Endocrinology and Metabolism*. 299:E1096-1105.

Zhang, C., Z. Xu, X.R. He, L.H. Michael, and C. Patterson. 2005. CHIP, a cochaperone/ubiquitin ligase that regulates protein quality control, is required for maximal cardioprotection after myocardial infarction in mice. *American Journal of Physiology. Heart and Circulatory Physiology*. 288:H2836-2842.

Zhang, M., A. Perino, A. Ghigo, E. Hirsch, and A.M. Shah. 2013. NADPH oxidases in heart failure: poachers or gamekeepers? *Antioxidants & Redox Signaling*. 18:1024-1041.

Zhang, Y., S. Goldman, R. Baerga, Y. Zhao, M. Komatsu, and S. Jin. 2009. Adipose-specific deletion of autophagy-related gene 7 (atg7) in mice reveals a role in adipogenesis. *Proceedings of the National Academy of Sciences of the United States of America*. 106:19860-19865.

Zhang, Y., D.A. Wick, A.L. Haas, B. Seetharam, and N.M. Dahms. 1995. Regulation of lysosomal and ubiquitin degradative pathways in differentiating human intestinal Caco-2 cells. *Biochimica et biophysica acta*. 1267:15-24.

Zhao, T., X. Huang, L. Han, X. Wang, H. Cheng, Y. Zhao, Q. Chen, J. Chen, H. Cheng, R. Xiao, and M. Zheng. 2012. Central role of mitofusin 2 in autophagosome-lysosome fusion in cardiomyocytes. *The Journal of Biological Chemistry*. 287:23615-23625.

Zhu, H., P. Tannous, J.L. Johnstone, Y. Kong, J.M. Shelton, J.A. Richardson, V. Le, B. Levine, B.A. Rothermel, and J.A. Hill. 2007. Cardiac autophagy is a maladaptive response to hemodynamic stress. *The Journal of Clinical Investigation*. 117:1782-1793.

Zolk, O., C. Schenke, and A. Sarikas. 2006. The ubiquitin-proteasome system: focus on the heart. *Cardiovascular Research*. 70:410-421.